การใช้ปริมาณรังสีอย่างเหมาะสมเพื่อให้เกิดภาพเอกซเรย์คอมพิวเตอร์ทรวงอกที่มีคุณภาพยอมรับได้ด้วยเทคนิคการปรับกระแสหลอด-เวลาบนพื้นฐานการเปลี่ยนค่าดัชนีย์นอยส์: ศึกษาในหุ่นจำลอง

นางภาวนา อินธิบาล

วิทยานิพนธ์นี้เป็นส่วนหนึ่งของการศึกษาตามหลักสูตรปริญญาวิทยาศาสตรมหาบัณฑิต
สาขาวิชาฉายาเวชศาสตร์ ภาควิชารังสีวิทยา
คณะแพทยศาสตร์ จุฬาลงกรณ์มหาวิทยาลัย
ปีการศึกษา 2555

ลิขสิทธิ์ของจุฬาลงกรณ์มหาวิทยาลัย
บทคัดย่อและแฟ้มข้อมูลฉบับเต็มของวิทยานิพนธ์ตั้งแต่ปีการศึกษา 2554 ที่ให้บริการในคลังปัญญาจุฬาฯ (CUIR)
เป็นแฟ้มข้อมูลของนิสิตเจ้าของวิทยานิพนธ์ที่ส่งผ่านทางบัณฑิตวิทยาลัย
The abstract and full text of theses from the academic year 2011 in Chulalongkorn University Intellectual Repository(CUIR)
are the thesis authors' files submitted through the Graduate School.

OPTIMIZATION IN 64- MDCT OF THE CHEST USING TUBE CURRENT MODULATION BASED ON NOISE INDEX: PHANTOM STUDY

Mrs. Pawana Inthibal

A Thesis Submitted in Partial Fulfillment of the Requirements
for the Degree of Master of Science Program in Medical Imaging
Department of Radiology
Faculty of Science
Chulalongkorn University
Academic Year 2012
Copyright of Chulalongkorn University

Thesis Title	OPTIMIZATION IN 64- MDCT OF THE CHEST USING TUBE CURRENT MODULATION BASED ON NOISE INDEX: PHANTOM STUDY
By	Mrs. Pawana Inthibal
Field of Study	Medical Imaging
Thesis Advisor	Associate Professor Anchali Krisanachinda, Ph.D.
Thesis Co-advisor	Associate Professor Kiat Arjhansiri, M.D.

Accepted by the Faculty of Medicine, Chulalongkorn University in Partial Fulfillment of the Requirements for the Master's Degree

……..…….....Dean of the Faculty of Medicine
(Associate Professor Sophon Napathorn, M.D.)

THESIS COMMITTEE

……..Chairman
(Assistant Professor Panruethai Trinavarat, M.D.)

……..Thesis Advisor
(Associate Professor Anchali Krisanachinda, Ph.D.)

……..Thesis Co-advisor
(Associate Professor Kiat Arjhansiri, M.D.)

…….External Examiner
(Professor Franco Milano, Ph.D.)

ภาวนา อินธิบาล : การใช้ปริมาณรังสีอย่างเหมาะสมเพื่อให้เกิดภาพเอกซเรย์คอมพิวเตอร์ทรวงอกที่มีคุณภาพยอมรับได้ด้วยเทคนิคการปรับกระแสหลอด-เวลาบนพื้นฐานการเปลี่ยนค่าดัชนีย์นอยส์: ศึกษาในหุ่นจำลอง (OPTIMIZATION IN 64 – MDCT OF THE CHEST USING TUBE CURRENT MODULATION BASED ON NOISE INDEX: PHANTOM STUDY) อ.ที่ปรึกษาวิทยานิพนธ์หลัก: รศ.ดร. อัญชลี กฤษณจินดา, อ.ที่ปรึกษาวิทยานิพนธ์ร่วม: รศ.นพ. เกียรติ อาจหาญศิริ: 101 หน้า.

เทคนิคการปรับกระแสหลอดเป็นวิธีการลดปริมาณรังสีแก่ผู้ป่วยได้อย่างมีประสิทธิภาพ, ค่าดัชนีนอยส์เป็นพารามิเตอร์หนึ่งของระบบควบคุมปริมาณรังสีแบบอัตโนมัติตามการเบาบางรังสีจากเครื่องเอกซเรย์คอมพิวเตอร์ชนิด 64 สไลซ์ ซึ่งกำหนดปริมาณสัญญาณรบกวนบนภาพและคุณภาพของภาพเอกซเรย์คอมพิวเตอร์ สัมพันธ์กับปริมาณรังสีที่ผู้ป่วยได้รับ การศึกษานี้มีวัตถุประสงค์เพื่อหาปริมาณรังสีเมื่อมีการตั้งค่าดัชนีย์นอยส์ที่ต่างกัน และค่าดัชนีย์นอยส์ที่เหมาะสมเพื่อให้ได้ภาพเอกซเรย์คอมพิวเตอร์ทรวงอกของหุ่นจำลองที่มีคุณภาพยอมรับได้และปริมาณรังสีต่ำ

หุ่นจำลองทรวงอกขนาดมาตรฐานและขนาดใหญ่ ภายในมีเนื้อเยื่อทรงกลมจำลอง ขนาดเส้นผ่านศูนย์กลาง 12, 10, 8, 5, และ 3 มิลลิเมตร บรรจุอยู่ ถูกนำมาสแกนด้วยเครื่องเอกซเรย์คอมพิวเตอร์ชนิด 64 สไลซ์ ด้วยการตั้งค่าพารามิเตอร์ที่แตกต่างกันของฟิลเตอร์สร้างภาพ 4 แบบ คือ STD, CHEST, LUNG, และ BONE+, ความหนาของสไลซ์ 4 ขนาด คือ 0.625, 1.25, 2.5 และ 5.0 มิลลิเมตร และ ค่าดัชนีย์นอยส์ 10, 12.5, 15, 17.5 และ 20 ด้วยค่ากระแสหลอดต่ำที่สุดถึงสูงที่สุดคือ 75-380 มิลลิแอมแปร์. ค่า $CTDL_{vol}$ และ DLP ที่ได้ถูกบันทึกจากหน้าจอแสดงภาพ การประเมินคุณภาพของภาพในเชิงปริมาณกระทำโดยวิธี การหาอัตราส่วนความคมชัดบนภาพต่อสัญญานรบกวน (ซีเอ็นอาร์) และการประเมินในเชิงคุณภาพโดย ความสามารถ ในการมองเห็นเนื้อเยื่อทรงกลมจำลอง และขนาดของเนื้อเยื่อทรงกลมจำลองที่เล็กที่สุดโดยนักรังสีการแพทย์ 2 ท่านที่มีประสบการ์ทางด้านเอกซเรย์คอมพิวเตอร์มากกว่าสิบปี ข้อมูลปริมาณรังสีและคุณภาพของภาพถูกนำมาประเมินเพื่อหาค่าดัชนีย์นอยส์ที่เหมาะสมเพื่อการใช้รังสีปริมาณต่ำและคุณภาพของภาพที่ยอมรับได้

ผลการศึกษาพบว่า สำหรับหุ่นจำลองขนาดมาตรฐานเมื่อมีการเพิ่มขึ้นของค่าดัชนีย์นอยส์ จาก 10-20 และ ความหนาของสไลซ์เพิ่มขึ้น 0.625- 5.0 มิลลิเมตรค่า $CTDL_{vol}$ ลดลงจาก 16.52 เหลือ 3.38 มิลลิเกรย์, และจะลดลงเพียงเล็กน้อยเมื่อความหนาของสไลซ์บาง แต่จะลดลงอย่างมากเมื่อความหนาของสไลซ์หนาขึ้น สำหรับหุ่นจำลองขนาดใหญ่ พบว่าค่า $CTDL_{vol}$ และ DLP ไม่เปลี่ยนแปลงที่ความหนาของสไลซ์บาง, ค่า $CTDL_{vol}$ ลดลงจาก 16.52 เหลือ 7.09 มิลลิเกรย์, ฟิลเตอร์สร้างภาพชนิด STD ให้ค่าเปอร์เซนต์ซีเอ็นอาร์มากที่สุด เมื่อเปรียบเทียบกับฟิลเตอร์สร้างภาพ แบบ CHEST ซึ่งให้ 50-60 เปอร์เซนต์ ในขณะที่ฟิลเตอร์สร้างภาพ แบบ BONE+ ให้ค่าซีเอ็นอาร์ต่ำที่สุด ผลการให้คะแนนเชิงคุณภาพจากนักรังสีการแพทย์ 2 ท่านมีความเห็นตรงกัน

ค่าดัชนีย์นอยส์และความหนาของสไลซ์เป็นปัจจัยหลักที่มีผลต่อปริมาณรังสีที่ผู้ป่วยได้รับ การเพิ่มขึ้นของค่าดัชนีย์นอยส์ในช่วง 10-20 มีผลช่วยลดปริมาณรังสีลงได้ 18.2, 32.1, 64.9 และ 65.9 เปอร์เซนต์ตามลำดับ สำหรับหุ่นจำลองขนาดใหญ่ ความหนาของสไลซ์เพียงอย่างเดียวที่เป็นปัจจัยหลัก โดยปริมาณรังสีจะลดลง 12.8 และ 57.07 เปอร์เซนต์ ที่ความหนาของสไลซ์ 2.5 และ 5.0 มิลลิเมตร ตามลำดับ ดังนั้น เมื่อใช้ค่าดัชนีย์นอยส์ 10-20 ค่าปริมาณรังสีของการเอกซเรย์คอมพิวเตอร์ทรวงอก คือ 16.52-3.38 มิลลิเกรย์ สำหรับหุ่นจำลองขนาดปกติ และ 16.52-7.09 มิลลิเกรย์ สำหรับหุ่นขนาดใหญ่, ดัชนีย์นอยส์, ความหนาของสไลซ์ และชนิดของฟิลเตอร์สร้างภาพล้วนมีผลต่อปริมาณรังสีและคุณภาพของภาพ, ฟิลเตอร์ชนิด STD ถูกออกแบบมาเพื่อให้ได้ภาพที่มีคุณภาพที่ดีที่สุดและมีสัญญาณรบกวนเหมาะสมเมื่อเปรียบเทียบกับฟิลเตอร์ชนิดอื่น การพิจารณาการใช้ค่าดัชนีย์นอยส์ ขึ้นอยู่กับชนิดของฟิลเตอร์ที่จะนำมาสร้างภาพและพยาธิสภาพของโรคปอด ค่าดัชนีย์นอยส์ 20 ที่ กระแสหลอด 75-380 มิลลิแอมแปร์ด้วยฟิลเตอร์สร้างภาพชนิด LUNG และ BONE+ เหมาะสมกับการตรวจเนื้อเยื่อปอด ให้ภาพที่มีคุณภาพยอมรับได้จากการประเมินด้วยวิธีเชิงคุณภาพ, ส่วนค่าดัชนีย์นอยส์ 15-17.5 ด้วยฟิลเตอร์สร้างภาพชนิด STD ให้ภาพที่มีคุณภาพที่ยอมรับได้จากการประเมินด้วยวิธีเชิงปริมาณสำหรับการเอกซเรย์คอมพิวเตอร์ทรวงอกที่ต้องการดูอวัยวะต่าง ๆ ทั่วไปในทรวงอก

ภาควิชา ……..รังสีวิทยา……..... ลายมือชื่อนิสิต……

สาขาวิชา ……ฉายาเวชศาสตร์…… ลายมือชื่อ อ. ที่ปรึกษาวิทยานิพนธ์หลัก……

ปีการศึกษา……..2555……..... ลายมือชื่อ อ. ที่ปรึกษาวิทยานิพนธ์ร่วม……

##5474147630: MAJOR MEDICAL IMAGING
KEYWORDS: NOISE INDEX/ AUTOMATIC EXPOSURE CONTROL
PAWANA INTHIBAL: OPTIMIZATION IN - 64 MDCT OF THE CHEST USING TUBE CURRENT MODULATION BASED ON NOISE INDEX: PHANTOM STUDY.ADVISOR: ASSOC.PROF. ANCHALI KRISANACHINDA, Ph.D., 101 pp.

Tube current modulation is the great potential method for the radiation dose reduction. Noise Index is an indicative parameter of the image quality controlled by the AEC system for the noise level in the image associated with radiation dose. The purpose of this study is to determine the radiation dose when varying Noise Index and the optimal Noise Index for the acceptable image quality of the chest phantom.

The standard and large sizes Lung Man Chest phantom with +100 HU of 12, 10, 8, 5, and 3 mm in diameter of spheres simulated nodules were scanned with various reconstruction filters, 0.625-5.0 mm of slice thickness, Noise Index 10-20 and 75-380 of mA. The $CTDI_{vol}$ (mGy) and DLP (mGy.cm) were recorded from the CT console. The quantitative image quality was assessed by the contrast to noise ratio (CNR) values. The nodule detectability and spatial resolution were independently evaluated by two radiological technologists for qualitative image quality.

With the variation on Noise Index of 10-20 and the slice thickness of 0.625-5.0 mm on the standard size phantom, the radiation dose was decreasing, $CTDI_{vol}$ from 16.52 to 3.38 mGy. The $CTDI_{vol}$ and DLP slightly decreased at the thin slice thickness and rapidly decreased at thick slice thickness on varying Noise Index. There were no variation of $CTDI_{vol}$ and DLP at the thin slice thickness for the large size phantom, the range of $CTDI_{vol}$ was 16.52-7.09 mGy. The STD filter offered the highest percent CNR when compared to the CHEST filter at 50-60%, the LUNG and BONE+ offered the lowest percent CNR respectively. The LUNG filter produced the best spatial resolution image. The scoring on image quality by two observers for standard, and large size phantoms were similar with good agreement.

Noise Index and slice thickness are the major parameters affecting the radiation dose. Increasing of Noise Index 10-20 results in decreasing radiation dose to 18.2, 32.1, 64.9, and 65.9% for 0.625-5.0 mm slice thickness respectively. The slice thickness had a major impact on radiation dose for the large size phantom with the reduction from 12.82% to 57.07 % for 2.5-5.0 mm of slice thickness respectively. The STD filters were designed for good spatial resolution with reasonably low image noise. The Noise Index has little affected on CNR.

When varying Noise Index from 10-20, the reduction in $CTDI_{vol}$ was 9.91-3.38 mGy for standard size phantom, and 16.52-7.09 mGy for large size phantom. The factors affecting on radiation dose and image quality were Noise Index, slice thickness and reconstruction filters. The selection on Noise Index depends on clinical applications. Using the Noise Index of 20 at 75-380 mA with LUNG and Bone+ filters resulted in acceptable subjective image quality whereas Noise Index 15-17.5 at 75-380 mA with STD filters resulted in acceptable objective image quality for routine chest CT.

Department…....Radiology…… Student's Signature……
Field of Study…….Medical Imaging..... Advisor's Signature……
Academic Year……2012…… Co-advisor's Signature……...

ACKNOWLEDGEMENTS

I would like to express gratitude and deepest appreciation to Associate Professor Anchali Krisanachinda, Ph.D., Division of Nuclear Medicine, Department of Radiology, Faculty of Medicine, Chulalongkorn University, my advisor for her guidance, helpful suggestion, supervision, constructive comments and polishing of the thesis writing to improve the readability and English expression.

I would like to extremely grateful Associate Professor Kiat Arjhansiri, M.D. Department of Radiology, Faculty of Medicine, Chulalongkorn University, my co-advisor for his helpful suggestion, constructive comments.

I would like to extremely grateful Associate Professor Sivalee Suriyapee, Chief Physicist at Division of Radiation Oncology, Department of Radiology, Faculty of Medicine, Chulalongkorn University, my teacher for her invaluable advices, constructive comments in this research.

I would like to deeply thank Associate Professor Somjai Wangsuphachart, M.D., Department of Radiology, Faculty of Medicine, Chulalongkorn University, for her help suggestion, constructive comments in this research.

I would like to thank Professor Franco Milano from University of Florence Italy, who is the external examiner of the thesis defense for his helpful recommendation, constructive comments and teaching of knowledge in Medical Imaging.

I would like to deeply grateful Mr. Krisadang Thasenhod, M.Sc., Department of Radiology, Rajavithi Hospital for his of invaluable advices, contribution in QC part, image scoring, helpful suggestion and all his kind supports in this research.

I would like to deeply grateful Mr. Kitiwat Kamwan Ph.D., Department of Radiology, King Chulalongkorn Memorial Hospital for his advices, constructive comment, his contribution in QC part and image scoring in this research.

I am extremely grateful for all teachers, lecturers and staffs at Master of Science Program in Medical Imaging, Faculty of Medicine, Chulalongkorn University for their helps, and unlimited teaching of knowledge during the course in Medical Imaging. My grateful is forwarded to the Graduate Studies for supply the knowledge as tutor, especially, Mrs. Petcharleeya Suwanpradit for her contribution in part QC phantom, and all technologist at Rajavithi Hospital for their kind supports.

Finally, I am extremely grateful to my family for their invaluable encouragement, entirely care, financial support and understanding during course of the study.

CONTENTS

	Page
ABSTRACT (THAI).....	iv
ABSTRACT (ENGLISH).....	v
ACKNOWLEDGEMENTS.....	vi
CONTENTS.....	vii
LIST OF TABLES.....	x
LIST OF FIGURES.....	xii
LIST OF ABBREVIATIONS.....	xiv
CHAPTER I INTRODUCTION.....	1
1.1 Background and rationale.....	1
1.2 Research objectives.....	3
CHAPTER II REVIEW OF RELATED LITERATURE.....	4
2.1 Theory.....	4
2.1.1 The introduction of Computed Tomography (CT).....	4
2.1.2 Multislice CT.....	4
2.1.3 Image reconstruction.....	6
2.1.4 CT number.....	7
2.1.5 Slice thickness: multiple detector array scanner.....	8
2.1.6 Volume CT Dose Index ($CTDI_{vol}$)	8
2.1.7 Dose Length Product (DLP).....	9
2.1.8 Image quality.....	10
2.1.8.1 Spatial resolution.....	10
2.1.8.2 Contrast resolution.....	10
2.1.8.3 Image noise.....	11
2.1.8.4 Factor affecting noise.....	11
2.1.9 Automatic Exposure Control (AEC).....	12
2.1.9.1 Angular modulation.....	13
2.1.9.2 Z-Axis modulation.....	14
2.1.10 Noise Index.....	14
2.2 Review of Related Literature.....	15
CHAPTER III RESEARCH METHODOLOGY.....	17
3.1 Research design.....	17
3.2 Research design Model.....	17
3.3 Conceptual framework.....	18
3.4 Research question.....	18
3.5 Materials.....	19
3.5.1 CT scanner.....	19
3.5.2 Lung Man Chest Phantom.....	19
3.5.3 Simulated lung nodules.....	20
3.5.4 Catphan phantom® 600	21

3.5.5 PMMA phantom……. 22
3.5.6 Radiation detector - Pencil ion chamber ……..... 23
3.6 Methods……... 23
3.6.1 Perform the quality control of 64 MDCT GE VCT LightSpeed 23
3.6.2 Verification of $CTDI_{vol}$……..... 23
3.6.3 Study of image quality in Catphan phantom……... 24
3.6.4 Lung man chest phantom study……. 25
3.6.5 Optimization the radiation dose and image quality…… 27
3.7 Data analysis…… 27
3.8 Sample size determination……..... 28
3.9 Outcome measurement……. 28
3.10 Statistical analysis…….. 29
3.11 Expected benefits……... 29
3.12 Ethical consideration…….. 29

CHAPTER IV RESULTS……..... 30
4.1 Quality control of the CT scanner……..... 30
4.2 Verification of Computed Tomography Dose Index (CTDI)……... 31
4.2.1 $CTDI_{100}$ in air……... 31
4.2.2 $CTDI_{100}$ in head phantom compared with IMPACTSCAN values for 120 kVp…….. 31
4.2.3 $CTDI_{100}$ in body phantom compared with IMPACTSCAN values for 120 kVp……. 32
4.2.4 $CTDI_{vol}$ of monitor and calculated $CTDI_{w}$……. 33
4.3 Characteristic of image quality in Catphan phantom……..... 33
4.3.1 High contrast resolution……... 34
4.3.2 Low contrast detectability…… 34
4.3.3 Image noise…….. 37
4.4 Radiation dose…… 37
4.5 Image quality……... 49
4.5.1 Quantitative image quality……... 49
4.5.1.1 Contrast to Noise Ratio (CNR)……..... 49
4.5.2 Qualitative image quality……..... 69
4.5.2.1 Image scoring…….. 69
4.5.2.2 Spatial resolution……..... 70

CHAPTER V DISCUSSION AND CONCLUSIONS……... 72
5.1 Discussion…… 72
5.1.1 Measurement of CTDI ……..... 72
5.1.2 Radiation dose, slice thickness and Noise Index……..... 73
5.1.3 Characteristic of image quality in Catphan phantom…….. 74
5.1.4 The assessment of image quality…… 74
5.1.4.1 Contrast to noise ratio…….. 75
5.1.4.2 The assessment of qualitative image quality……... 75
5.1.4.3 Optimization of radiation dose, image quality and Noise Index……. 76
5.2 Conclusion…….. 77

REFERENCES……. 78

APPENDICES……. 80

Appendix A: Case record form……. 81

Appendix B: Quality Control of CT system……. 87

VITAE…….. 101

LIST OF TABLES

Table		Page
3.1	The five point scale of image quality……..	28
4.1	Report of CT system performance……..	30
4.2	The measured $CTDI_{100}$ in air for head and body protocols compared with ImPACTSCAN values for each kVp……..	31
4.3	The measured $CTDI_{100}$ in the head phantom compared with ImPACTSCAN values for 120 kVp……...	32
4.4	The measured $CTDI_{100}$ in the body phantom compared with ImPACTSCAN values for 120 kVp……...	32
4.5	$CTDI_{vol}$ of monitor and $CTDI_w$ using head technique ……...	33
4.6	$CTDI_{vol}$ of monitor and $CTDI_w$ using body technique……	33
4.7	High contrast resolution study …….....	34
4.8	Low contrast detectability at supra-slice…….....	35
4.9	Low contrast detectability at sub-slice……	35
4.10	The standard deviation of CT number with variation of filters……..	37
4.11	$CTDI_{vol}$, DLP for standard size Lung Man chest phantom with STD filter……	38
4.12	$CTDI_{vol}$, DLP for standard size Lung Man chest phantom with BONE+ filter……..	39
4.13	$CTDI_{vol}$, DLP for standard size Lung Man chest phantom with CHEST filter……...	40
4.14	$CTDI_{vol}$, DLP for standard size Lung Man chest phantom with LUNG filter…….	41
4.15	$CTDI_{vol}$, DLP for large size of Lung Man chest phantom with STD filter…….	42
4.16	$CTDI_{vol}$, DLP for large size Lung Man chest phantom with BONE+ filter…….	43
4.17	$CTDI_{vol}$, DLP for large size Lung Man chest phantom with CHEST filter…….	44
4.18	$CTDI_{vol}$, DLP for large size Lung Man chest phantom with LUNG filter…….	45
4.19	The percent $CTDI_{vol}$ reduction when vary the noise index from 10 to 20at different slice thickness of standard size phantom…….	46
4.20	The percent $CTDI_{vol}$ reduction when vary the noise index from 10 to 20 at different slice thickness for the large size phantom……...	47
4.21	The percent CNR of nodule 12 mm in diameter for standard size phantom……..	49

Table **Page**

4.22	The percent CNR of nodule 10 mm in diameter for standard size phantom……..	50
4.23	The percent CNR of nodule 8 mm in diameter for standard size phantom……..	51
4.24	The percent CNR of nodule 5 mm in diameter for standard size phantom……..	52
4.25	The percent CNR of nodule 3 mm in diameter for standard size phantom……..	53
4.26	The percent CNR of nodule 12 mm in diameter for large size phantom	54
4.27	The percent CNR of nodule 10 mm in diameter for large size phantom	55
4.28	The percent CNR of nodule 8 mm in diameter for large size phantom.	56
4.29	The percent CNR of nodule 5 mm in diameter for large size phantom.	57
4.30	The percent CNR of nodule 3 mm in diameter for large size phantom.	58
4.31	The image scoring of standard size phantom……..	69
4.32	The image scoring of large size phantom……..	69
4.33	The weighted Kappa of image quality scored by two radiological technologist……..	70
4.34	The spatial resolution (mm) of standard size phantom……..	71
4.35	The spatial resolution (mm) of large size phantom……	71
5.1	The percent $CTDI_{vol}$ reduction of standard size phantom……..	74
5.2	Comparison of the percent of noise level among manufacturer…….	74

LIST OF FIGURES

Figure		Page
2.1	Detector array designs for CT scanner 64 images per gantry rotation	5
2.2	Process involved in CT image reconstruction…….	6
2.3	The relationship between spatial resolution and image noise of difference convolution kernel……..	7
2.4	Dose profile of a single CT section…….	9
2.5	Automatic adjustment of tube current…….	12
2.6	Angular modulation of tube current performed at different projections in the x-y plane within each 360º …….	13
3.1	64 –MDCT GE VCT LightSpeed…….....	19
3.2	Lung Man Chest phantom……...	20
3.3	Simulated lung nodules of 12,10, 8, 5, and 3 mm diameter……	20
3.4	Catphan phantom ® 600……..	21
3.5	Diagram of Catphan phantom ® 600 with dimensions……	21
3.6	PMMA phantoms with chamber insert at center…….	22
3.7	The Ray Safe Xi CT detector with reader……...	23
3.8	Measurement of noise…….	25
3.9	Measurement the CT number of nodule and background……...	26
4.1	Low contrast detectability obtained from various filters, STD, CHEST, LUNG and BONE+ filters……	36
4.2	The relationship between the average $CTDI_{vol}$ and Noise Index at different sizes of slice thickness for the standard size phantom……..	46
4.3	The relationship between the average $CTDI_{vol}$ and Noise Index of at varying slice thickness of large size phantom…….	47
4.4	The relationship between the average DLP and Noise Index of at different slice thickness for the standard size phantom……...	48
4.5	The relationship between the average DLP and Noise Index of at different slice thickness for the large size phantom…….	48
4.6	The percent CNR of nodule 12 mm, at slice thickness 0.625, 1.25, 2.5 and 5.0 mm respectively for standard size phantom……..	59
4.7	The percent CNR of nodule 10 mm, at slice thickness 0.625, 1.25, 2.5 and 5.0 mm respectively for standard size phantom……..	60
4.8	The percent CNR of nodule 8 mm, at slice thickness 0.625, 1.25, 2.5 and 5.0 mm respectively for standard size phantom……	61
4.9	The percent CNR of nodule 5 mm, at slice thickness 0.625, 1.25, 2.5 and 5.0 mm respectively for standard size phantom……..	62
4.10	The percent CNR of nodule 3 mm, at slice thickness 0.625, 1.25, 2.5 and 5.0 mm respectively for standard size phantom…….	63
4.11	The percent CNR of nodule 12 mm, at slice thickness 0.625, 1.25, 2.5 and 5.0 mm respectively for large size phantom……..	64

Figure **Page**

4.12 The percent CNR of nodule 10 mm, at slice thickness 0.625, 1.25, 2.5 and 5.0 mm respectively for large size phantom…….. 65
4.13 The percent CNR of nodule 8 mm, at slice thickness 0.625, 1.25, 2.5 and 5.0 mm respectively for large size phantom……. 66
4.14 The percent CNR of nodule 5 mm, at slice thickness 0.625, 1.25, 2.5 and 5.0 mm respectively for large size phantom……. 67
4.15 The percent CNR of nodule 3 mm, at slice thickness 0.625, 1.25, 2.5 and 5.0 mm respectively for large size phantom……. 68
5.1 The chest CT with 5 mm nodule, 1.25 mm slice thickness, NI 20, of LUNG and BONE+ filters…….. 76
5.2 The chest CT with 5 mm nodule, 1.25 mm slice thickness with STD filter of NI 15 and 17.5…… 76

LIST OF ABBREVIATIONS

ABBREVIATION	TERMS
3D	Three dimensions
AEC	Automatic Exposure Control
CT	Computed Tomography
cm	Centimeter
CNR	Contrast to Noise Ratio
CTDI	Computed Tomography Dose Index
$CTDI_{vol}$	Volume Computed Tomography Dose Index
$CTDI_{w}$	Weighted Computed Tomography Dose Index
DAS	Data Acquisition System
DFOV	Display Field Of View
DLP	Dose Length Product
GE	General Electric
g/cm^3	Gram per centimeter square
HRCT	High Resolution Computed Tomography
HU	Hounsfield Unit
kVp	Kilo Voltage peak
lp/cm	Line pair per centimeter
mA	Milliampere
mAs	Milliampere-second
mGy	Milligray
mm	Millimeter
mm^2	Millimeter square
NI	Noise Index
PMMA	Polymethylmethacrylate
ROI	Region Of Interest
QC	Quality Control
SC	Section Collimator
SD	Standard Deviation
SFOV	Scan Field Of View
STD	Standard
μ	Attenuation coefficient
WW	Window Width
WL	Window Level

CHAPTER I

INTRODUCTION

1.1 Background and rationale

Since the first invention of CT scanner by G.N. Hounsfield in 1972, CT has been developed and the number of CT systems increase rapidly. It becomes the important modalities in medical imaging. Current CT systems offer fast scanning speed and isotropic spatial resolution corresponding with specific software applications. CT provides better visualization to diagnose disease more quickly, safety and accurately than alternative radiographic modalities.

According to the United Nation Scientific Committee on the Effects of the Atomic Radiation (UNSCEAR), CT constitutes approximately 5% of all radiological examinations in the world but contributed to about 34% of the collective dose to the population **[1]**. The overall increasing in patient irradiation cause by the growing use of the multi-detectors row CT. The cancer risk is associated with the radiation dose in CT. The reducing patient radiation dose becomes top priorities of the radiologist, medical physicist and manufacturer. There are two guideline principles that must be followed. First, CT examinations must be appropriately justified for each individual patient. The requesting clinicians and radiologist share the major responsibility to the patient for the most appropriate imaging modality for required diagnostic task. Second, for each CT examination, all technique aspects of the examination must be optimized, such that the required level of image quality can be obtained while keeping the doses as low as possible **[2]**.

The attempt to reduce the patient radiation dose occurs although the benefits of CT excess the harmful effect. The strategies that used for dose reduction become an important practice. There are several factors that affect radiation dose associated with the multi detector, MDCT scanning. The factors can and cannot be modified or adjusted by user. Factors that can be adjusted to optimize radiation dose include tube potential, tube current, gantry rotation time, automatic exposure control, detector configuration, pitch, table speed, slice collimation, scan length, scan mode, scan region of interest, scanning phases, post processing image base filters, metal artifact reduction software and shielding devices. In addition, there are several scan features that users cannot change, including scanner geometry, x-ray beam filters, pre patient tracking of x-ray tube focal spot and projection adaptive reconstruction filters **[3]**.

Tube current modulation is one technical innovation that can reduce radiation dose with great potential. The concept of an automatic tube current modulation is based on the assumption that pixel noise on a CT scan is attributable to quantum noise in the projections by adjusting the tube current to follow the changing patient anatomy. There are two methods used on CT scanner, longitudinal tube modulation (z-axis) and angular tube modulation (x-y axis). Both methods have a complementary role in minimizing patient dose **[4]**.

The AEC system of GE Medical was studied for the optimization of patient dose using the combined tube current modulation system, auto mA 3D, which consists of two parts, Auto mA provides longitudinal automatic exposure control and Smart mA provides angular automatic exposure control. These two parts can be used separately. The image quality was specified in terms of Noise Index (NI). Noise Index is an indicator of the noise level in the image associated with radiation dose. The GE CT system use Noise Index prescribed the image quality. Noise is an important determinant of CT image quality, which is inversely related to the radiation dose.

Radiation dose is one of most significant factors determining CT image quality. Radiation dose should only be reduced under the condition that the diagnostic image quality is not sacrificed. The understanding how the radiation dose can be reduced is necessary with the relationship to image quality and radiation dose which can be achieved through system and operator controls.

The image quality is an important function of CT system. There are many characteristics affect on the image quality relate to the adjusting parameters by operator. The relationship between the slice thickness, Noise Index and reconstruction filters result in contrast to noise ratio which is an indicator of image quality of this study, however the adjusting of this parameters have also affect on radiation dose. CT parameters are necessary for the image quality and radiation dose trade off.

In this study, the optimization of the CT chest has been chosen as it is the study on an anatomical region where radiation dose could be reduced for high natural contrast between structures, such as air in the lungs and fat in the mediastinum, CT is a powerful modality for screening of the asymptomatic patient, the lung disease especially the lung cancer which the early detection with a smaller size is possible as compared with chest radiography. The major role of MDCT to solitary pulmonary nodule is accurately identified the malignant from benign lesions. It can improve the nodule detection and characterization by improving spatial resolution and decreasing artifact so the patients with the small solitary pulmonary lung nodules could be followed up the nodule several times for malignancy evaluation. The clinical application for MDCT chest such a CT angiography, the thin slice thickness was used to obtain the good image quality and the low radiation dose. The optimization for the radiation dose and image quality is important for the CT operators and radiologist. Moreover in female chest, breasts are radiosensitive organ directly exposed to x-ray beam, It is therefore necessary to keep the radiation as low as possible.

1.2 Research objectives

1.1.1 To determine radiation dose when varying Noise Index in chest phantom of various thickness.

1.1.2 To determine the optimal Noise Index for the chest phantom of different thickness.

Definition

Noise Index	The technique parameter entered by the user to determine the desired noise level. It is referenced to the standard deviation of pixel values in a specific size water phantom and is compared to a patient attenuation measured from the scout in order maintain image noise.

CHAPTER II
REVIEW OF RELATED LITERATURES

2.1 Theory

2.1.1 The introduction of Computed Tomography (CT) [5]

Computed tomography (CT) has been one of the biggest breakthroughs in diagnostic radiology. In 1917 Austrian mathematician Johann Radon presented an algorithm for creating an image from a set of measured data. After further theoretic work by Cormack between 1950 and 1970, the first clinical CT scanner was developed by Godfrey N. Hounsfield for examinations of the head and was installed in 1971 at Atkinson Morley's hospital in Wimbledon, England. Before the end of the 1970s the basics technical evolution was complete. The first body CT scanner was installed in 1974. Technical details were refined during the 1980s, and CT technology remained on a plateau until the early 1990s, when the advent of spiral (helical) CT scanning initial a further, rapid evaluation leading to improve diagnostic capabilities, 3D imaging techniques and CT angiography. The latest innovation is the introduction of multislice CT in 1998. This new technology is vastly expanding the performance of CT scanners, it truly transforms CT from a transaxial imaging modality to a 3D technique that yields high quality images in arbitrary planes and forms the basis for an expanding variety of 3D visualization technique, including virtual endoscopy. In addition, these scanners have the potential to revolutionize cardiac imaging with CT.

The first and second generations of CT scanners were superseded in the late 1970s by third and fourth generation scanners, which are still in use today. In third generation scanners, tube and detector array rotate synchronously around the patient. The detector array covers the full width of the fan beam. In fourth generation scanners, the detectors elements cover a full circle around the scanner opening and remain stationary during the scan, while only the x-ray tube rotates around the patient. However, third generation scanner offer better scatter suppression and require less detector elements, therefore all multislice CT scanners use third generation technology.

2.1.2 Multislice CT [5]

The high performances of Multislice CT are the reduction of scan time, and section collimation, including increased scan length. Multislice CT system is equipped with two or more parallel detector arrays and utilize a third generation technology with synchronously rotating tube and detector array as well as solid state detectors.

Multidetector row system

Multidetector systems are able to acquire at least four simultaneous sections. To be able to choose between various section collimation, the detector arrays have to be subdivided into multiple detector rows. Data from each of the scanned sections is recorded by *a data acquisition systems* (DAS), which consists of one detector row or a combination of detector rows, depending on the chosen section collimation. There are the three basic types of detectors as the matrix, adaptive array and hybrid detectors.

- ***Matrix detector***

  Matrix detectors consist of multiple detector rows of identical width. The GE matrix detector is a typical example. It use 64 parallel detector arrays with a width of 0.625 mm each.

- ***Adaptive array detector***

  Adaptive array detector consists of detector rows that grow in width from the center of the section to the periphery.

- ***Hybrid detectors***

  Hybrid detectors are similar to matrix detectors with the exception that the innermost detectors rows are thinner than the outer.

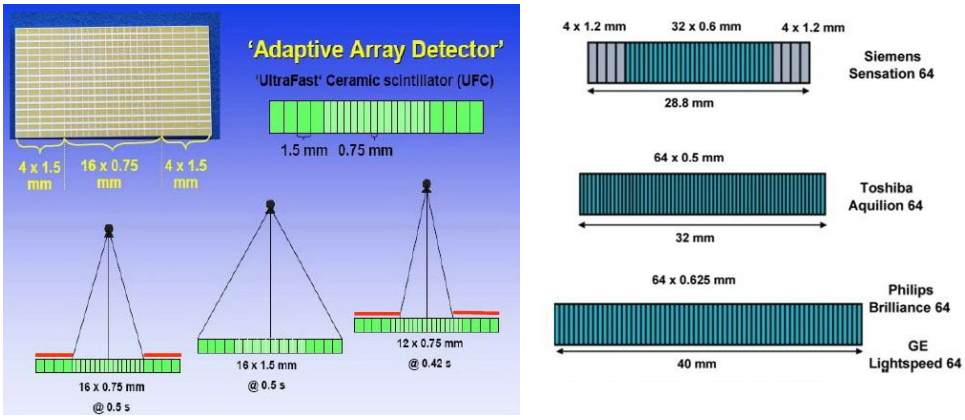

Figure 2.1 Detector array designs for CT scanner 64 images per gantry rotation.

2.1.3 Image reconstruction [5]

The detector signal registered during a scan is preprocessed to compensate for inhomogeneities in the detector system and to correct for beam-hardening effects within the patient. After various correction steps and transformation from signal intensities into x-ray attenuation values these data called "CT raw data" as shown in Figure 2.2

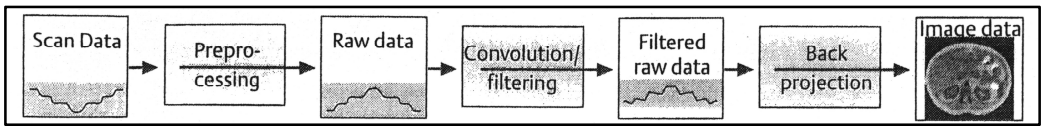

Figure 2.2 Process involved in CT image reconstruction.

The raw data sets for third and fourth generation scanners consist of the attenuation profile of some 500 to 1500 projections for 360º rotation of the x-ray tube. Each projection is composed of 500 to 1500 attenuation values. Image reconstruction from the raw data sets finally yields the image data set.

Image reconstruction starts with the selection of the desired field of view. Each ray from the tube to the detectors that passes through this field of view is used for reconstruction. The attenuation coefficient for each image point is determined by averaging the attenuation values for all rays that cross this point (back projection). This type of unfiltered back projection yields a very unsharp image with blurred edges Therefore multiple rays are assembled into a projection and the resulting attenuation profile subjected to an edge enhancing mathematic filtering (convolution) process.
The "convolution kernel" determines the type of filtering.

The convolution kernel used for the filter backprojection determines the properties of the reconstructed CT sections in terms of spatial resolution and image noise. Contrast resolution is the ability to differentiate objects with very little attenuation difference from their surroundings. High resolution convolution kernels improve spatial resolution but increase noise. The soft or smooth kernels lead to a reduction in noise and spatial resolution as shown in Figure 2.3. Standard kernel is designed as a compromise for good spatial resolution and reasonably low image noise for most CT applications.

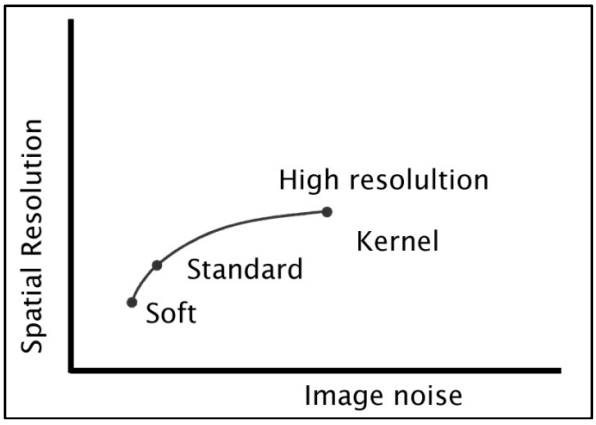

Figure 2.3 The relationship between spatial resolution and image noise of different convolution kernels.

2.1.4 CT number or Hounsfield Unit [6]

After CT reconstruction, each pixel in the image is represented by a high precision floating point number that is useful for computation but less useful for display. Consequently, after CT reconstruction, but before storing and displaying, CT images are normalized and truncated to integer values. The CT number *(x, y)* in each pixel, *(x, y),* of the image is determined by using the following equation:

$$CT(x, y) = 1000 \frac{\mu(x, y) - \mu_{water}}{\mu_{water}}$$

where $\mu(x, y)$ is the floating point number of the *(x, y)* pixel before conversion, μ_{water} is the attenuation coefficient of water, and CT*(x, y)* is the CT number that ends up in the final clinical CT image. The value of μ_{water} is about 0.195 for the x-ray beam energies typically used in CT scanning. This normalization results in CT numbers ranging from about -1,000 to +3,000, where -1,000 corresponds to air, soft tissues range from-300 to -100, water is 0, and dense bone and areas filled with contrast agent range up to +3,000.

CT numbers are corresponding to the physical of the patient. CT images are produced with a highly filtered, high kV x-ray beam, with an average energy of about 75 keV. At this energy in muscle tissue, about 91% of x-ray interactions are Compton scatter. For fat and bone, Compton scattering interactions are 94% and 74% respectively. Therefore, CT numbers and hence CT images derive their contrast mainly from the physical properties of tissue that influence Compton scatter. Density (g/cm^3) is a very important discriminating property of tissue (especially in lung tissue, bone, and fat), and the linear attenuation coefficient.

2.1.5 Slice thickness: multiple detector array scanners [6]

The slice thickness of multiple detector array CT scanners is determined not by collimator, but rather by the width of detectors in the slice thickness dimension. The width of the detectors is changed by *binning* different numbers of individual detector element together. The electronic signals generated by adjacent detectors element are electronically summed. Multiple detector arrays can be used both in conventional axial scanning and in helical scanning protocols. In axial scanning for example, four detectors are used, the width of the two center detector array almost completely dictates the thickness of the slice. For the two slices at the edges of the scan (detector arrays 1 and 4 of the four active detector arrays), the inner side of the slice is determined by the edge of the detector, but the outer edge is determined either by the collimator penumbra or the outer edge of the detector, depending on the collimation adjustment. With a multiple detector array scanner in helical mode, each detector array contributes to every reconstructed image, and therefore the slice sensitivity profile for each detector array needs to be similar to reduce artifacts. To accommodate this condition, it is typical to adjust the collimation so that the focal spot collimation blade penumbra falls outside the edge detectors. This cause the radiation dose to be a bit higher (especially for the small slice widths) in multislice scanners, but it reduces artifacts by equalizing the slice sensitivity profiles between the detectors array.

2.1.6 Volume CT Dose Index ($CTDI_{vol}$) [5]

The volume CT dose index ($CTDI_{vol}$) is a tool to indicate the average local dose to patient within the scan volume. Its unit is the mGy and there are separate data provided for body applications (measured in 32 cm diameter PMMA phantom) or head scans (16 cm diameter PMMA phantom). The $CTDI_{vol}$ is a measured of the average local dose delivered by CT (conventional slice by slice, single slice or multislice spiral scanning) to a cross section of such a phantom.

The $CTDI_{vol}$ is the most accessible dose indicator because it can be directly displayed on the user interface of the modern CT scanners. It provides immediate feedback about the dose delivered to the patient. The $CTDI_{vol}$ allows for direct comparison of the radiation dose from different scan parameter setting, even for scanners of different manufacturers.

The $CTDI_{vol}$ is derived from the primary direct measurement of dose in CT, the CT dose index defines as the integral under the dose profile D(z) of a CT section:

$$CTDI = \frac{1}{N.SC} . \int D(z)dz$$

CTDI measurements are made at various positions within a body (32 cm diameter) or head (16 cm diameter) PMMA phantom. The phantom provides scattering media similar to a patient. The dose profile is markedly wider than the

section collimation SC or section profile because of beam divergence and scatter radiation the area under the curve describes the CT dose index. Acquisition of multiple contiguous sections increases the local dose due to contributions from adjacent sections. As a result, increasing of the local radiation dose during scanning of whole body region as shown in Fig 2.4

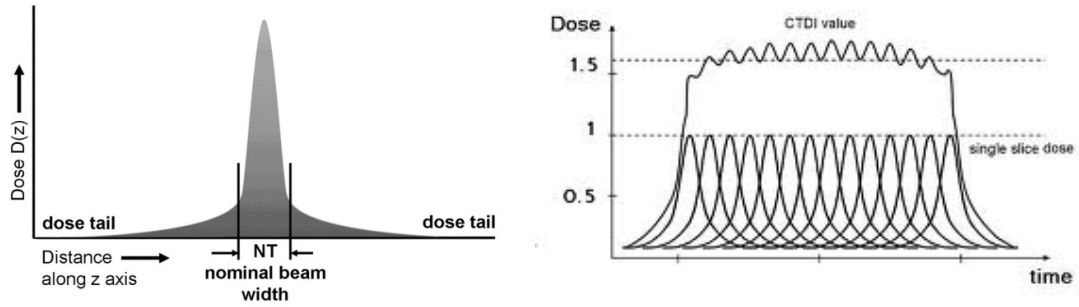

Figure 2.4 Dose profile of a single CT section

The term $CTDI_w$ (weighted CIDI) represent the average radiation dose across the diameter of the phantom (in body scanning, the peripheral and center measurement can vary by a factor of 2). The $CTDI_w$ is measured using a 100 mm ionization chamber that is placed at various positions within a 32 cm (body) phantom. The $CTDI_w$ is then calculated from the measurement in the center and the average of the four measurements in the periphery, 1 cm below the phantom surface

$$CTDI_w = \frac{1}{3} CTDI_c + \frac{2}{3} CTDI_p$$

2.1.7 Dose Length Product (DLP) [5]

The dose length product DLP is a measure of the cumulative dose (total energy) delivered to a patient. Its unit is mGy.cm It not only takes into account the average dose within the scan volume ($CTDI_{vol}$) but also the scan length L:

$$DLP = CTDI \times L$$

For conventional (non spiral) scanning the scan length L is the sum of all section collimations (e.g. 25x1 mm for HRCT = 25 mm). For spiral scanning, one can use the difference in table positions of the first and last section as a good estimate for the scan length L. However, spiral and multislice CT oversample data at the beginning and the end of the scan range because this data is needed for raw data interpolation of the first and last section. An approximately one half a rotation at the beginning and another half rotation at the end have to be added to the radiation

exposure of the patient. Thus the scan length, as provided by the scanner, should be expanded by at least one table feed.

2.1.8 Image quality [7]

Image quality in CT depends on four basic factors, spatial resolution, contrast resolution, image noise, and artifacts.

2.1.8.1 Spatial resolution

Spatial resolution is the ability of the system to image an object without blurring. It is often described as the 'sharpness' of an image. It may be quoted as the smallest object size able to be discerned, and as such is evaluated using high contrast test objects where signal to noise level is high and does not influence perception. It can also be specified in terms of spatial frequency, in line pairs per cm (lp/cm), for particular levels of the modulation transfer function (MTF); usually at the 50%, 10% and 2 % or 0% levels. The 0% MTF level is referred to as the 'cut-off frequency' and reflects the limit of the spatial resolution. The visual limit of spatial resolution, as the minimum size of high contrast objects, in millimeters, that can be distinguished, more generally relates to the frequency values between approximately the 2 and 5% modulation of the MTF. Sometimes a visual limited value is given by the manufacturers, either from a visual test object, or by converting the 2% value on the MTF to its size in mm.

The z-axis resolution is often referred to as z-sensitivity and is quoted in terms of the full width at half maximum (FWHM) of the imaged slice dose profile, but it may also be determined by the MTF. The z-axis resolution is primarily determined by the z-axis detector dimensions. Z-axis detector array design on MDCT scanners varies considerably between systems, with minimum dimensions ranging from 0.50 to 0.75 mm. With variable arrays, the z-axis spatial resolution will be reduced when the full extent of the array is used for imaging, as data from adjacent detectors are combined, increasing the effective detector size.

2.1.8.2 Contrast resolution

Contrast resolution is the ability to resolve an object from its surroundings where the CT numbers are similar *(e.g.* in the imaging of liver metastases). It is sometimes referred to as low as contrast resolution or low contrast detectability. The ability to detect an object will be dependent on its contrast, the level of image noise and its size. Contrast resolution is usually specified as the minimum size of object of a given contrast difference that can be resolved for a specified set of scan and reconstruction parameters.

Generator power is an important factor in low contrast examination. Low noise image require high tube current (mA) values, particularly when coupled with fast rotation speeds and narrow slice acquisitions. Fast rotation speeds reduce movement artifacts, thin slices improve spatial resolution as well as reduce partial

volume effects. Dose efficiency of the scanner is a significant factor in these types of examinations, as it will determine the dose required for a given level of contrast resolution. Contrast resolution specifications should give a guide to a scanner's dose efficiency. However, there is no standard methodology of data acquisition and image quality scoring to enable a good comparison of manufacturers' data.

2.1.8.3 Image noise [8]

In CT, x-rays contribute to detector measurements and not to individual pixels. CT image noise is thus associated with the number of x-rays contributing to each detector measurement. Because CT noise appears as fluctuations in CT numbers, a measurement of image noise is a measurement of these fluctuations, and such a measurement can be made using regions of interest (ROIs) on a scan of a uniform phantom. A statistical ROI function (available on most CT scanners) allows users to place a rectangular or oval ROI on the image, within which is calculated the average and standard deviation (SD) of the CT numbers for the enclosed pixels. The SD indicates the magnitude of random fluctuations in the CT number and thus is related to noise: the larger the SD, the higher the image noise.

2.1.8.4 Factor affecting noise [9]

a) Pixel size

Noise can be decreased by increasing the dimension of the pixel (voxel), this increase image blurring and reduces visibility of detail.

b) Slice thickness

Since slice thickness forms one dimension of the voxel, it affects image noise. Thin slices, which produce better detail and fewer partial-volume artifacts, produce higher noise levels.

c) Radiation exposure

The amount of radiation used to create a CT image can usually be varied by changing either the mA or the scanning time. Changing either produces a proportional change in patient dose and the radiation absorbed in individual voxels. Image noise can be decreased by increase the mAs, but the radiation dose absorbed by the tissue will also increase.

d) Window setting

The visibility of noise in a CT image depends on the setting of the window used to view the image. Small window, which enhance contrast, also increase the contrast and visibility of noise.

e) Filtration

Some of the mathematical filters algorithms used in the reconstruction process can reduce image noise by smoothing, or blurring, the image. The compromise that must be considered in using these filter functions is the reduction in image detail.

2.1.9 Automatic Exposure Control (AEC) [10]

AEC is a set of techniques that enable automatic adjustment of the tube current in the x-y plane (angular modulation) or along the z-axis (z-axis modulation) according to the size and attenuation characteristics of the body part being scanned. AEC techniques allow maintenance of constant image quality at a required radiation exposure level because AEC rapidly responds to large variations in beam attenuation. AEC is based on the fact that image noise is determined by x-ray quantum noise in the transmitted beam projections. This technique aims to modulate tube current on the basis of regional body anatomy for adjustment of x-ray quantum noise to maintain constant image noise with improved dose efficiency. There are two distinct techniques are available for AEC. Both techniques modulate tube current is an effort to maintain constant image quality at the lowest dose while simultaneously reducing tube loading (heating) and minimizing streak artifacts caused by a minimal number of photons.

The adjustment of tube current can be considered on three levels **[10]**. at the first level the mA is adjusted to take account of overall patient size as shown in Figure 2.5. The aim is to have a similar value of image noise for patients of different sizes. If used in isolation, this level of AEC maintains the same mA throughout the scan. However it is usually used in combination with the other levels of mA adjustment described below, which take into account attenuation variations within the patient.

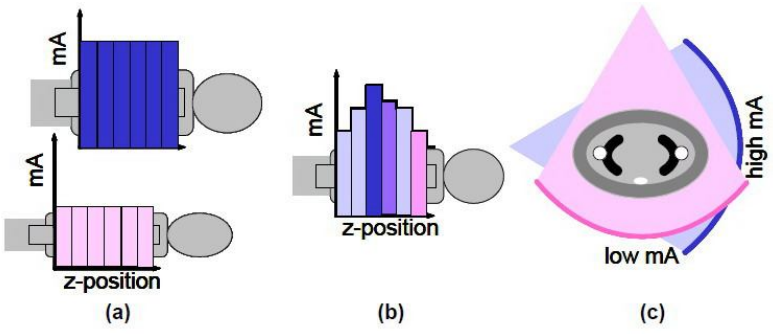

Figure 2.5 Automatic adjustment of tube current to account for (a) overall patient size, (b) attenuation variations along patient's long axis and (c) varying attenuation throughout a rotation

At the second level of automatic mA control, z-axis modulation, the mA is varied on a rotation by rotation basis to account for variations in attenuation along the patient's long axis (z-axis) as shown in Figure 2.5(b). With this type of tube current control, the mean level of image noise within a slice should remain approximately constant for different positions along the z-axis.

At the third level of automatic mA control, angular modulation, the mA is varied during the course of each tube rotation to compensate for the varying attenuation at different angles through the patient as shown in Figure 2.5(c). At some anatomical levels, e.g. the shoulders and pelvis, there is a considerable difference in attenuation between the lateral and anterior-posterior (AP) directions through the patient. The highest tube current is usually required for the lateral projections. Using this technique, a more uniform level of image noise is obtained across the imaged plane, and a given noise level can be achieved at a lower average mA.

2.1.9.1 Angular modulation [10]

The angular-modulation technique was introduced in 1994 for a single–detector row helical CT scanner. This software-based technique modulated tube current on the basis of the measured density of regional structures and the absorption values of the object of interest. A recent refinement of the angular-modulation approach is an online, real-time, anatomy-adapted, attenuation-based tube current modulation technique.

Angular-modulation techniques automatically adjust the tube current for each projection angle to the attenuation of the patient to minimize x-rays in projection angles (antero-posterior or postero-anterior angles are less important than are lateral projections because the former cause less beam attenuation and are associated with less noise) that are less important with regard to reducing the overall noise content as shown in Figure 2.6

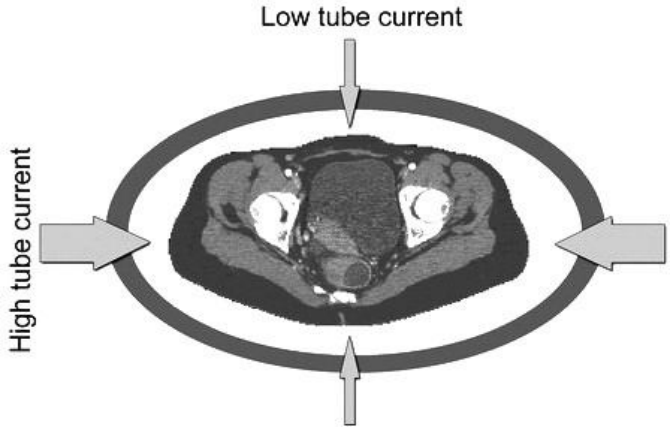

Figure 2.6 Angular modulation of tube current is performed at different projections in the x-y plane within each 360º x-ray tube rotation.

The angular-modulation technique reduces tube current as a function of projection angles for low-attenuation projections (antero-posterior vs lateral projections).This technique calculates the modulation function (an objective image quality parameter) from the online attenuation profile of the patient. The modulation function data are processed and sent to the generator control for tube current modulation with a delay of 180° from the x-ray generation angle. In regions with marked asymmetry, such as the shoulders in CT scanning of chest, where attenuation is substantially less in the antero-posterior direction than in the lateral direction, a reduction in radiation dose of up to 90% can be achieved in the antero-posterior or postero-anterior direction by using the angular-modulation technique. In summary, the technique of angular modulation aids in improving dose efficiency in the x-y axis by reducing radiation exposure in a particular scanning plane.

2.1.9.2 Z-Axis modulation [10]

In the z-axis–modulation technique, the system determines the tube current by using the patient's localizer radiograph projection data and a set of empirically determined noise prediction coefficients by using the reference technique. The projection data from a single localizer radiograph can be used to determine the density, size, and shape information of the patient. The total projection attenuation data of a single localizer radiograph contain the patient's density and size information about the projection area, whereas the amplitude and area of the projection contain the patient's shape information, which gives an estimate of the patient's elliptic asymmetry expressed as an oval ratio at a given z-axis position. The oval ratio is the ratio of the *a* and *b* parameters (lengths of the long and short axes) of an ellipse. The ellipse parameters can be determined for the patient by using the equation for the area of an ellipse. These characteristics of the localizer radiograph predict the amount of x-rays that will reach the detector for a specified technique and determine the image standard deviation due to x-ray noise for a given reconstruction algorithm. The predicted x-ray noise at a given z-axis position for the reference technique (reference noise) is calculated from the projection area and oval ratio from the localizer radiograph by using the polynomial coefficients that were determined from the noise measurements in a set of phantoms representing a wide range of patient sizes and shapes.

Automatic mA adjustment requires prior knowledge of the attenuation characteristics of a patient. The attenuation information to adapt the mA for patient size is obtained from the planning scan projection radiograph (SPR). The SPR information is also used to adjust the mA for each rotation.

2.1.10 Noise Index (NI) [10]

The LightSpeed VCT 64-MDCT scanner provides both longitudinal (*z*-axis) and angular (*x*/*y*-axis) automatic tube current modulation. This modulation adjusts tube current to maintain an operator-defined noise level in the reconstructed images that is predominantly independent of patient size and anatomy. The NI value is

specified by the vendor as approximately equal to the SD in the central region of the image when a uniform (20-cm water) phantom is scanned and reconstructed using the standard reconstruction algorithm. In general, radiation dose is reduced with automatic tube current modulation protocols versus fixed tube current protocols because the tube current is adjusted automatically according to patient size and anatomy.

2.2 Review of Related Literature

Kubo, T., et al [11] reviewed the radiation dose reduction in CT chest. The objective was to present the available data on reducing radiation exposure in routine protocol in CT. There was an argument that radiation exposure in medical imaging had a significant impact on a cancer risk related to radiation exposure. It was reported that exposure to ionizing radiation during diagnostic imaging may be responsible for 0.6-3.2% of malignant tumors in 15 developed countries and CT examinations were responsible for most of the collective patient dose. Second, a large variation in CT scanning parameters was an important factor for dose delivered in chest CT. The ways to reduce the radiation dose were summarized, lowering tube current or tube voltage was the most direct way of achieving dose reduction because tube current was easier to modify and the result was more predictable modification. Their articles assessed the image quality by the visualization of structures in the lung, level of noise, and severity of artifacts with scores and compared between reduced-dose and standard dose CT. The result of the studies indicated that current - time product could be reduced from the typical 200 mAs to 110-140 mAs without significant degradation of image quality. There was an alternative approach to evaluating diagnostic quality of reduced dose CT images particularly detection of nodules in low dose CT. Their studies suggested that current-time product of 50-20 mAs was sufficient for the detection of pulmonary nodules. Most lung cancer screening programs using CT use a tube current-time product in this range. The use of
automatic exposure control in chest CT examinations, 22% radiation dose was reported with angular modulation and 26% was reported with z-axis modulation, without significant changes in image quality.

Kalra, K.M., et al [12] studied sixteen detector row CT of abdomen and pelvis for optimization of Z-Axis modulation technique in 153 patients. The optimal Noise Index required to obtain diagnostically acceptable computed tomographic (CT) image of the abdomen and pelvis with Z- axis modulation was determined. Ninety five patients underwent 16 - section MDCT (GE LightSpeed 4.x) of the abdomen and pelvis with z-axis modulation at Noise Index of 10.5, 11.0, 11.5 and 12.0 with 10-380 mA. Subsequently, 58 patients were scanned at Noise Index of 12.5 and 15.0 with 75-380 mA. The weights of all subjects were recorded, and transverse and antero-posterior diameters were measured. CT images were evaluated for abnormalities and graded for image quality in terms of noise and diagnostic acceptability by using five point scales. Objective noise (noise measurement by quantitative study) in the liver parenchyma were measured. Statistical analyses were performed to determine the

appropriate noise indices and to assess the effect of patient weight and abdominal diameters on image noise and diagnostic acceptability at noise indices. The result showed no statistical significant in subjective image noise or diagnostic acceptability at Noise Index of 10.5-15.0 and objective noise was significantly inferior only at a Noise Index of 15.0. Compared with CT scanning at a 10.5 of Noise Index, CT scanning at 12.5 and 15.0 of Noise Index yielded, 10.0 % and 41.3 % reductions in radiation exposure respectively.

Kanal M. K., et al [13] studied the impact of operator selected image Noise Index and reconstruction slice thickness on patient radiation dose in 64-MDCT. Their objective was to develop a better understanding of the complex interrelationship between image noise, reconstruction slice thickness, and patient radiation dose on 64-MDCT scanner that use automated tube current modulation. Better understand the theoretical and actual (measured) relationship between Noise Index and radiation dose at a given reconstruction slice thickness were expected by reviewed physics theory and performed phantom dose measurement while altering operator-selectable image noise and reconstruction slice thickness. The radiation dose was affected by Noise Index value selected and Noise Index also varies with reconstruction slice thickness. A spreadsheet and graph were created to help operator understand the trade-off when trying to minimize dose and optimize image noise. Because the delivery dose was affected by Noise Index value selected and Noise Index also varies with reconstruction slice thickness, the appropriate Noise Index can have a major impact on delivery dose. The Noise Index table may be used to determine how the dose changes as a function of Noise Index at a constant reconstruction slice thickness. Noise Index values were read down the columns and matched up for each isodose row with relative dose column and dose difference (%) column values to obtain the difference in dose caused by a specific change in Noise Index.

CHAPTER III

RESEARCH METHODOLOGY

3.1 Research design

This study is an experimental prospective study research.

3.2 Research design model

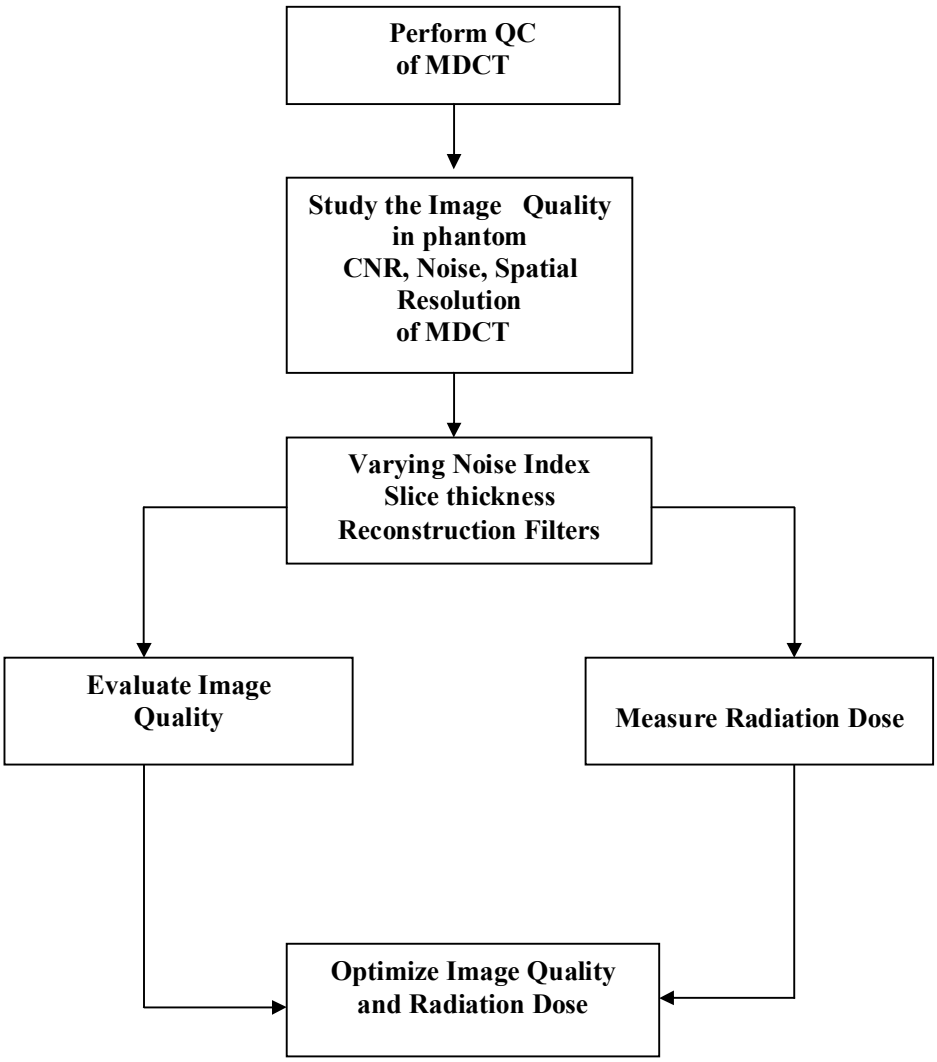

3.3 Conceptual framework

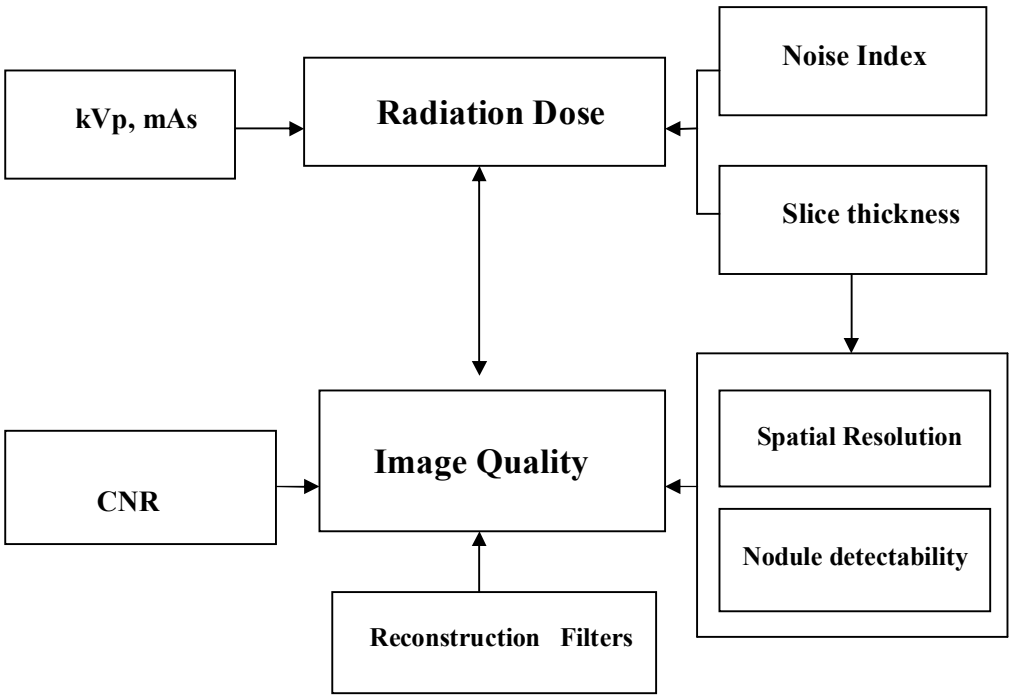

3.4. Research question

What are the optimal Noise Index and image quality for radiation dose reduction in 64-MDCT using tube current modulation and two phantom sizes?

3.5 Materials

3.5.1 CT scanner, 64 –MDCT

The 64-MDCT scanner from manufacturer GE Medical System, Model VCT LightSpeed at the Department of Diagnostic Radiology, Rajavithi Hospital has been installed in 2007 as shown in Figure3.1

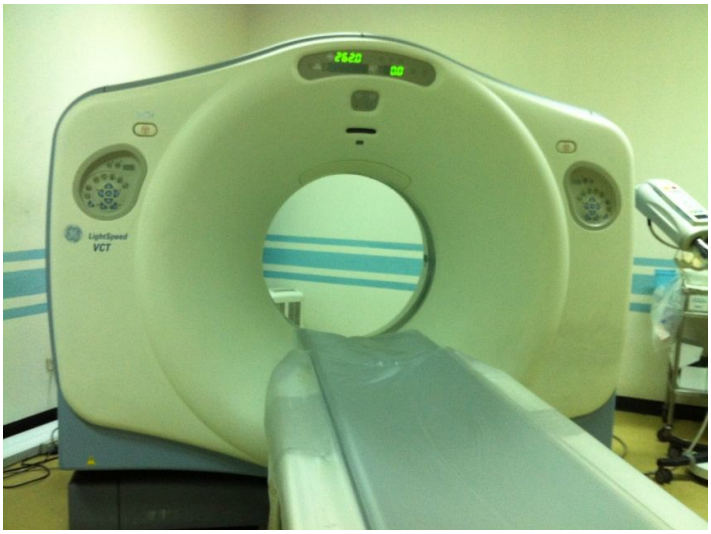

Figure 3.1 64 –MDCT GE VCT LightSpeed

3.5.2 Lung man chest phantom

Lung Man Chest Phantom (Kyoto Kagaku Co. Ltd.) is designed and constructed commercially to simulate standard human chest. The inner components consist of mediastinum, pulmonary vasculature and an abdomen block. The phantom is an accurate life-size anatomical model of a human torso. The standard size is 17 cm chest thickness as the standard man at 70 kg and the large size is 24 cm chest thickness as the man at 90 kg. The thickness of the chest wall is based on measurement of clinical data. The soft tissue substitute material and synthetic bones have the x-ray absorption very close to those of human tissues as shown in Figure3.2

Figure 3.2 Lung Man Chest phantom

3.5.3 Simulated lung nodules

Simulated lung nodules were inserted in Lung man chest phantom. There are 5 sizes of simulated circular nodules at 12, 10, 8, 5 and 3 mm in diameters. The CT number of each nodule had been measured at approximately +100 as shown in Figure3.3

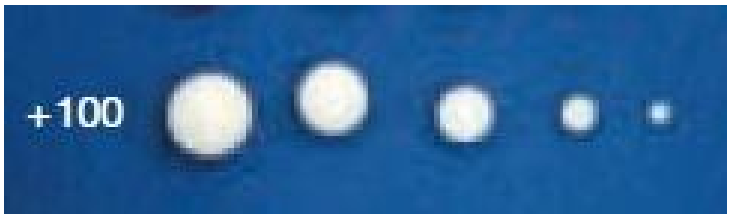

Figure 3.3 Simulated circular lung nodules of 12, 10, 8, 5, and 3 mm diameter

3.5.4 Catphan phantom ® 600

The **Catphan phantom ® 600 (The Phantom Laboratory, New York, NY, USA)** contains five modules. The phantom in Figure 3.4 can be assessed for both mechanical integrity and image quality of CT scanner. It has the module design, and within each module, different image quality parameters can be evaluated. Each module is illustrated in Figure 3.4

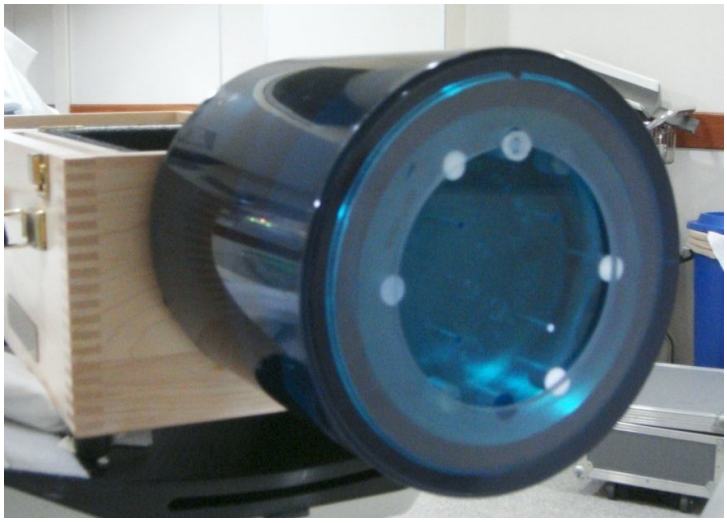

Figure 3.4 Catphan phantom ® 600

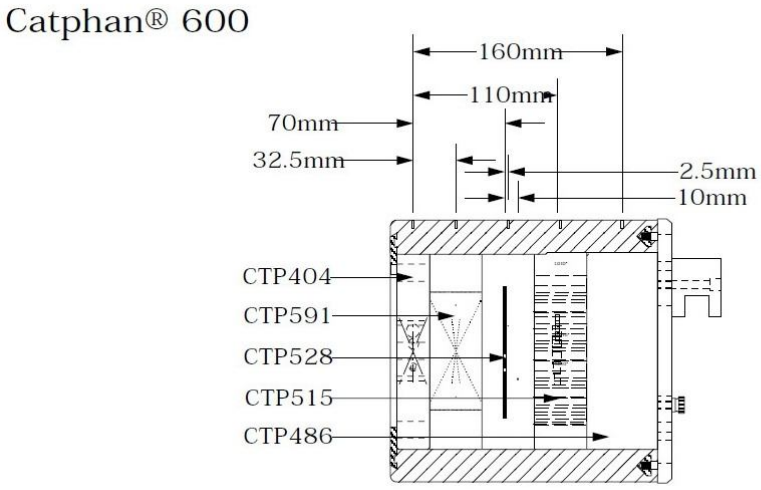

Figure 3.5 Diagram of Catphan phantom ® 600 with dimensions

The Catphan phantom ®600 is designed so all test sections can be located by precisely indexing the table from center of section 1 (CTP404) to the center of each subsequence test module. The indexing distance from section 1 of Catphan phantom® 600 test module locations are:

Module Purpose of Study	Distance from section 1 center (mm)
CTP404, Slice width, sensitometry and pixel size	
CTP591, Bead geometry	32.5
CTP528, 21 line pair high resolution	70
CTP528, Point source	80
CTP515, Subslice and supra-slice low contrast	110
CTP486, Solid image uniformity module	150

3.5.5 PMMA phantom

The CT phantoms were used to perform QC for CT system. Two phantom diameters of 16 cm, represent head and 32 cm represent body were used to determine CT Dose Index. CTDI phantom is made of PMMA. The 10 cm length CT pencil ionization chamber was placed in each hole of the phantom as shown in figure 3.6.

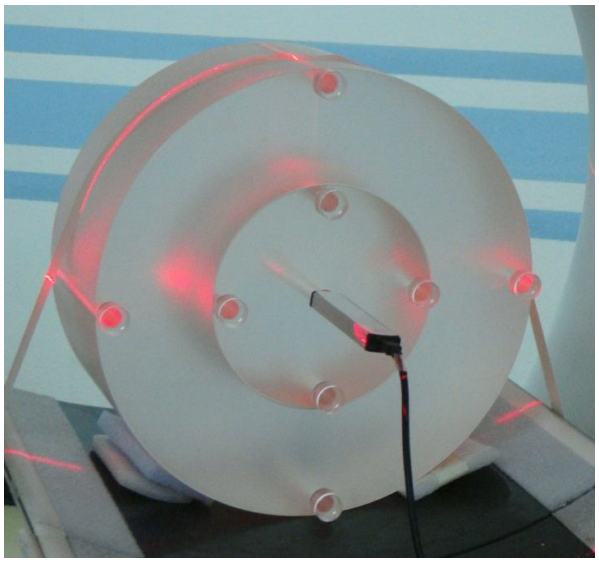

Figure 3.6 PMMA phantoms with chamber insert at center

3.5.6 Radiation detector - Pencil ion chamber

The RaySafe Xi CT detector is a hybrid ion chamber combined with electronics into one unit measure both temperature and pressure to actively compensate for this dependency (Figure3.7). The temperature is actually measured inside the ion chamber giving very precise compensations both with and without a CT phantom. With no baseline drift, this carbon fiber ion chamber is ready to use within one minute.

Figure 3.7 The Ray Safe Xi CT detector with reader (http://www.raysafe.com)

3.6 Methods

3.6.1 Perform the quality control of 64 –MDCT GE VCT LightSpeed

The quality control of 64 –MDCT GE VCT LightSpeed was performed by following the IAEA Human Health No. 19 which includes Radiation safety, Mechanical accuracy, Dosimetry of CTDI in air, CTDI in phantom and imaging performance.

3.6.2 Verification of $CTDI_{vol}$

The $CTDI_{vol}$ displayed on the monitor of the console of the scanner, must be verified to make confidence in using these values prior all studies. The procedures are as followings:

- Pencil ionization chamber was inserted in the 16 and 32 diameter of PMMA phantom. The positioning of the phantom and chamber were investigated to avoid the alignment errors.
- Computed Tomography Dose Index (CTDI) was recorded from monitor and from Ray Safe detector readout, where the chamber was inserted at the center

and the peripheral positions in the phantom. The phantom was scanned three times for each kVp setting.

- The acquisition parameters were 5.0 mm collimation, 1.0 sec rotation time, and effective mAs 100. The $CTDI_{vol}$ that initial displayed on CT console were recorded after running the scan.
- The data shown on dosimeter was recorded for the calculation of $CTDI_{vol}$ and compared to the displayed values on CT monitor and the ImPACTSCAN values for each kVp.

3.6.3 Study of image quality in Catphan phantom

The Catphan® 600 was mounted on the phantom holder and placed at the center on the CT gantry. The CTP515 (subslice and supra-slice low contrast) was used to study the low contrast resolution, the CTP528 (21 line pair resolution) was used to study the high contrast resolution and the CTP486 (Solid image uniformity module) was used to study the uniformity and image noise.

a) High contrast resolution

Select the CTP 528 module containing the high resolution test objects, select the head technique, set the four size slice thickness 0.625, 1.25, 2.5, and 5.0 mm and four types filters STD, CHEST, LUNG, BONE+.

Perform a single transverse scan with setting parameters 120 kVp, 300 mA, 1 sec rotation time, small head, DFOV 250 mm. Select the area containing the high resolution test objects and zoom as necessary. Select appropriate window and level for the best visualization of the test objects. Record the smallest test object visualized on the monitor.

b) Low contrast detectability

Select the CTP515 module containing subslice and supra-slice low contrast. Set four sizes of slice thickness 0.625, 1.25, 2.5, and 5.0 mm and four types of reconstruction filters STD, CHEST, LUNG, and BONE+.

Perform a single transverse scan utilizing the same technique as high resolution. Select appropriate window and level for the best visualization of the test objects. Record the smallest test object visualized on the monitor.

c) Image noise

Select the CTP486 module containing solid image uniformity. Select the head technique, small head, 120 kVp, 300 mA, 1 sec rotation time, and slice collimation 5 mm. Set four types of filters. Perform a single transverse scan. The circular ROI area 400 mm^2 was placed at the center of the phantom image as shown in Figure 3.8.

Record the standard deviation of CT number. The noise was evaluated when using the various types of reconstruction filters.

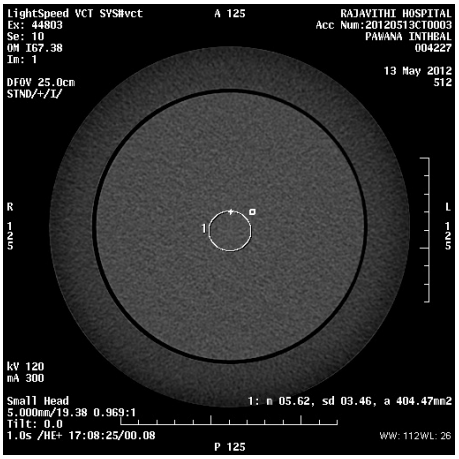

Figure 3.8 Measurement of Noise

3.6.4 Lung man chest phantom study

- The five sizes of simulated lung lesions were inserted within the Lung Man Chest phantom. The two sizes of Lung man chest phantom were scanned with variable parameters such as Noise Index, slice thickness, and reconstruction filter. The exposure technique for scanned the phantom were set by following parameters

kVp	120
Rotation time (s)	0.5
Pitch	0.981:1
Scan length (mm)	347.5
Location	Apex of lung to lower costal margin
SFOV	Medium
DFOV (mm)	400
Min mA-Max mA	75-380

- The $CTDI_{vol}$ and DLP were recorded from the CT console.
- The image quality was evaluated in three major characteristics of contrast to noise ratio, the nodule detectability and spatial resolution

a) Contrast to noise ratio (CNR)

The contrast to noise ratio were determined by placing the 2 circulars ROIs of equal area within the nodules and the background at the same slice as shown in Figure 3.9 with WW 1200, WL -600. The CT number within the ROI were recorded in order to calculated the contrast to noise ratio (CNR). CNR was defined as

$\boldsymbol{CNR = (CT_N - CT_B)/SD_B}$ where CT_N is the CT number of nodule, CT_B is the CT number of background and SD_B is standard deviation of background.

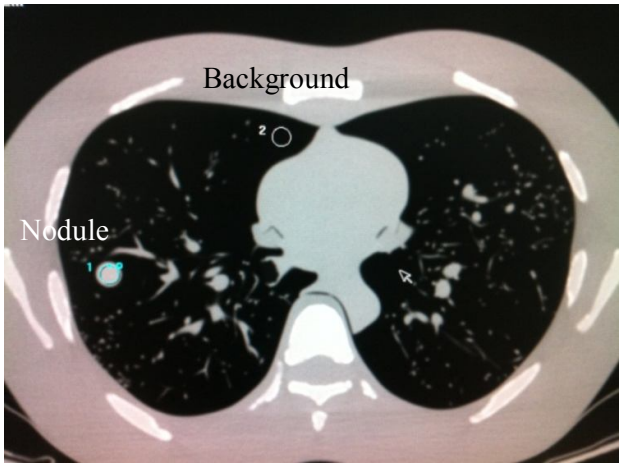

Figure 3.9 Measurement the CT number of nodule and background

To determine the percent of CNR, CNR was compared to those within the group of same slice thickness but varying filters and Noise Index. The CNR of different parameters in the group were normalized at Noise Index 10 at STD filters. The percent of CNR define as:

$$\% \text{ CNR} = \frac{\text{CNR x 100}}{\text{CNR } (NI_{10,\ STD})}$$

b) The nodule detectability

The nodule detectability was scored by two observers (radiological technologists with experience of more than 10 years in CT scan). They were blinded to the scanning techniques. The images will be displayed in a random order for each observer. Adjusting the window with lung window and soft tissue window until the best visualization occurs. The observers independently graded the image for nodule detectability by using a five-point scale: Score 1 means unacceptable; score 2, poor; score 3, acceptable; score 4, good; and score 5, excellent.

c) Spatial resolution

All of the Lung Man Chest phantom images were reviewed. The spatial resolution was evaluated by the best visualized of the smallest size of nodule with various parameters. Noise Index, slice thickness and reconstruction filters were the factors affecting the image quality.

3.6.5 Optimization the radiation dose and image quality

The correlation of radiation dose and the image quality was evaluated to obtain the optimal protocols for CT chest with the appropriate Noise Index according to the slice thickness and reconstruction filters by consider the lowest $CTDI_{vol}$ while maintain the acceptable the image quality.

3.7 Data analysis

The quantitative image quality was assessed from contrast to noise ratio (CNR) and the spatial resolution (size of smallest detected nodule). CNR was determined by using excel software to assess the mean, minimum, maximum values respectively.

The qualitative image quality was assessed by two radiological technologists who have experience in CT more than 10 years. The five point scale was used to evaluate the nodules detectability as shown in table 1.1. The agreement of image quality scored was assessed by calculating weighted Kappa of the variation of filters, slice thickness and Noise Index for two sizes of phantom.

Table 3.1 The five point scale of image quality

Score	Image Quality	Detail
1	Unacceptable	Visualized partly of 10 mm, completely 12 mm in diameter
2	Poor	Visualized partly of 8 mm completely 10 mm in diameter
3	Acceptable	Visualized partly of 5 mm completely 8 mm in diameter
4	Good	Visualized partly 3 mm completely 5 mm in diameter
5	Excellent	Visualize completely 3 mm in diameter

3.8 Sample size determination

This is an experimental study. There are variable setting parameters. The sample size between two related groups and calculated are;

- Five values of Noise Index
- Four sizes of slice thickness
- Four types of filter
- Two sizes of phantom

3.9 Outcome measurement

Variable: Independent variables = Noise Index, Reconstruction filter, Slice thickness
Dependent variables = CNR, Nodules detectability, Radiation Dose

3.10 Statistical analysis

3.10.1 Descriptive statistics as mean, minimum, maximum by using Excel program.

3.10.2 Weighted kappa for inter observer reliability was to evaluate qualitative image quality analysis form *www.medcalc.org/manual/kappa.php*

3.11 Expected benefits

3.11.1 An optimal Noise Index for optimization of image quality of chest at the lowest radiation dose.

3.11.2.The optimal protocols benefit to patient and increase confidence in MDCT chest nodule detectability.

3.12 Ethical consideration

This study was performed in phantom to evaluate the radiation dose and image quality of chest MDCT. The ethical had been approved by the Ethics Committee, Faculty of Medicine, Chulalongkorn University and Rajavithi hospital.

CHAPTER IV

RESULT

4.1 Quality control of the CT scanner: GE VCT LightSpeed

The quality control of CT scanner was performed following IAEA Human Health No.19 **[14]** and ImPACTSCAN Information Leaflet **[15]** including the test of electromechanical component, image quality and radiation dose. Table 4.1 and Appendix B, the detail of quality control of CT scanner are shown with the summarized report of CT scanner performance test.

Table 4.1 Report of CT system performance

Location	CT room, Department of Radiology, Rajavithi Hospital
Date	May 13, 2012
Manufacturer	GE Medical
Model	VCT LightSpeed

Pass	Scan Localization Light Accuracy
Pass	Alignment of Table to Gantry
Pass	Table Increment Accuracy
Pass	Slice Increment Accuracy
Pass	Gantry Tilt
Pass	CT No. Position Dependence and SNR
Pass	Reproducibility of CT Number
Pass	mAs Linearity
Pass	Linearity of CT Numbers
Pass	Image Uniformity
Pass	High Contrast Resolution
Pass	Low Contrast Resolution
Pass	Radiation Profile Width

4.2 Verification of Computed Tomography Dose Index (CTDI)

4.2.1 $CTDI_{100}$ in air

Measure the $CTDI_{100}$ in air using head and body protocols and the 100 mm pencil chamber is set at the isocenter of the CT gantry. The scan parameter is 100 mA tube current, 1 sec scan time for all measurements at kilovoltage setting of 80, 100, 120, and 140.The measured CTDI was compared with ImPACTSCAN values for each kVp. The results of CTDI in air are shown in Table 4.2

Table 4.2 The measured $CTDI_{100}$ in air for head and body protocols compared with ImPACTSCAN values for each kVp.

kVp	$CTDI_{100}$ in air (mGy/100mAs)					
	Head		%diff	Body		%diff
	Measured	ImPACTSCAN		Measured	ImPACTSCAN	
80	12.27	14.8	17.09	12.27	14.8	17.09
100	20.01	24.2	17.41	20.01	24.2	17.41
120	28.78	35.0	17.70	28.78	35.0	17.70
140	38.39	46.9	18.22	38.39	46.9	18.22

4.2.2 $CTDI_{100}$ in head phantom compared with ImPACTSCAN values for 120 kVp

The $CTDI_{100}$ in head phantom was determined by using a 100 mm pencil ionization chamber placed in each hole of 16 cm diameter PMMA phantom at the isocenter of the CT gantry. The scan parameters were 100 mA, 1 sec scan time, small head 250 mm FOV and 5 mm collimation setting for all measurement at 120 kVp. The results of CTDI in air are shown in Table 4.3

Table 4.3 The measured $CTDI_{100}$ in the head phantom compared with ImPACTSCAN values for 120 kVp.

kVp	$CTDI_{100}$ in head phantom (mGy)									
	At center		%diff	At periphery						%diff
	Measured	ImPACT SCAN		North	East	South	West	Average	ImPACT SCAN	
120	18.45	22.40	17.63	18.60	18.56	18.76	18.62	18.63	22.50	17.20

4.2.3 $CTDI_{100}$ in body phantom compared with ImPACTSCAN values for 120 kVp

The $CTDI_{100}$ in body phantom was determined by using a 100 mm pencil ionization chamber placed in each hole of 16 cm diameter PMMA phantom at the isocenter of the CT bore. The scan parameters were 100 mA, 1 sec scan time, large body 360 mm FOV and 5 mm collimation setting for all measurement at 120 kVp. The results of CTDI in air are shown in Table 4.4

Table 4.4 The measured $CTDI_{100}$ in the body phantom compared with ImPACTSCAN values for 120 kVp

kVp	$CTDI_{100}$ in body phantom (mGy)									
	At center		%diff	At periphery						%diff
	Measured	ImPACT SCAN		North	East	South	West	Average	ImPACT SCAN	
120	5.52	6.50	15.07	10.77	11.05	9.79	11.04	10.66	13.10	18.62

4.2.4 $CTDI_{vol}$ of monitor and calculated $CTDI_w$

The $CTDI_w$ was determined by using 16 and 32 cm diameter PMMA cylindrical phantom for head and body phantoms. The scan techniques were 120 kVp, 100 mA, 1sec, STD filter for head and body protocol. The displayed $CTDI_{vol}$ on CT monitor were recorded to compare with the calculated values and the ImPACTSCAN values as shown in Table 4.5 for $CTDI_{vol}$ in head phantom and Table 4.6 for $CTDI_{vol}$ in body phantom.

Table 4.5 $CTDI_{vol}$ of monitor and $CTDI_w$ using head technique 120 kVp mA 100, 1 sec scan time, collimation 5 mm and STD filter.

kVp	$CTDI_{vol}$ (mGy) in head phantom				
	Calculated	Monitor	% difference (monitor and calculated)	ImPACTSCAN	%difference (monitor and ImPACTSCAN)
120	**18.57**	**18.33**	**-1.31**	**19.81**	**-7.47**

Table 4.6 $CTDI_{vol}$ of monitor and $CTDI_w$ using body technique 120 kVp, mA 100, 1 sec scan time, collimation 5 mm and STD filter.

kVp	$CTDI_{vol}$ (mGy) in body phantom				
	Calculated	Monitor	% difference (monitor and calculated)	ImPACTSCAN	%difference (monitor and ImPACTSCAN)
120	**8.95**	**8.39**	**-6.67**	**9.15**	**-8.31**

4.3 Characteristic of image quality in Catphan phantom

The Catphan phantom ® 600 was used to study the image quality which included the three characteristics, high contrast resolution, low contrast resolution and noise. The CTP515 (Subslice and supra-slice low contrast) was used to study the low contrast resolution, the CTP528 (21 line pair resolution) was used to study the high contrast resolution and the CTP486 (Solid image uniformity module) was used to study the noise.

4.3.1 High contrast resolution

The scanning parameters of head technique 120 kVp, 300 mA, 1 sec rotation time, small head, DFOV 250 mm. were used by varying the slice thickness and filters. Appropriate window and level were adjusted for the best visualization of the test objects. The result of lp/cm and the gap size (cm) were shown in table 4.7

Table 4.7 High contrast resolution study

Slice Thickness (mm)	Filters							
	STD		CHEST		LUNG		BONE+	
	lp/cm	Gap size (cm)	lp/cm	Gap size (cm)	lp/cm	Gap size (cm)	lp/cm	Gap size (cm)
5	7	0.071	7	0.071	5	0.100	11	0.045
2.5	7	0.071	7	0.071	8	0.063	11	0.045
1.25	7	0.071	7	0.071	8	0.063	11	0.045
0.625	7	0.071	7	0.071	8	0.063	11	0.045

Table 4.7 shows the high contrast resolution with variation of slice thickness and filters. The results indicate the BONE+ filter provide the highest contrast resolution for all slice thickness. There are no difference between the STD, CHEST, LUNG and BONE+ filters at 0.625-2.5 mm slice thickness except at 5 mm slice thickness, the LUNG filter give a poor high contrast resolution.

4.3.2 Low contrast detectability

The scanning parameter of head technique 120 kVp, 300 mA, 1 sec rotation time, small head, DFOV 250 mm. were used with various filters. The window and level (WW 60, WL 60) were adjusted with the same contrast for every images. The amount of hole and percent contrast perform at supra-slice and sub-slice are shown in Table 4.8 and 4.9

Table 4.8 Low contrast detectability at supra-slice

	Filers	Nominal target contrast level					
		1%		0.50%		0.3%	
		Hole	% contrast	Hole	% contrast	Hole	% contrast
Supraslice	**STD**	9	2	9	1	6	1.5
	LUNG	9	2	3	4	-	-
	CHEST	9	2	9	1	6	1.5
	BONE+	6	5	6	2.5	-	-

Table 4.9 Low contrast detectability at sub-slice

	Filters	Nominal target contrast level					
		7 mm length		5mm length		3 mm length	
		Hole	% contrast	Hole	% contrast	Hole	% contrast
Subslice	**STD**	4	7	4	5	4	3
	LUNG	4	7	2	2.5	-	-
	CHEST	4	7	4	5	3	2.25
	BONE+	4	7	3	3.75	2	1.5

Table4.8 and 4.9 show the low contrast detectability at supra-slice and subslice. At supra-slice the STD, CHEST, and LUNG filters were applied for the low contrast detectability of 2 mm at 1% contrast level whereas the BONE+ filter obtained 5 mm 1% contrast level. The LUNG filter obtained 4 mm at 0.50% contrast level, however, the LUNG and BONE+ filters cannot identify the amount of hole at 0.3 % contrast level.

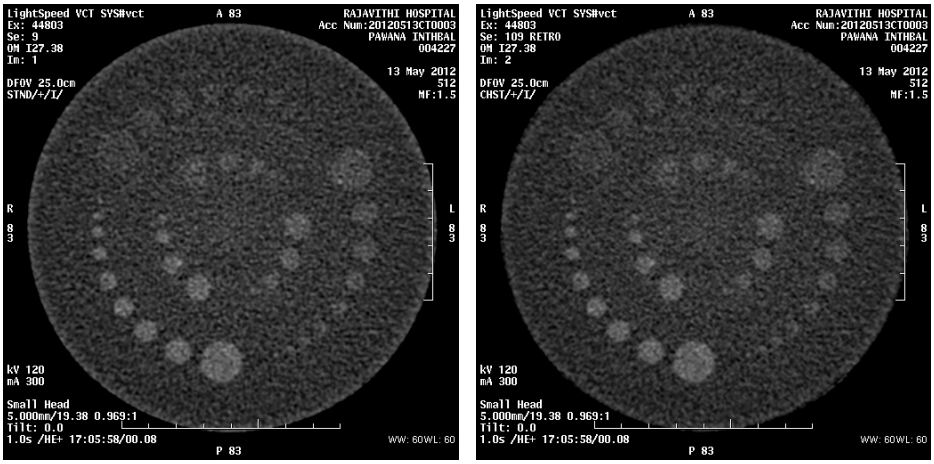

STD CHEST

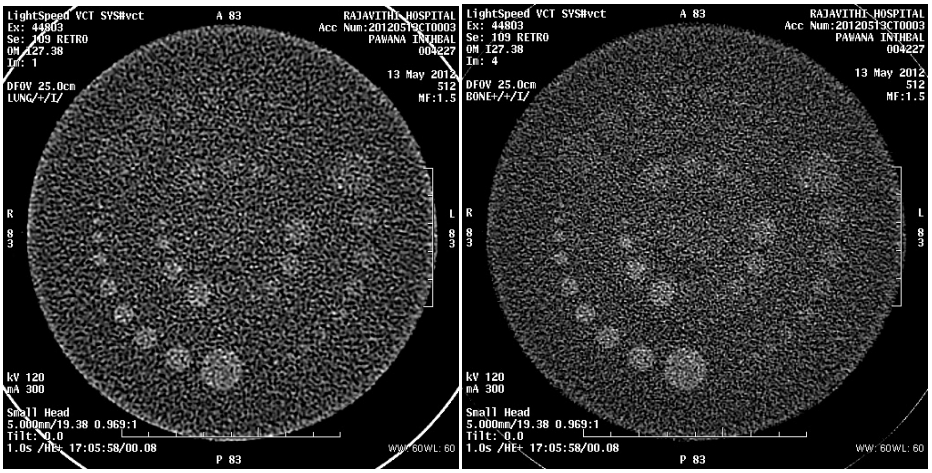

LUNG BONE+

Figure 4.1 Low contrast detectability obtained from various filters, STD, CHEST, LUNG and BONE+ filters.

Figure 4.1 shows the low contrast detectability obtained from various filters, STD, CHEST, LUNG and BONE+ filters.

4.3.3 Noise

The scanning parameter of head technique 120 kVp, 300 mA, 1 sec rotation time, 5 mm collimation, small head, DFOV 250 mm. were used with various filters. The circular ROI area 400 mm^2 was placed at the center of the phantom to determine the noise. The standard deviation of CT number is an indicator of the noise level in the image. The standard deviation was normalized with the STD filter as shown in Table 4.10

Table 4.10 The standard deviation of CT number with variation of filters.

Filter	S.D of CT number (HU)	Normalized of S.D
STD	3.46	0.000
CHEST	3.54	0.004
LUNG	15.59	0.701
BONE+	20.76	1.000

Table 4.10 shows the standard deviation of CT number with various filters. The highest noise level obtained from the BONE+, LUNG, CHEST and STD filters respectively.

4.4 Radiation dose

$CTDI_{vol}$ and DLP were recorded from monitor displayed with scanning the 2 thicknesses of Lung Man Chest phantom using scanning parameters 120 kVp, 0.5 sec rotation time, 0.981:1 pitch factor, 75-380 min- max mA value, scan length 347.5 mm, location: apex of lung to lower costal margin, medium SFOV and 40 cm DFOV by vary the noise index, slice thickness, and reconstruction filters. The data was shown in Table 4.11- 4.18

Table 4.11 $CTDI_{vol}$, DLP for standard size Lung Man chest phantom with STD filter.

Filter	Slice thickness (mm)	Noise Index	$CTDI_{vol}$ (mGy)	DLP (mGy.cm)
STD	0.625	10	16.52	650.53
STD	0.625	12.5	16.52	650.53
STD	0.625	15	16.14	635.80
STD	0.625	17.5	15.16	597.12
STD	0.625	20	13.57	534.29
STD	1.25	10	16.52	650.53
STD	1.25	12.5	16.37	644.71
STD	1.25	15	15.33	630.79
STD	1.25	17.5	13.61	535.77
STD	1.25	20	11.25	443.04
STD	2.5	10	15.46	608.76
STD	2.5	12.5	12.75	502.28
STD	2.5	15	9.54	375.88
STD	2.5	17.5	7.04	277.27
STD	2.5	20	5.46	214.96
STD	5.0	10	9.95	394.06
STD	5.0	12.5	6.45	255.38
STD	5.0	15	4.65	184.34
STD	5.0	17.5	3.73	147.99
STD	5.0	20	3.78	133.86

Table 4.12 $CTDI_{vol}$, DLP for standard size Lung Man chest phantom with BONE+ filter.

Filter	Slice thickness (mm)	Noise Index	$CTDI_{vol}$ (mGy)	DLP (mGy.cm)
BONE+	0.625	10	16.52	650.53
BONE+	0.625	12.5	16.52	650.53
BONE+	0.625	15	16.14	635.63
BONE+	0.625	17.5	15.15	596.66
BONE+	0.625	20	13.44	529.04
BONE+	1.25	10	16.47	650.53
BONE+	1.25	12.5	16.37	644.54
BONE+	1.25	15	16.52	630.45
BONE+	1.25	17.5	13.47	530.29
BONE+	1.25	20	11.10	437.05
BONE+	2.5	10	15.45	608.47
BONE+	2.5	12.5	12.60	496.34
BONE+	2.5	15	9.38	369.43
BONE+	2.5	17.5	6.92	272.43
BONE+	2.5	20	5.36	211.31
BONE+	5.0	10	9.78	387.69
BONE+	5.0	12.5	6.33	251.07
BONE+	5.0	15	4.57	180.95
BONE+	5.0	17.5	3.68	146.03
BONE+	5.0	20	3.37	133.52

Table 4.13 $CTDI_{vol}$, DLP for standard size Lung Man chest phantom with CHEST filter.

Filter	Slice thickness (mm)	Noise Index	$CTDI_{vol}$ (mGy)	DLP (mGy.cm)
CHEST	0.625	10	16.52	650.53
CHEST	0.625	12.5	16.52	650.53
CHEST	0.625	15.0	16.10	634.09
CHEST	0.625	17.5	15.05	592.84
CHEST	0.625	20	13.37	526.47
CHEST	1.25	10	16.52	650.53
CHEST	1.25	12.5	16.33	643.00
CHEST	1.25	15	15.23	599.68
CHEST	1.25	17.5	13.40	527.72
CHEST	1.25	20	11.12	437.85
CHEST	2.5	10	15.37	605.27
CHEST	2.5	12.5	12.55	494.06
CHEST	2.5	15	9.36	368.75
CHEST	2.5	17.5	6.91	271.91
CHEST	2.5	20	5.36	211.25
CHEST	5.0	10	9.81	388.60
CHEST	5.0	12.5	6.32	250.32
CHEST	5.0	15	4.57	181.18
CHEST	5.0	17.5	3.70	146.61
CHEST	5.0	20	3.36	133.17

Table 4.14 $CTDI_{vol}$, DLP for standard size Lung Man chest phantom with LUNG filter.

Filter	Slice thickness (mm)	Noise Index	$CTDI_{vol}$ (mGy)	DLP (mGy.cm)
LUNG	0.625	10	16.52	650.53
LUNG	0.625	12.5	16.52	650.53
LUNG	0.625	15.0	16.19	637.69
LUNG	0.625	17.5	15.22	599.34
LUNG	0.625	20	13.36	538.23
LUNG	1.25	10	16.52	650.53
LUNG	1.25	12.5	16.43	646.93
LUNG	1.25	15	15.39	606.19
LUNG	1.25	17.5	13.70	539.42
LUNG	1.25	20	11.44	450.29
LUNG	2.5	10	15.52	611.32
LUNG	2.5	12.5	12.85	506.10
LUNG	2.5	15	9.69	381.53
LUNG	2.5	17.5	7.14	281.21
LUNG	2.5	20	5.53	217.87
LUNG	5.0	10	10.08	399.63
LUNG	5.0	12.5	6.54	259.11
LUNG	5.0	15	4.70	181.40
LUNG	5.0	17.5	3.76	149.19
LUNG	5.0	20	3.39	134.20

Table 4.15 $CTDI_{vol}$, DLP for large size of Lung Man chest phantom with STD filter.

Filter	Slice thickness (mm)	Noise Index	$CTDI_{vol}$ (mGy)	DLP (mGy.cm)
STD (L)	0.625	10	16.52	650.53
STD (L)	0.625	12.5	16.52	650.53
STD (L)	0.625	15	16.52	650.53
STD (L)	0.625	17.5	16.52	650.53
STD (L)	0.625	20	16.52	650.53
STD (L)	1.25	10	16.52	650.53
STD (L)	1.25	12.5	16.52	650.53
STD (L)	1.25	15	16.52	650.53
STD (L)	1.25	17.5	16.52	650.53
STD (L)	1.25	20	16.52	650.53
STD (L)	2.5	10	16.52	650.53
STD (L)	2.5	12.5	16.52	650.53
STD (L)	2.5	15	16.47	648.47
STD (L)	2.5	17.5	15.75	620.51
STD (L)	2.5	20	13.68	538.51
STD (L)	5.0	10	16.50	653.97
STD (L)	5.0	12.5	15.19	601.94
STD (L)	5.0	15	11.88	470.66
STD(L)	5.0	17.5	9.21	365.12
STD (L)	5.0	20	7.05	279.32

(L) – Large size of Lung Man Chest phantom

Table 4.16 $CTDI_{vol}$, DLP for large size Lung Man chest phantom with BONE+ filter.

Filter	Slice thickness (mm)	Noise Index	$CTDI_{vol}$ (mGy)	DLP (mGy.cm)
BONE+(L)	0.625	10	16.52	650.53
BONE+(L)	0.625	12.5	16.52	650.53
BONE+(L)	0.625	15	16.52	650.53
BONE+(L)	0.625	17.5	16.52	650.53
BONE+(L)	0.625	20	16.52	650.53
BONE+(L)	1.25	10	16.52	650.53
BONE+(L)	1.25	12.5	16.52	650.53
BONE+(L)	1.25	15	16.52	650.53
BONE+(L)	1.25	17.5	16.52	650.53
BONE+(L)	1.25	20	16.52	650.53
BONE+(L)	2.5	10	16.52	650.53
BONE+(L)	2.5	12.5	16.52	650.53
BONE+(L)	2.5	15	16.47	648.47
BONE+(L)	2.5	17.5	15.47	620.51
BONE+(L)	2.5	20	13.71	538.51
BONE+(L)	5.0	10	16.51	653.97
BONE+(L)	5.0	12.5	15.22	601.94
BONE+(L)	5.0	15	11.99	470.66
BONE+(L)	5.0	17.5	9.27	365.12
BONE+(L)	5.0	20	7.10	279.32

(L) – Large size of Lung Man Chest phantom

Table 4.17 $CTDI_{vol}$, DLP for large size Lung Man Chest phantom with CHEST filter.

Filter	Slice thickness (mm)	Noise Index	$CTDI_{vol}$ (mGy)	DLP (mGy.cm)
CHEST (L)	0.625	10	16.52	650.53
CHEST (L)	0.625	12.5	16.52	650.53
CHEST (L)	0.625	15	16.52	650.53
CHEST (L)	0.625	17.5	16.52	650.53
CHEST (L)	0.625	20	16.52	650.53
CHEST (L)	1.25	10	16.52	650.53
CHEST (L)	1.25	12.5	16.52	650.53
CHEST (L)	1.25	15	16.52	650.53
CHEST (L)	1.25	17.5	16.52	650.53
CHEST (L)	1.25	20	16.52	650.53
CHEST (L)	2.5	10	16.52	650.53
CHEST (L)	2.5	12.5	16.52	650.53
CHEST (L)	2.5	15	16.45	647.96
CHEST (L)	2.5	17.5	15.65	616.46
CHEST (L)	2.5	20	13.52	532.35
CHEST (L)	5.0	10	16.49	653.45
CHEST (L)	5.0	12.5	15.07	597.35
CHEST (L)	5.0	15	17.71	464.35
CHEST (L)	5.0	17.5	9.04	358.17
CHEST (L)	5.0	20	6.91	273.81

(L) – Large size of Lung Man Chest phantom

Table 4.18 $CTDI_{vol}$, DLP for large size Lung Man chest phantom with LUNG filter.

Filter	Slice thickness (mm)	Noise Index	$CTDI_{vol}$ (mGy)	DLP (mGy.cm)
LUNG (L)	0.625	10	16.52	650.53
LUNG (L)	0.625	12.5	16.52	650.53
LUNG (L)	0.625	15	16.52	650.53
LUNG (L)	0.625	17.5	16.52	650.53
LUNG (L)	0.625	20	16.52	650.53
LUNG (L)	1.25	10	16.52	650.53
LUNG (L)	1.25	12.5	16.52	650.53
LUNG (L)	1.25	15	16.52	650.53
LUNG (L)	1.25	17.5	16.52	650.53
LUNG (L)	1.25	20	16.52	650.53
LUNG (L)	2.5	10	16.52	650.53
LUNG (L)	2.5	12.5	16.52	650.53
LUNG (L)	2.5	15	16.47	648.47
LUNG (L)	2.5	17.5	15.74	620.06
LUNG (L)	2.5	20	13.69	539.19
LUNG (L)	5.0	10	16.50	653.97
LUNG (L)	5.0	12.5	15.20	602.28
LUNG (L)	5.0	15	11.95	473.76
LUNG (L)	5.0	17.5	9.25	366.72
LUNG (L)	5.0	20	7.06	280.12

(L) – Large size of Lung Man Chest phantom

The mean values $CTDI_{vol}$ from STD, BONE+, CHEST, and LUNG filters of standard size phantom were plotted when vary Noise Index from 10-20 and four sizes of slice thickness 0.625, 1.25, 2.5, and 5.0 mm as shown in figure 4.2

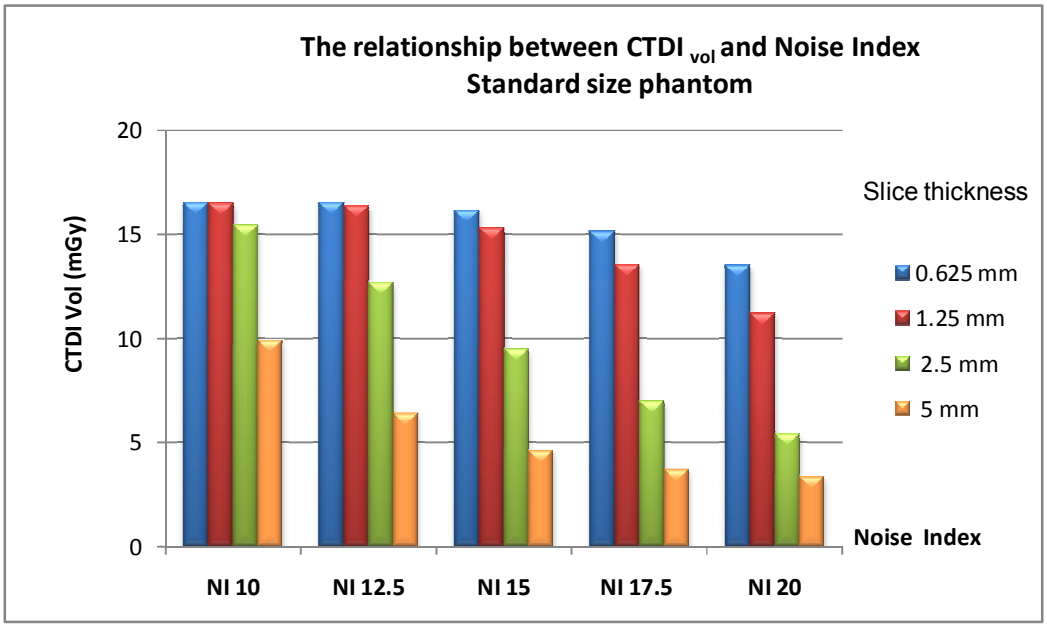

Figure 4.2 The relationship between the average $CTDI_{vol}$ and Noise Index at different sizes of slice thickness for the standard size phantom.

Table 4.19 The % $CTDI_{vol}$ reduction when vary the Noise Index from 10 to 20 at different slice thickness of standard size phantom.

Slice thickness (mm)	% $CTDI_{vol}$ Reduction				
	NI10	NI12.5	NI 15	NI17.5	NI20
0.625	0	0	2.3	8.3	18.2
1.25	0	0.9	7.3	18.0	32.1
2.5	0	17.9	38.5	54.7	64.9
5.0	0	35.3	53.4	62.5	65.9

From Table 14.20 increasing Noise Index from 10 to 20, $CTDI_{vol}$ reduced, the slice thickness 5 mm at Noise Index 20 obtained the 65.9 % $CTDI_{vol}$ reduction.

The mean values $CTDI_{vol}$ from STD, BONE+, CHEST, and LUNG filters of large size phantom were plotted when vary Noise Index from 10-20 and four sizes of slice thickness 0.625, 1.25, 2.5, and 5.0 mm as shown in figure 4.3

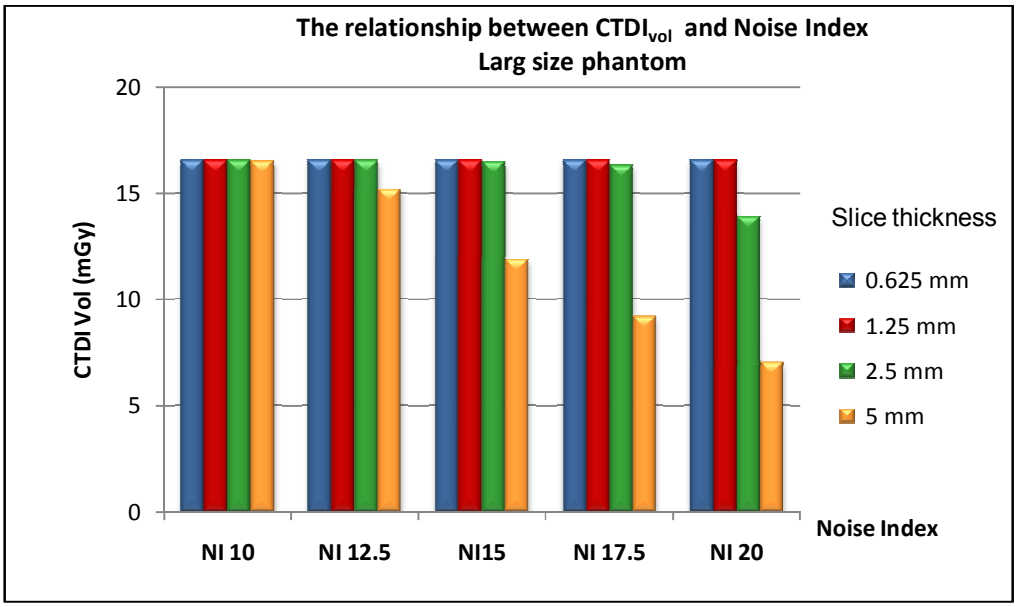

Figure 4.3 The relationship between the average $CTDI_{vol}$ and Noise Index of at varying slice thickness of large size phantom.

Table 4.20 The percent $CTDI_{vol}$ reduction when vary the Noise Index from 10 to 20 at different slice thickness for the large size phantom.

Slice thickness (mm)	% $CTDI_{vol}$ Reduction				
	NI10	NI12.5	NI 15	NI17.5	NI20
0.625	0	0	0	0	0
1.25	0	0	0	0	0
2.5	0	0	0.30	1.39	12.82
5.0	0	7.9	27.56	43.91	57.07

From the Table 14.20 increasing Noise Index from 10 to 20, There are no change of $CTDI_{vol}$ at slice thickness 0.625 and 1.25 mm, the slice thickness 5 mm at Noise Index 20 obtained 57.07 % $CTDI_{vol.}$ reduction.

The mean values DLP from STD, BONE+, CHEST, and LUNG filters of standard size phantom were plotted when vary Noise Index from 10-20 and four sizes of slice thickness 0.625, 1.25, 2.5, and 5.0 mm as shown in figure 4.4.

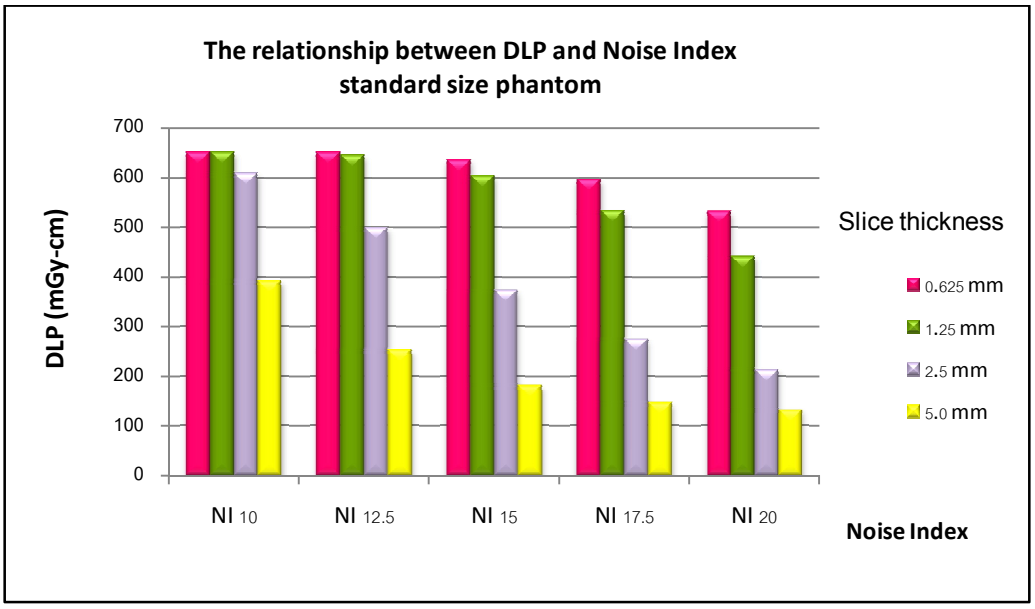

Figure 4.4 The relationship between the average DLP and Noise Index of at different slice thickness for the standard size phantom.

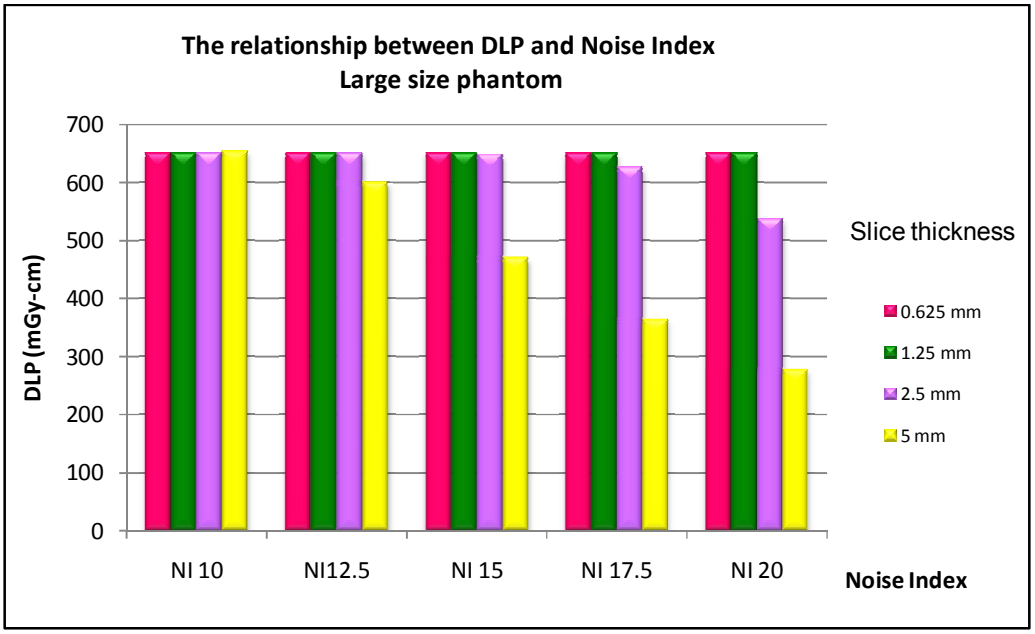

Figure 4.5 The relationship between the average DLP and Noise Index of at different slice thickness for the large size phantom.

4.5 Image quality

4.5.1 Quantitative image quality

4.5.1.1 Contrast to Noise Ratio (CNR)

The percent CNR of standard size and the large size phantom were compared within the group of same both nodules and slice thickness but various filters and the Noise Index. The CNR of different parameters in the group were normalized at Noise Index 10 at STD filter as shown in table 14.21 to 14.30

Table 4.21 The percent CNR of nodule 12 mm in diameter for standard size phantom.

Slice thickness (mm)	Noise Index	% CNR Nodule 12 mm			
		Filter			
		STD	CHEST	LUNG	BONE+
0.625	10	100.00	54.64	27.62	30.42
	12.5	99.58	56.71	31.32	32.91
	15	93.97	52.99	32.72	32.68
	17.5	88.82	46.77	28.19	28.64
	20	80.49	39.71	25.11	24.55
1.25	10	100.00	54.50	32.74	31.40
	12.5	105.34	53.77	35.02	32.70
	15	94.84	45.88	29.15	30.17
	17.5	83.64	40.13	26.02	25.54
	20	69.51	35.95	26.69	23.74
2.5	10	100.00	44.21	29.52	31.52
	12.5	82.72	37.67	27.47	26.72
	15	71.75	32.63	23.50	22.66
	17.5	62.17	26.17	20.44	18.02
	20	56.75	22.66	19.17	17.84
5	10	121.40	51.23	35.64	37.75
	12.5	100.00	42.89	28.63	31.34
	15	93.56	39.76	27.10	33.11
	17.5	91.32	36.81	27.32	29.38
	20	93.25	38.71	27.61	30.12

Table 14.21 shown the percent CNR of nodule 12 mm diameter for standard size phantom.

Table 4.22 The percent CNR of nodule 10 mm in diameter for standard size phantom.

Slice thickness (mm)	Noise Index	% CNR Nodule 10 mm			
		Filter			
		STD	CHEST	LUNG	BONE+
0.625	10	100.00	73.75	45.81	41.69
	12.5	86.45	68.82	43.07	45.90
	15	86.26	67.68	43.21	45.95
	17.5	73.79	65.65	40.39	44.35
	20	67.20	56.52	37.44	38.77
1.25	10	100.00	68.22	49.91	49.94
	12.5	89.47	69.22	40.11	52.29
	15	85.80	53.24	36.51	48.64
	17.5	78.70	52.39	33.44	36.36
	20	80.23	52.77	31.94	34.09
2.5	10	100.00	68.25	30.77	54.43
	12.5	81.97	63.81	33.82	42.80
	15	81.14	53.39	26.41	39.57
	17.5	72.36	47.96	26.04	39.23
	20	63.76	39.77	27.77	31.69
5	10	100.00	72.29	90.12	74.15
	12.5	89.98	55.42	67.10	58.25
	15	87.53	64.47	58.36	56.57
	17.5	84.24	60.92	52.37	54.95
	20	84.31	52.59	50.85	56.75

Table 14.22 shows the percent CNR of nodule 10 mm in diameter for standard size phantom.

Table 4.23 The percent CNR of nodule 8 mm in diameter for standard size phantom.

Slice thickness (mm)	Noise Index	% CNR Nodule 8 mm			
		Filter			
		STD	CHEST	LUNG	BONE+
0.625	10	100.00	44.17	36.89	36.13
	12.5	101.57	48.89	34.33	29.21
	15	90.73	52.75	44.57	34.87
	17.5	99.08	49.92	42.10	40.35
	20	104.85	48.38	34.21	34.01
1.25	10	100.00	29.20	24.13	22.63
	12.5	72.86	33.40	23.00	23.97
	15	78.35	26.80	23.35	21.92
	17.5	60.10	32.52	26.64	22.16
	20	79.91	27.87	23.30	24.76
2.5	10	100.00	37.25	35.36	30.92
	12.5	93.04	38.19	32.32	34.43
	15	76.85	32.24	33.95	23.98
	17.5	73.61	30.55	26.91	22.70
	20	56.94	23.51	22.67	23.07
5	10	100.00	47.00	40.17	32.18
	12.5	67.70	39.07	32.89	24.04
	15	60.00	28.83	22.77	25.55
	17.5	65.14	22.73	25.38	21.26
	20	65.81	20.96	20.11	17.89

Table 14.23 shows the percent CNR of nodule 8 mm in diameter for standard size phantom.

Table 4.24 The percent CNR of nodule 5 mm in diameter for standard size phantom.

Slice thickness (mm)	Noise Index	% CNR Nodule 5 mm			
		Filter			
		STD	CHEST	LUNG	BONE+
0.625	10	100.00	66.15	34.73	35.84
	12.5	85.48	52.49	35.59	37.44
	15	121.51	51.58	27.20	34.20
	17.5	65.33	37.84	28.83	28.70
	20	87.35	34.12	28.95	37.56
1.25	10	100.00	41.66	29.99	56.21
	12.5	81.52	43.81	29.99	41.76
	15	81.52	34.74	30.00	39.83
	17.5	99.75	30.87	27.12	32.01
	20	69.27	24.29	24.94	27.53
2.5	10	100.00	54.80	44.80	40.65
	12.5	67.82	43.35	33.56	47.94
	15	67.30	29.21	24.78	39.04
	17.5	54.16	27.87	25.98	27.23
	20	50.76	32.83	26.03	27.59
5	10	100.00	29.75	20.27	36.39
	12.5	76.73	25.95	24.88	38.56
	15	71.40	22.71	19.32	30.60
	17.5	81.85	21.38	36.74	27.31
	20	80.18	20.15	23.11	27.48

Table 14.24 shows the percent CNR of nodule 5 mm in diameter for standard size phantom.

Table 4.25 The percent CNR of nodule 3 mm in diameter for standard size phantom.

Slice thickness (mm)	Noise Index	% CNR Nodule 3 mm			
		Filter			
		STD	CHEST	LUNG	BONE+
0.625	10	100.00	56.47	40.07	47.44
	12.5	100.25	65.19	35.31	34.31
	15	97.83	58.52	40.39	28.55
	17.5	86.14	43.60	29.98	35.37
	20	109.33	35.05	40.00	34.41
1.25	10	100.00	53.51	52.68	38.26
	12.5	119.35	61.77	47.67	38.82
	15	99.45	51.72	39.57	45.63
	17.5	90.73	56.59	39.16	25.98
	20	80.42	28.68	31.18	30.40
2.5	10	100.00	49.93	68.60	41.95
	12.5	95.48	49.93	68.60	41.95
	15	95.48	45.14	46.16	28.40
	17.5	74.40	34.73	47.60	27.88
	20	63.42	26.40	33.94	15.96
5	10	100.00	26.66	20.22	23.66
	12.5	93.78	31.76	19.61	17.63
	15	57.44	17.57	18.78	17.26
	17.5	63.47	16.08	12.59	20.74
	20	73.04	18.59	15.86	21.98

Table 14.25 shows the percent CNR of nodule 3 mm in diameter for standard size phantom.

Table 4.26 The percent CNR of nodule 12 mm in diameter for large size phantom.

Slice thickness (mm)	Noise Index	% CNR Nodule 12 mm			
		Filter			
		STD(L)	CHEST(L)	LUNG(L)	BONE+(L)
0.625	10	100.00	54.18	34.19	34.06
	12.5	101.03	55.06	33.37	34.77
	15	109.07	53.18	32.51	34.53
	17.5	105.35	55.70	31.65	36.59
	20	105.29	52.18	35.76	35.70
1.25	10	100.01	40.72	29.36	30.19
	12.5	97.59	44.88	30.10	30.22
	15	94.20	37.92	28.54	29.86
	17.5	88.53	44.36	27.09	29.63
	20	86.13	41.64	29.56	30.22
2.5	10	100.00	45.30	30.85	31.73
	12.5	97.79	44.75	30.71	31.90
	15	101.66	42.44	32.90	33.59
	17.5	98.89	43.46	31.28	32.60
	20	87.23	36.49	28.97	28.58
5	10	100.00	47.86	47.86	33.92
	12.5	94.88	41.79	41.79	30.73
	15	84.35	34.27	34.27	25.72
	17.5	73.36	31.12	31.12	20.47
	20	71.36	27.11	27.11	20.43

(L) – Large size of Lung Man Chest phantom

Table 14.26 shows the percent CNR of nodule 12 mm in diameter for large size phantom.

Table 4.27 The percent CNR of nodule 10 mm in diameter for large size phantom.

Slice thickness (mm)	Noise Index	% CNR Nodule 10 mm			
		Filter			
		STD(L)	CHEST(L)	LUNG(L)	BONE+(L)
0.625	10	99.99	53.26	34.13	37.34
	12.5	88.91	49.97	38.87	35.98
	15	107.29	58.04	34.69	40.82
	17.5	100.55	59.19	32.93	38.45
	20	115.81	54.73	33.21	39.77
1.25	10	100.00	49.98	35.61	35.62
	12.5	104.22	43.89	34.00	40.14
	15	93.32	49.00	31.97	38.06
	17.5	90.20	42.22	32.94	37.52
	20	107.90	45.46	31.31	37.60
2.5	10	100.00	73.30	66.86	70.99
	12.5	100.78	76.18	61.86	67.13
	15	97.94	76.71	66.26	69.46
	17.5	93.23	65.15	56.20	71.60
	20	101.83	61.65	51.95	62.09
5	10	100.01	66.13	71.38	54.95
	12.5	102.71	61.79	64.18	58.03
	15	90.25	49.14	53.03	56.31
	17.5	96.05	45.22	56.37	43.83
	20	101.89	34.64	44.82	38.09

(L) – Large size of Lung Man Chest phantom

Table 14.27 shows the percent CNR of nodule 10 mm in diameter for large size phantom.

Table 4.28 The percent CNR of nodule 8 mm in diameter for large size phantom.

Slice thickness (mm)	Noise Index	% CNR Nodule 8 mm			
		Filter			
		STD(L)	CHEST(L)	LUNG(L)	BONE+(L)
0.625	10	100.01	58.48	37.80	37.47
	12.5	101.88	57.97	34.57	40.28
	15	91.61	54.41	34.76	43.56
	17.5	105.82	50.81	38.72	40.13
	20	123.91	52.73	42.79	37.26
1.25	10	100.00	42.24	38.44	35.02
	12.5	98.93	44.41	38.55	35.91
	15	94.28	47.77	33.45	35.31
	17.5	97.30	50.55	41.05	36.94
	20	102.34	47.29	36.02	37.64
2.5	10	100.00	34.16	46.75	32.73
	12.5	93.09	37.80	42.06	32.44
	15	95.06	34.01	47.50	29.57
	17.5	102.27	39.49	38.04	30.27
	20	87.33	32.79	37.14	28.95
5	10	100.00	32.07	38.01	32.16
	12.5	73.83	33.82	36.46	27.78
	15	73.51	29.87	30.52	27.89
	17.5	79.36	24.06	28.08	22.57
	20	59.24	23.94	23.11	19.36

(L) – Large size of Lung Man Chest phantom

Table 14.28 shows the percent CNR of nodule 8 mm in diameter for large size phantom.

Table 14.29 The percent CNR of nodule 5 mm in diameter for large size phantom.

Slice thickness (mm)	Noise Index	% CNR Nodule 5 mm			
		Filter			
		STD(L)	CHEST(L)	LUNG(L)	BONE+(L)
0.625	10	99.99	55.50	53.82	43.93
	12.5	115.51	60.71	46.52	44.86
	15	96.53	74.89	38.33	44.16
	17.5	118.33	62.85	43.00	34.18
	20	100.41	57.71	39.61	39.50
1.25	10	99.99	40.47	40.81	46.77
	12.5	111.18	48.65	32.77	36.47
	15	89.59	43.81	46.36	57.23
	17.5	101.05	40.56	42.48	39.97
	20	132.40	51.19	41.33	33.15
2.5	10	100.00	56.64	51.98	50.95
	12.5	105.20	41.70	47.37	42.62
	15	113.31	44.70	41.33	57.76
	17.5	138.23	57.11	42.23	56.36
	20	118.70	40.70	36.05	35.75
5	10	100.00	55.57	43.90	55.33
	12.5	131.80	57.48	39.39	32.75
	15	76.95	35.12	26.22	24.38
	17.5	87.24	28.94	27.00	24.28
	20	65.50	28.16	25.04	18.15

(L) – Large size of Lung Man Chest phantom

Table 14.29 shows the percent CNR of nodule 5 mm in diameter for large size phantom.

Table 4.30 The percent CNR of nodule 3 mm in diameter for large size phantom.

Slice thickness (mm)	Noise Index	% CNR Nodule 3 mm			
		Filter			
		STD(L)	CHEST(L)	LUNG(L)	BONE+(L)
0.625	10	100.00	37.31	36.37	30.40
	12.5	81.92	58.68	39.56	32.06
	15	78.53	40.94	32.65	34.83
	17.5	114.54	42.46	40.56	33.47
	20	84.76	34.11	35.25	27.86
1.25	10	100.00	39.83	24.59	29.71
	12.5	76.98	26.76	28.65	28.04
	15	71.40	38.42	29.87	21.87
	17.5	90.67	30.55	30.74	30.93
	20	98.17	28.68	28.20	25.28
2.5	10	100.00	32.04	51.49	30.45
	12.5	129.24	62.61	52.62	28.12
	15	78.25	43.98	42.51	36.09
	17.5	161.21	42.82	46.76	28.61
	20	97.05	39.68	39.39	38.55
5	10	100.01	33.17	15.16	24.17
	12.5	98.39	39.76	18.73	17.43
	15	82.63	30.69	17.68	22.60
	17.5	46.69	21.22	17.19	19.50
	20	51.32	21.29	11.15	11.65

(L) – Large size of Lung Man Chest phantom

Table 14.30 shows the percent CNR of nodule 3 mm in diameter for large size phantom.

The percent CNR of the standard size and large size phantoms were plotted separately for the relationship between the CNR and Noise Index when using the different type of filters compare within the same size of nodule as shown in Figure 4.6-4.10 for standard size phantom and Figure 4.11-4.15 for large size phantom.

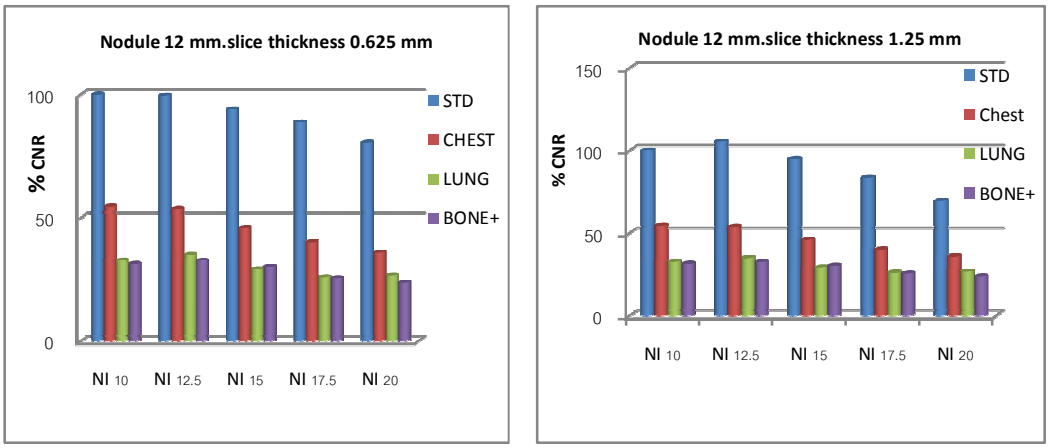

(a)

(b)

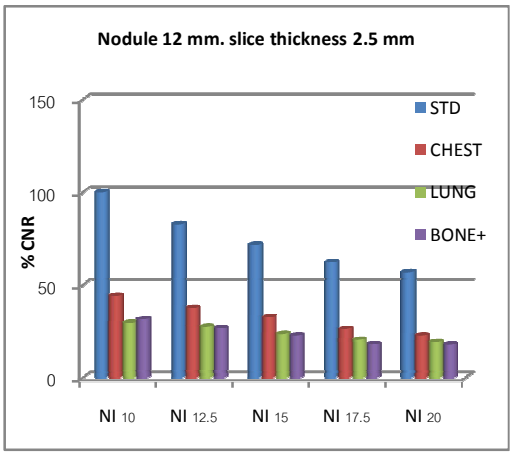

(c)

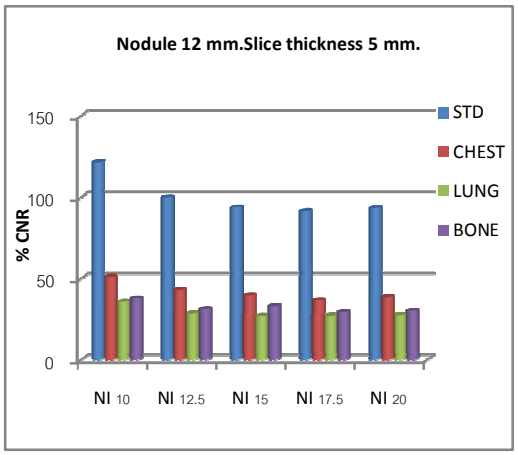

(d)

Figure 4.6 The percent CNR of nodule 12 mm, at slice thickness 0.625, 1.25, 2.5 and 5.0 mm respectively for standard size phantom.

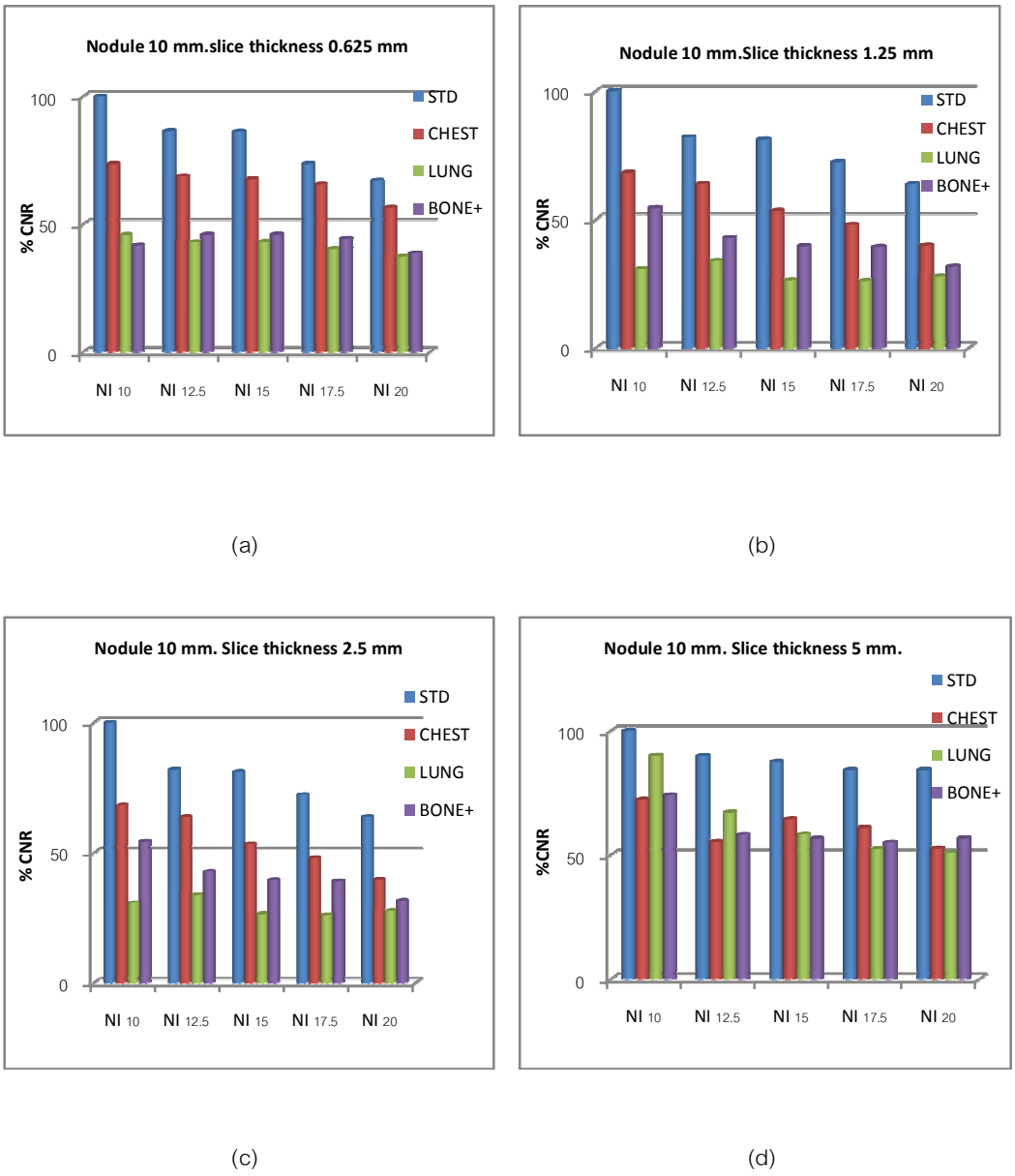

Figure 4.7 The percent CNR of nodule 10 mm, at slice thickness 0.625, 1.25, 2.5 and 5.0 mm respectively for standard size phantom

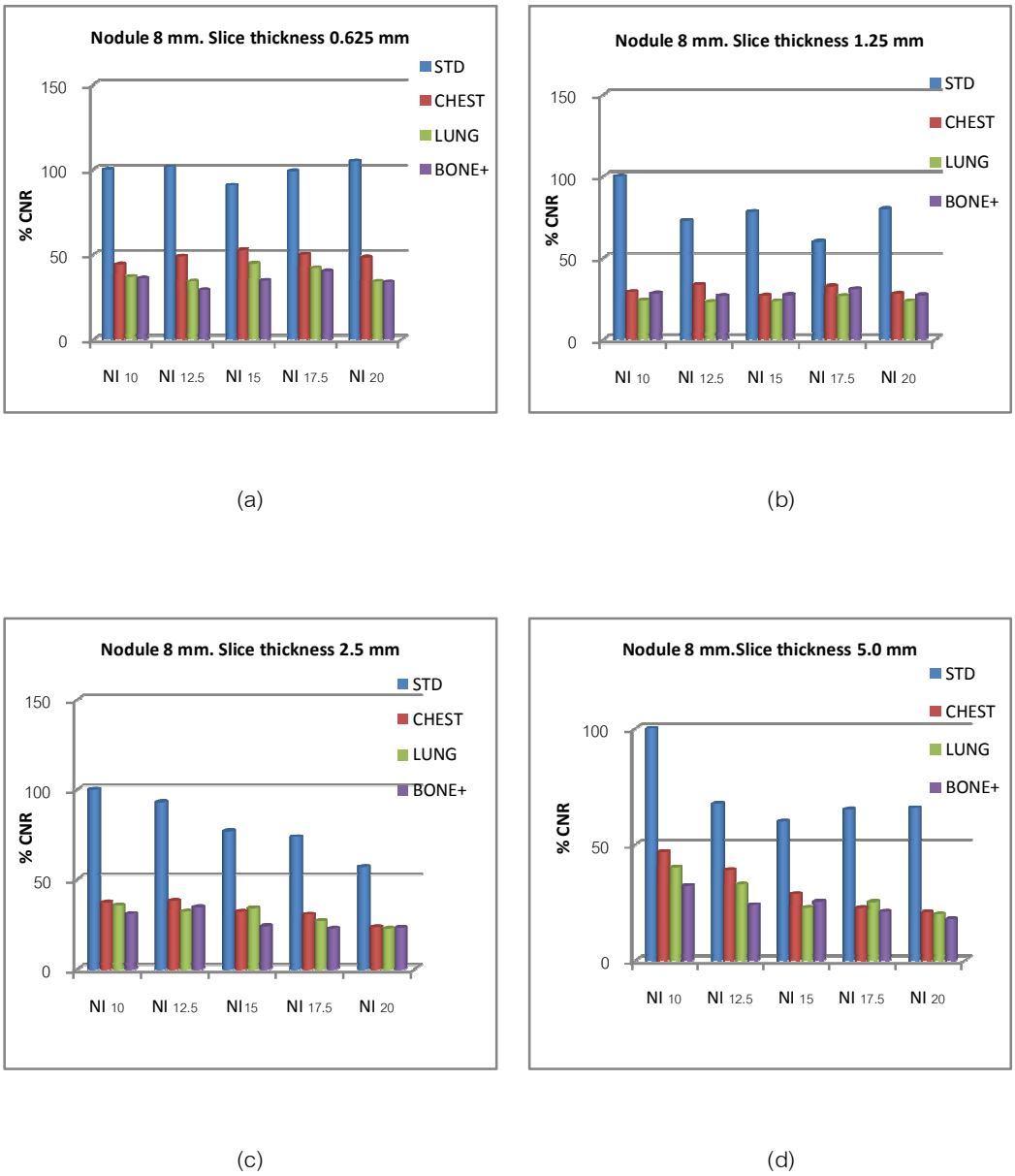

Figure 4.8 The percent CNR of nodule 8 mm, at slice thickness 0.625, 1.25, 2.5 and 5.0 mm respectively for standard size phantom.

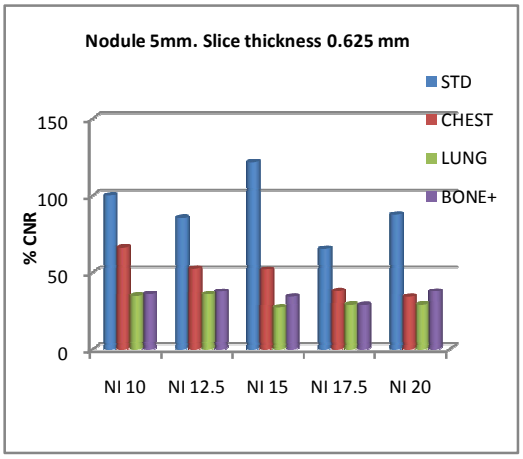

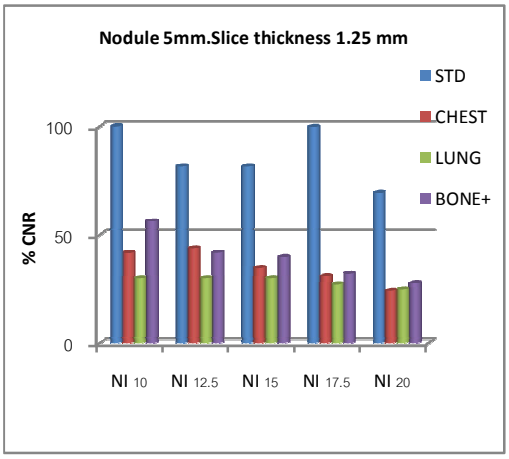

(a) (b)

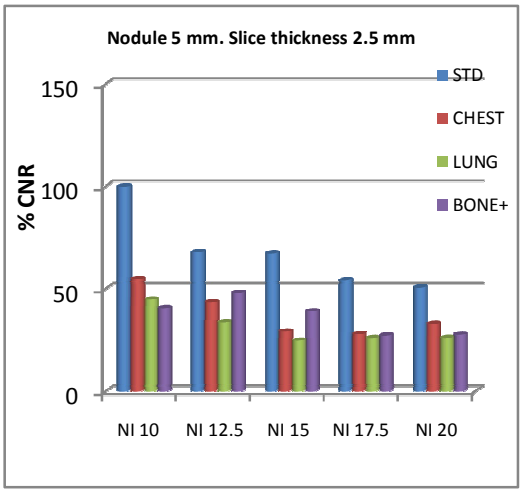

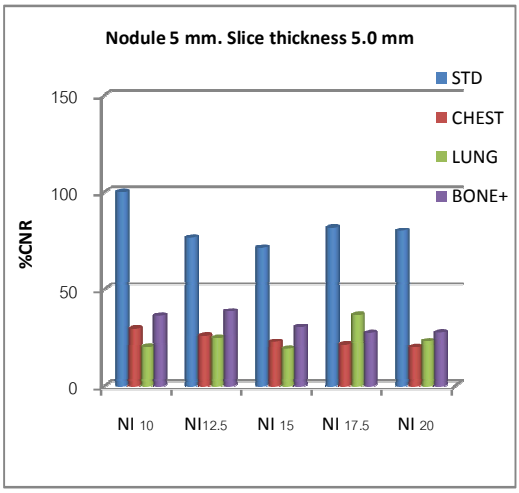

(c) (d)

Figure 4.9 The percent CNR of nodule 5 mm, at slice thickness 0.625, 1.25, 2.5 and 5.0 mm respectively for standard size phantom.

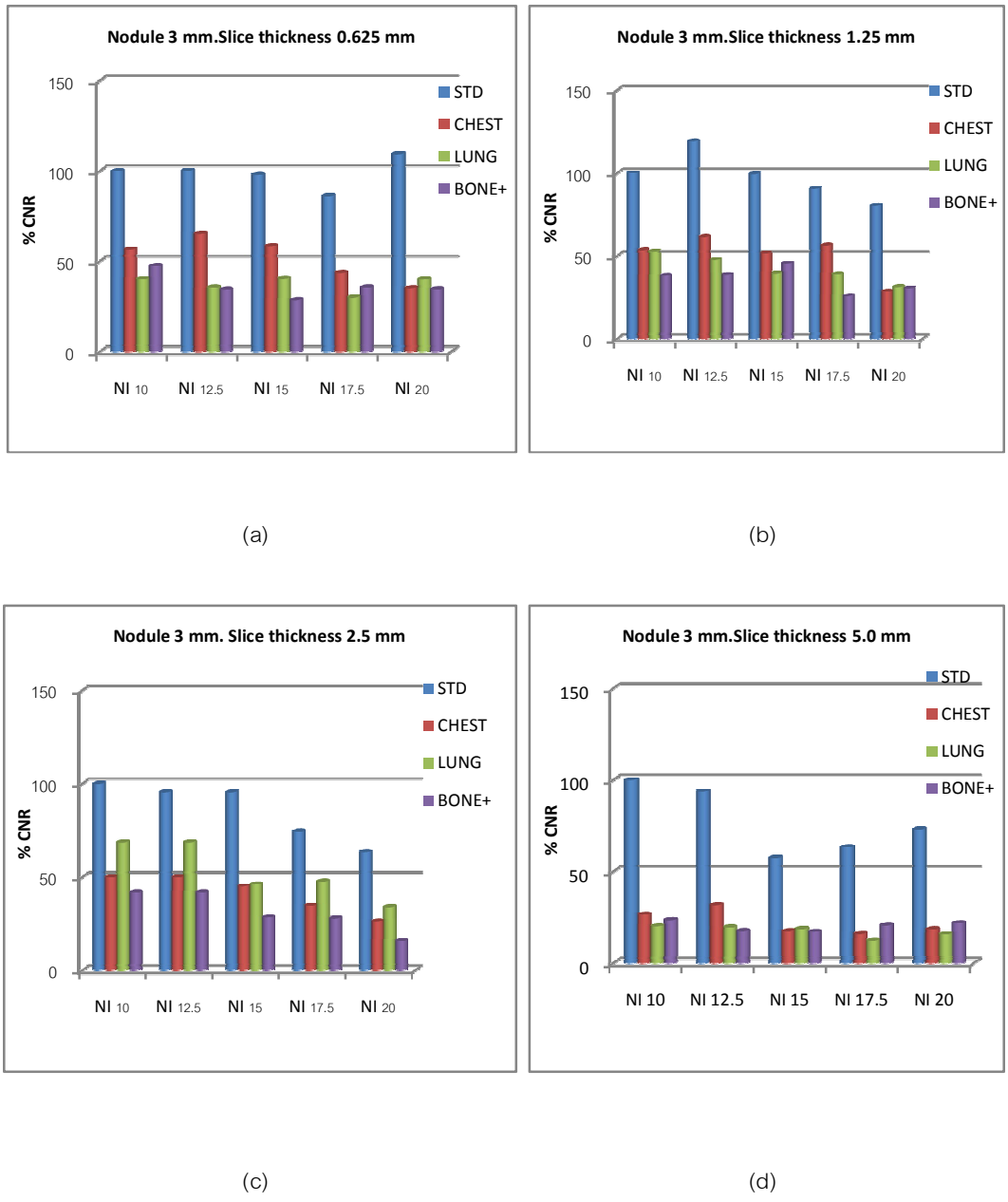

Figure 4.10 The percent CNR of nodule 3 mm, at slice thickness 0.625, 1.25, 2.5 and 5.0 mm respectively for standard size phantom.

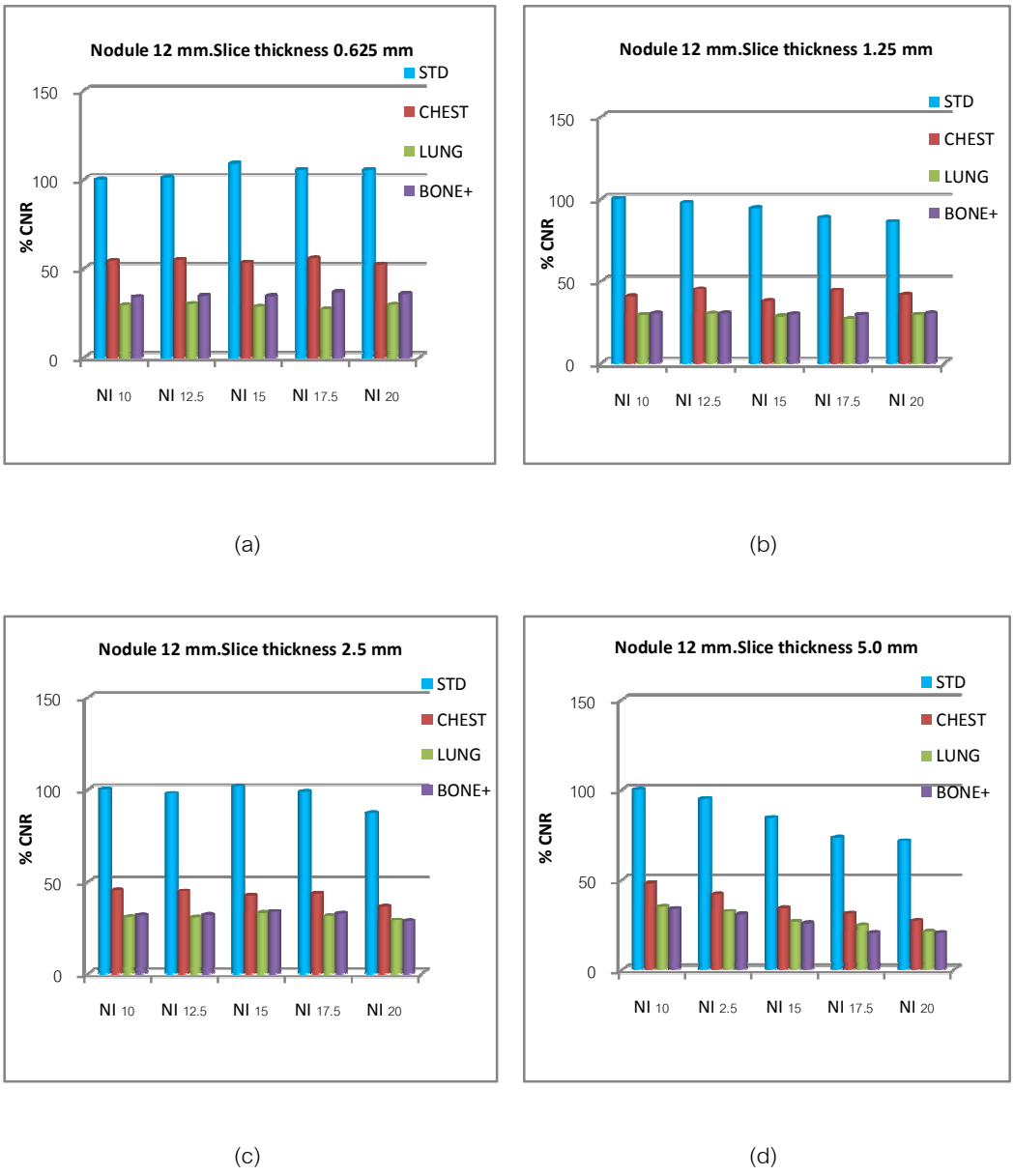

Figure 4.11 The percent CNR of nodule 12 mm, at slice thickness 0.625, 1.25, 2.5 and 5.0 mm respectively for large size phantom.

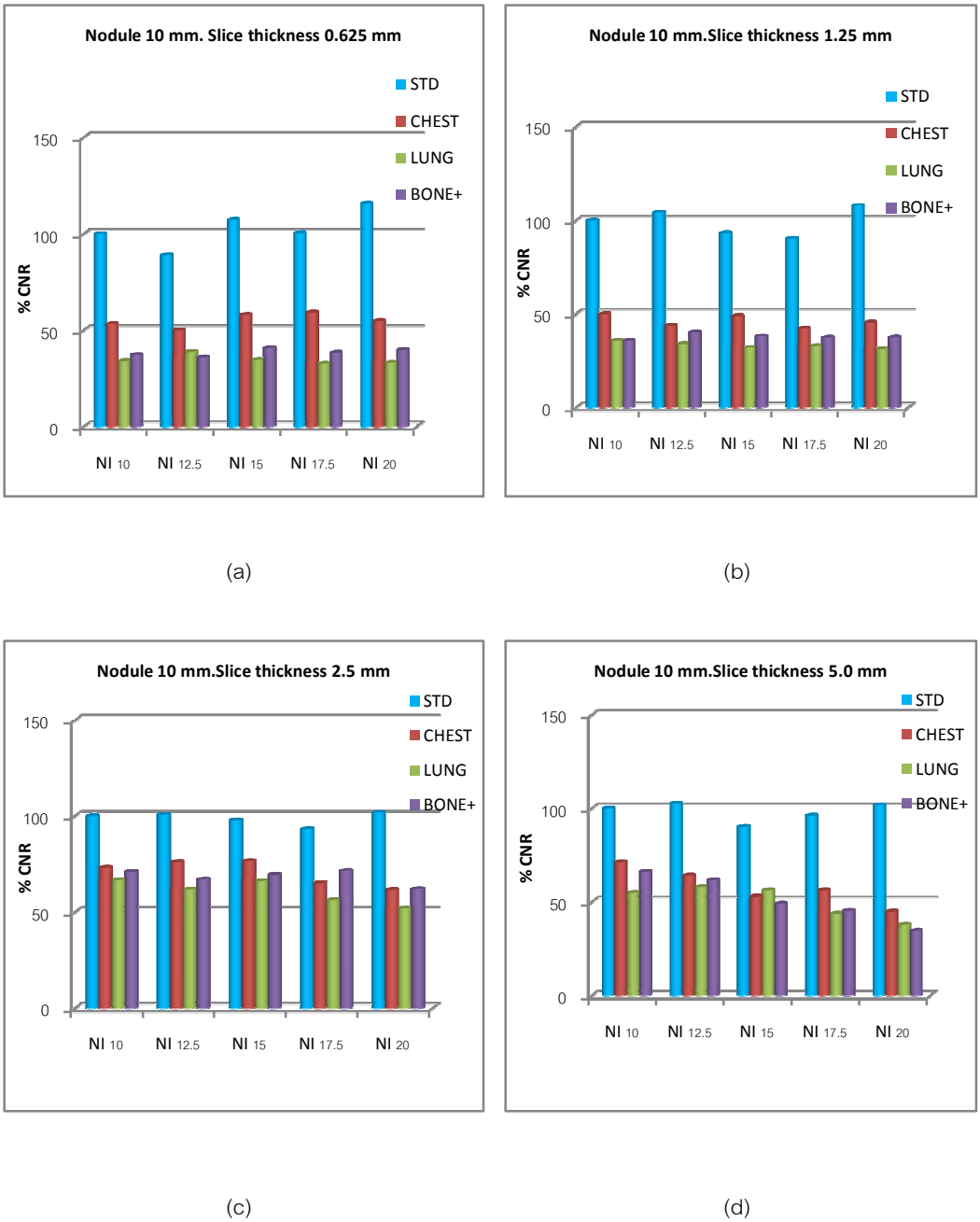

Figure 4.12 The percent CNR of nodule 10 mm, at slice thickness 0.625, 1.25, 2.5 and 5.0 mm respectively for large size phantom

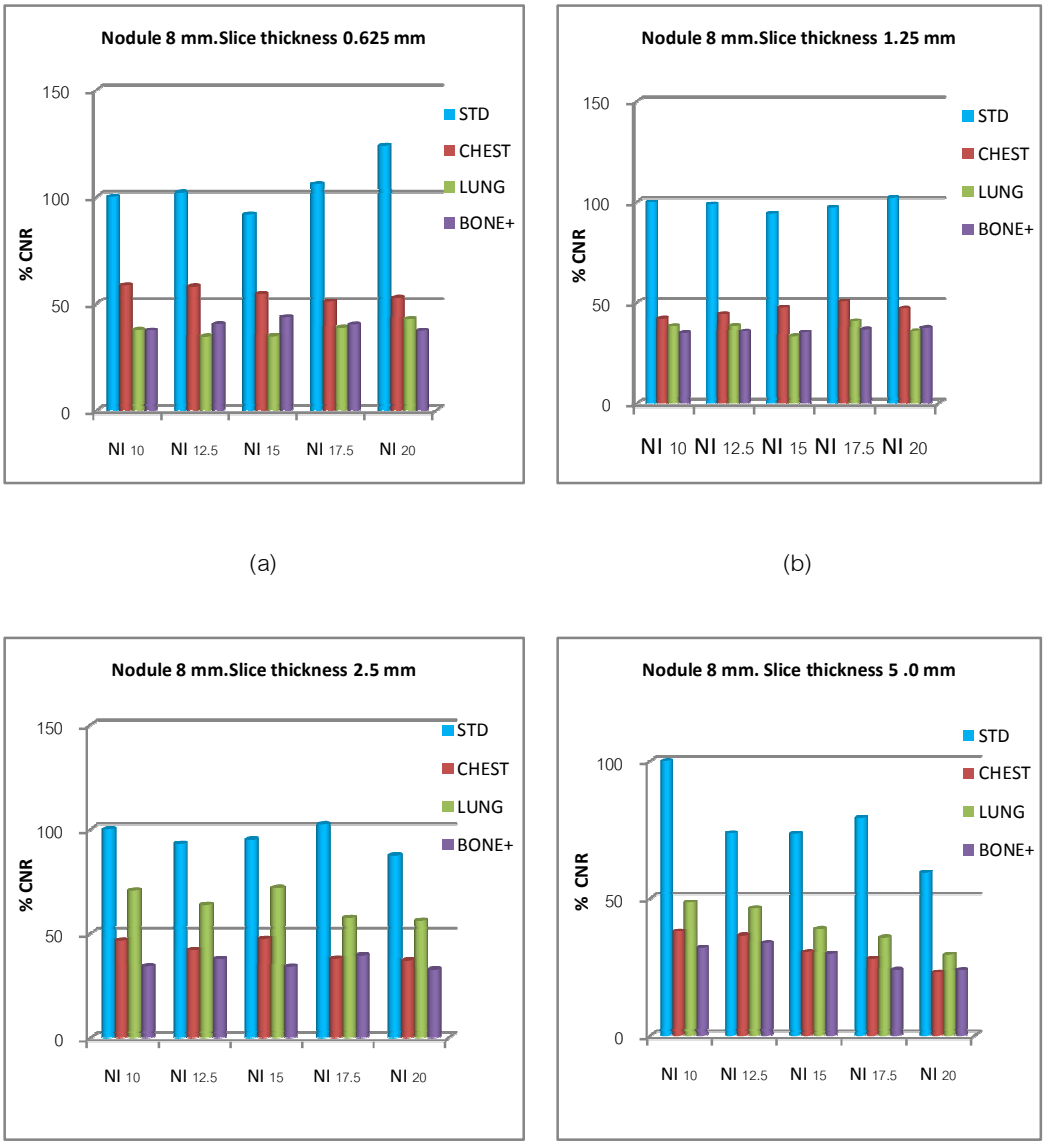

Figure 4.13 The percent CNR of nodule 8 mm, at slice thickness 0.625, 1.25, 2.5 and 5.0 mm respectively for large size phantom.

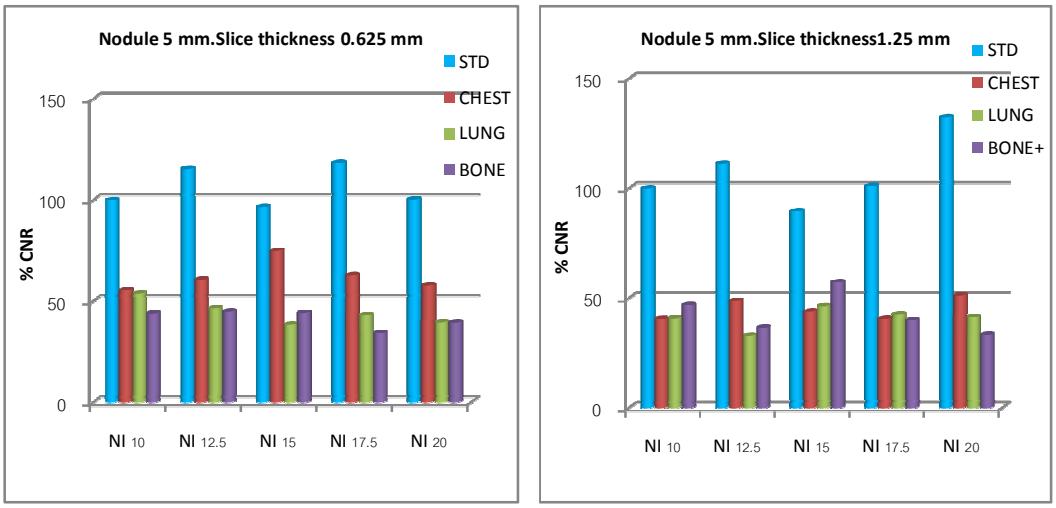

(a)

(b)

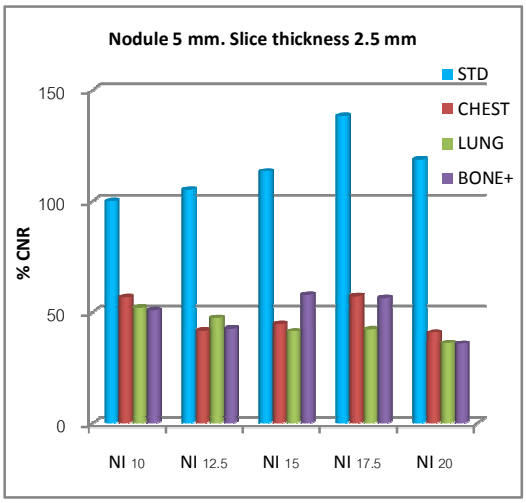

(c)

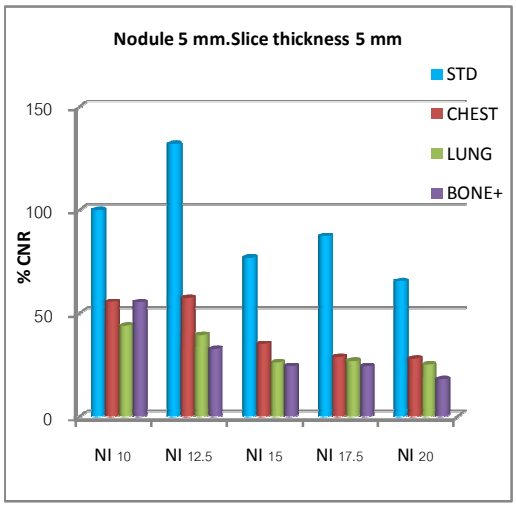

(d)

Figure 4.14 The percent CNR of nodule 5 mm, at slice thickness 0.625, 1.25, 2.5 and 5.0 mm respectively for large size phantom.

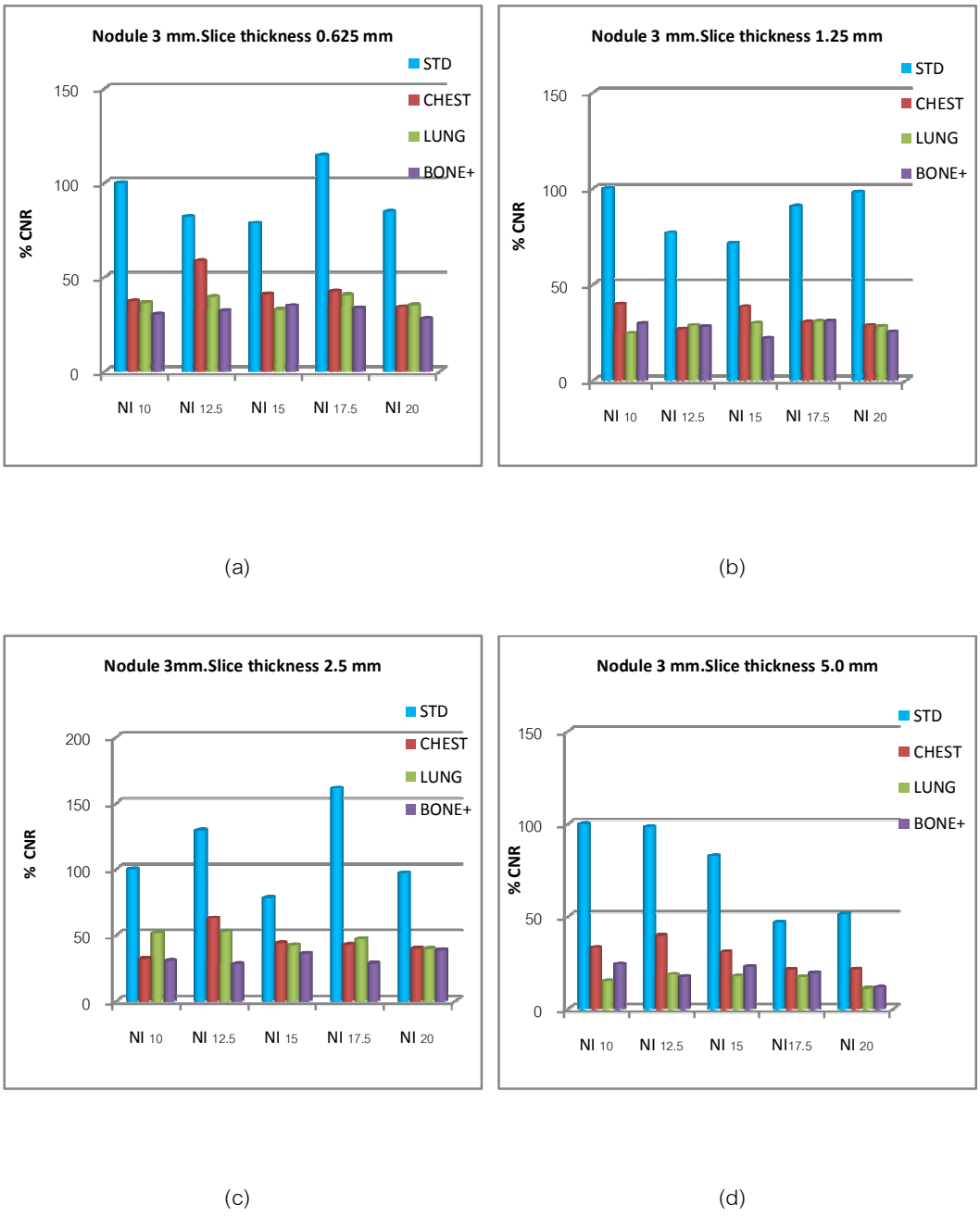

Figure 4.15 The percent CNR of nodule 3 mm, at slice thickness 0.625, 1.25, 2.5 and 5.0 mm respectively for large size phantom.

4.5.2 Qualitative image quality

4.5.2.1 Image scoring

Qualitative image quality was evaluated by two radiological technologists using criteria score 5 to 1 as described in the chapter III. The average score is shown in Table 4.31 and Table 4.32

Table 4.31 The image scoring of standard size phantom using different slice thickness and filters

Slice thickness (mm)	Image Scoring (standard size phantom)			
	Filters			
	STD	BONE+	CHEST	LUNG
0.625	4.5	5	4	5
1.25	4.5	4	3.5	4.5
2.5	3	3	3	4
5	1	3	1	2

Table 4.32 The image scoring of large size phantom using different slice thickness and filters

Slice thickness	Image Scoring (large size phantom)			
	Filters			
	STD	BONE+	CHEST	LUNG
0.625	4.5	4.5	4	5
1.25	4.5	4	3	4.5
2.5	3	3	3	4
5	1	2	1	2

(L) – Large size of Lung Man Chest phantom

Table 4.31-4.32 shows the image scoring of two sizes of Lung Man Chest phantom with variation of the slice thickness, Noise Index and reconstruction filters. The 0.625 slice thickness, scanning with STD and LUNG filters obtained the best scores.

The agreement of image quality scored by two radiological technologist was assessed by calculating weighted Kappa of the variation of reconstruction filters, slice thickness and Noise Index for two size of phantom. The data of weighted Kappa is shown in table 4.33

Table 4.33 The weighted Kappa of image quality scored by two radiological technologist.

Filters	Weighted Kappa
STD	0.889
BONE+	1.000
CHEST	0.909
LUNG	0.871
STD (L)	1.000
BONE+ (L)	0.875
CHEST (L)	1.000
LUNG (L)	1.000

Table 4.33 shows the agreement of scores by two radiological technologists using weighted Kappa. All reconstruction filters of standard and large size phantoms obtained very good agreement. For standard size, the BONE+ filters obtained score 1.000 whereas large size phantom STD, CHEST and LUNG obtained the score 1.000 as well.

4.5.2.2 Spatial resolution

The resolution was evaluated by the visualization of the amount of simulated nodules (12, 10, 8, 5, and 3 mm in diameter) with variation of the reconstruction filters, slice thickness and Noise Index. The spatial resolution of standard size phantom and large size phantom are shown in Table 14.34 and Table 14.35

Table 4.34 The spatial resolution, number of nodules visualization at various filters and slice thickness of standard size phantom.

Slice thickness (mm)	STD	BONE+	CHEST	LUNG
	Amount of visualized nodules			
0.625	4.5	5	4	5
1.25	4.5	4	3.5	4.5
2.5	3	3	3	4
5	1	1	1	2

Table 4.35 The spatial resolution, number of nodules visualization at various filters and slice thickness of large size phantom

Slice thickness (mm)	STD(L)	BONE+(L)	CHEST(L)	LUNG(L)
	Amount of visualized nodules			
0.625	4.5	5	4	5
1.25	4.5	4	3	4.5
2.5	3	3	3	4
5	1	2	1	2

(L) – Large size of Lung Man Chest phantom

Table 4.34 - 4.35 show number of visualized simulated nodules with variation of the reconstruction filters, slice thickness and Noise Index. The LUNG and BONE+ filters at 0.625 mm of slice thickness obtained the best resolution (visualized small nodule 3-5 mm in diameter), STD and CHEST obtained good resolution. Slice thickness 1.25 and 2.5 mm obtained the good resolution respectively whereas at 5.0 mm of slice thickness obtained the poorest resolution (visualized large nodules 10-12 mm in diameter) for both standard and large phantoms.

CHAPTER V

DISCUSSION AND CONCLUSION

5.1 Discussion

The CT technology has been rapidly emerged not only with the amount of detectors, the fast scanning speed and the isotropic spatial resolution but also the increasing of radiation dose associated with CT scanning. The modern MDCT scanner provides a useful function such as an automated tube current modulation program to reduce the patient dose while the tube current, mA and the gantry rotation time are modulated. Moreover, the operator can adjust a selectable parameter to alter the image quality corresponds to the radiation dose. The parameter indicative the level of the image noise is Noise Index (NI), a term used only for GE medical system. However changing the Noise Index alters the range of mA by the automatic exposure control (AEC) during gantry rotation to produce a selected level of average image noise. But average image noise depends on the reconstruction slice thickness **[13].** In this study, both x-y, and z-axis modulations were applied to obtain the high efficiency of the radiation dose reduction according to the image quality at the optimal Noise Index for the acceptable image quality and radiation dose.

5.1.1 Measurement of CTDI

The CT Dose Index displayed on the CT monitor was verified by comparison of the readout to the measurement of CTDI in air, phantoms and the ImPACTSCAN values at the same kVp and mAs. The measured CTDI in air, head and body phantom were greater than 10% of the ImPACTSCAN values. The main reason of the discrepancy in the CTDI measurement and the ImPACTSCAN values is the measurement uncertainty as described in IAEA Technical Report Series (TRS) No.457: **[16]**. The factors affecting the measurement uncertainty in the estimation of the CTDI were characteristic of the ionization chamber, electrometer, the measurement scenario, the precision of reading, tube loading chamber position, the phantom construction, the chamber response in phantoms and the inaccuracy on the laser beam alignment.

Comparison of the ImPACTSCAN and the displayed $CTDI_{vol}$ values at 120 kVp in air for the head and body protocols, the ImPACTSCAN values were higher than the displayed $CTDI_{vol}$ 7.41% and 8.31% respectively.

Comparison of the calculated $CTDI_{vol}$ and monitor display, the calculated $CTDI_{vol}$ values at 120 kVp for the head and body protocols were greater than the monitor display 1.31% and 6.67 % respectively.

The CTDI on monitor display was the least when compare to the measurement CTDI and the ImPACTSCAN values.

5.1.2 Radiation Dose, slice thickness and Noise Index

The relationship between $CTDI_{vol}$ and Noise Index for standard size phantom is that, the increasing of Noise Index from 10-20 and slice thickness from 0.625 to 5.0 mm, $CTDI_{vol}$ decreased from 18.2, 32.1, 64.9 to 65.9% respectively. There are no difference of $CTDI_{vol}$ between Noise Index 10 and 12.5 for 0.625 mm of slice thickness, however the $CTDI_{vol}$ slightly decreased when increasing of Noise Index from 15 to 20. When the thicker slice at 2.5 and 5 mm were selected, $CTDI_{vol}$ decrease to 64.9 and 65.9 % as shown in Table 5.1

Table 5.1 The percent $CTDI_{vol}$ reduction of standard size phantom

Slice Thickness	% $CTDI_{vol}$ Reduction				
	Noise Index				
	10	12.5	15	17.5	20
0.625	0	0	2.3	8.3	18.2
1.25	0	0.9	7.3	18.0	32.1
2.5	0	17.9	38.5	54.7	64.9
5.0	0	35.3	53.4	62.5	65.9

The relationship between $CTDI_{vol}$ and Noise Index for large size phantom was no variation of $CTDI_{vol}$ when varying slice thickness at low Noise Index, until the thick slice thickness particularly 5.0 mm, the $CTDI_{vol}$ was rapidly decreased. Therefore the slice thickness had a major impact on radiation dose for the large size phantom, however the reduction of the radiation dose of large size was less than the standard size phantom because the tube modulation based on the phantom size. The AEC system estimated the attenuation value from the scan projection radiography (scout view) to adjust tube current **[10]** therefore the $CTDI_{vol}$ was high for the large phantom than standard phantom because of the greater of attenuation.

The AEC system provides the mA range, at 75-380 mA automatically selected in this study **[17]** to avoid excessive tube current in small patient. The maximum tube current 380 was restricted to prevent a high dose in large patient for the chest study.

The function of AEC is according to the first prospective reconstruction slice thickness with indicative Noise Index to estimate the tube current, therefore the second prospective reconstruction slice thickness was used with the same algorithm. The mA will be calculated based on the first prospective reconstruction slice thickness. This implies that the Noise Index will be changed to maintain the same radiation dose (relative to the first prospective reconstruction) **[4]**. Therefore the factors affecting on radiation dose are the slice thickness and Noise Index.

When Noise Index was increasing, the radiation dose would be decreasing. Kalra M K et al **[18]** studied for optimization of z-axis modulation technique with various Noise Index in chest study and concluded that Noise Index of 10, 12.5 and 15 yielded 18.0%, 26.0% and 41.3 % respectively in radiation dose reduction. However their studies performed in the 16 MDCT and our study in 64 MDCT.

5.1.3 Characteristic of image quality in Catphan phantom

The BONE+ filter provides the highest contrast resolution. There are no difference of the spatial resolution, lp/cm when vary the slice thickness for each filters. From the result in chapter IV, the slice thickness had few effects on the high contrast resolution but the filters have high effect on the high contrast resolution.

The STD and CHEST filters have more ability to visualize the smallest size of object at different contrast level to the background than the LUNG and BONE+ filters. However the visualization of both characteristic were subjective depend on an observer.

The noise level measurement in uniform phantom was highest for BONE+ and lower for LUNG, CHEST and STD filters respectively. They correspond with the measurement by manufacturer as shown in table 5.2. The high resolution kernel as a BONE+ and LUNG filters result in high image noise and edge enhancement.

Table 5.2 Comparison of the percent of noise level and reconstruction filters among the manufacturers. **[19]**

Reconstruction Kernel	Noise level (%)			
	Manufacturer			
	GE	Phillips	Siemens	Toshiba
STD	0.36	0.38	0.35	NA
CHEST	1.7	1.7	1.8	0.9
LUNG	2.3	2.3	2.5	3.2
BONE	4.2	4.2	4.7	10.6

5.1.4 The assessment of image quality

5.1.4.1 Contrast to noise ratio

In order to eliminate the variance from the nodules position, the CNR were grouped of the simulated nodules of 12, 10, 8, 5 and 3 mm. in diameter respectively. Noise Index 10 with STD filter was baseline for normalized percent CNR due to the expected lowest noise level.

The STD filter showed the highest CNR for all nodule sizes, slice thickness and Noise Index. Subsequently, the CHEST filter result in 50-60% of the STD filter, the LUNG and BONE+ filters showed the lowest percent CNR. For the large size nodules 12 and 10 mm. in diameter, the CNR decreased with the increasing Noise Index. The low Noise Index provided the high CNR, however there were variations for the small sizes of nodules 8, 5, and 3 mm. particularly nodule sizes 5 and 3 mm. in diameter, a lot of variation at all slice thickness. The major factors were the variation in positions of circular ROI especially a very small size nodule. These effects contribute to the variation of CT number of the nodule and the standard deviation values of the background. The partial volume effect and the effect on variation of slice thickness were greater than the effect on the nodules size. The attenuation of background occupied in the same voxel resulting in the CT number represents the sum of the different attenuation values **[5]**.

There was the difference of CNR between the standard and large size phantoms. The CT number of the simulated nodules in the large phantom was less than in the standard phantom. According to the same scanning parameters as a standard phantom, the maximum mA was restricted at 380 mA therefore the greater attenuation in the large size phantom resulting the fewer x-ray photons reached the detectors and increasing noise level. However when calculated to the percent CNR, it does not decrease by the effect of increasing of Noise Index for the 12, 10, and 8 mm nodules, however the variation of the percent CNR were less than the standard phantom. The percent CNR were highest for STD filter, and reduce for CHEST, LUNG, and BONE+ respectively.

The STD filter provides the highest percent CNR because the STD filter designed for good spatial resolution and reasonably low image noise. The manufacturer also include high resolution kernel with reduced noise level [5]. The STD filter offers the lowest noise level and the BONE+ filter offers the highest noise level [5]. The Noise Index has little effect on contrast to noise ratio

5.1.4.2 The assessment of qualitative image quality

The scoring of image quality of two size phantoms by two radiological technologists, the LUNG filter provided the best image quality at all slice thickness except 0.625 mm, both STD and LUNG filters showed the best scores. The 5 mm of slice thickness showed the worst score whereas 2.5 and 1.25 mm slice thickness showed the moderate and good score respectively. The agreement of two radiological technologists scoring for all filters of two size phantoms was very good.

The spatial resolution was considered from the visualization of smallest simulated nodules. The score 5 = visualized 3 mm, score 4 = visualized 5 mm, score 3 = visualized 8 mm, score 2 = visualized 10 mm and score 1 = visualized 12 mm in diameters. The LUNG filter provided the best resolution for all slice thicknesses. The score of two sizes phantom were similar with good agreement because the AEC system modulated the tube current in an effort to maintain constant image quality.

5.1.4.3 Optimization of radiation dose, image quality and Noise Index

The selection of Noise Index depends on the clinical applications for chest CT. High resolution CT (HRCT), 1-2 mm of slice thickness with high resolution kernel are necessary to define and evaluate fine structure details in the lung parenchyma **[5]**. 1.25 mm of slice thickness with the scoring of image quality from LUNG and BONE+ filters at Noise Index of 20 offered the low radiation dose with acceptable subjective image quality as shown in Figure 5.1

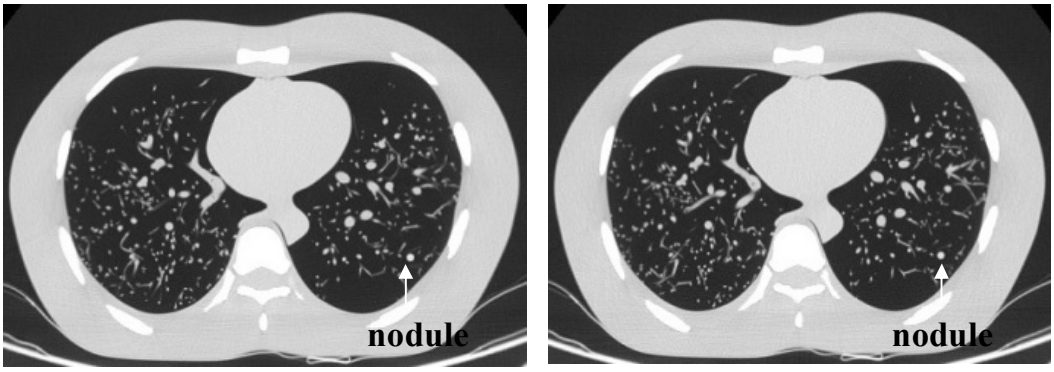

(a) (b)

Figure 5.1 The chest CT with 5 mm nodule, 1.25 mm slice thickness, NI 20, (a) LUNG, (b) BONE+ filter.

For routine chest CT, the mediastinum should be reconstructed using a soft kernel, 1-1.5 mm of slice thickness are selected for multislice CT therefore they are sufficient for routine interpretation **[5]**. Using Noise Index 15 and17.5 at 75-380 mA with STD filter result in acceptable objective image quality as shown in Figure 5.2

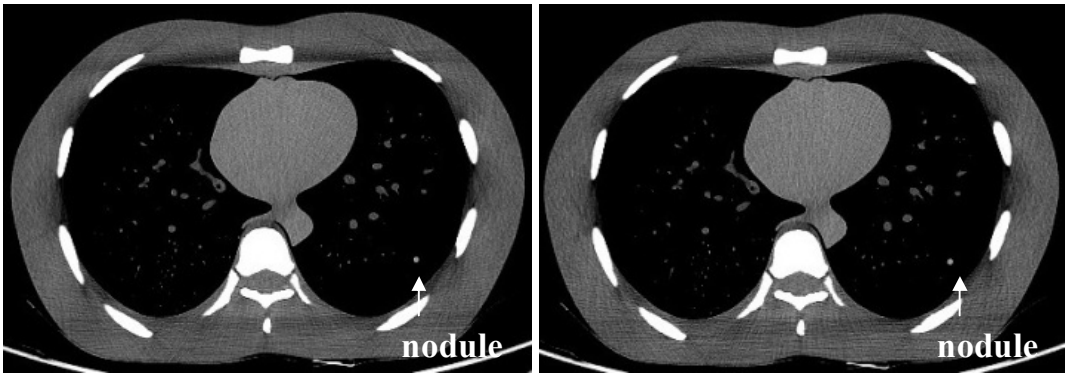

(a) (b)

Figure 5.2 The chest CT with 5 mm nodule, 1.25 mm slice thickness with STD filter, NI 15 (a), NI 17.5 (b)

CNR were only evaluated within the nodules, not for mediastinum therefore the optimization for routine chest CT were not exactly of objective image quality, however we expected that the CNR of mediastinum would be similar to the nodules because the nodules represented the soft tissue therefore we could optimize for the routine chest CT as well.

5.2 Conclusion

Automatic exposure control is the great potential method for radiation dose reduction. The use of both angular and z-axis modulations obtained the maximum dose reduction. Noise Index and slice thickness affected on the radiation dose. When vary Noise Index from 10-20, the radiation dose reduced from 16.52 to 3.38 mGy for standard size phantom, and 16.52 to 7.09 mGy for large size phantom. The factors affecting on radiation dose and image quality were Noise Index, slice thickness and reconstruction filters. The optimal Noise Index depends on the clinical applications. Using of Noise Index 20 at 75-380 mA, 1.25 mm slice thickness with LUNG and BONE+ filters result in acceptable subjective image quality whereas Noise Index 15-17.5 at 75-380 mA, 1.25 mm slice thickness with STD filter result in acceptable objective image quality for routine chest CT.

REFERENCES

[1] United Nations Scientific Committee on the Effects of Atomic Radiation. UNSCEAR 2000 report to the general assembly, Annex D: medical radiation exposure. New York: United Nations; 2000.

[2] Leng, L. Y. Radiation dose reduction in computed tomography: technique and future perspective. Imaging Med 1 (2009): 65-84.

[3] Kalra, K. M., MDCT Radiation Dose, In: Sanjay, S., Rubin, D. G., Kalra, K. M., editor. MDCT A Practical Approach. 30-35. Milan: Springer, 2006.

[4] Bruesewitz, R. M., Liffeng, Y., Vrieze, J. T., Kolfler, M. J., Macollough, H. C., editor. Smart mA – Automatic Exposure Control (AEC): Physics Principle and Practical Hint. [Internet]. Rochester: RSNA; 2008. [cited 2012 Jan 8]. Available from http://mayoresearch.mayo.edu/mayo/research/ctcic/upload/rsna2008-smart-ma.pdf

[5] Prokob, M., Galanski, M. Spiral and multislice computed tomography of the body. Stuttgart: Thieme, 2003.

[6] Bushberg, J. T., Seibert, J. A., Leidholdt, E. M., and Boone, J. M. The Essential Physics of Diagnostic Radiology. 2nd ed. Philadelphia: Lippincott Williams & Wilkins, 2002.

[7] The ImPACT Group. Buyer's guide: Multi-slice CT scanners CEP 08007. Medical Physics Department, Tooting, London 2009.

[8] Goldman, L.W. Principle of CT: Radiation dose and Image Quality. J Nucl Med Technol 35 (2007): 213-225.

[9] Perry Sprawls, Physical Principles of Medical Imaging. 2nd ed Mandison: Aspen Publisher, 1993.

[10] Kara, K. M., et al. Technique and applications of automatic tube current modulation for CT. J Radiology 233 (2004): 649-657.

[11] Kubo, T., et al. Radiation Dose Reduction in Chest CT : A Review. AJR 190 (Feb 2008): 335-343.

[12] Kalra, K. M., et al. Sixteen-detector row CT of abdomen and pelvis: study for optimization of z-axis modulation technique performed in 153 patients. AJR 233 (Feb 2004): 241-249.

[13] Kanal, M. K., Stewart, K. B., Kolokythas, O., and Shuman, P. W. Impact of operator- selected image noise index and reconstruction slice thickness on patient radiation. AJR 189 (Feb 2007): 219-225.

[14] IAEA. IAEA Human Health Series No 19. Quality Assurance Program for Computed Tomography: Diagnostic and therapy Application 2012.

[15] ImPACT. ImPACT information leaflet 1: CT scanner acceptance testing. Version 1.02 2001:1-8.

[16] International Atomic Energy Agency 2007.Dosimetry in Diagnostic Radilogy: An International Code of Practice-Vienna: International Atomic Agency (Technical report series, ISSN 007-1914; no 457). Vienna, Austria: IAEA

[17] Kalra, K. M., Rizzo, S., and Novelline, A. R. Reducing radiation dose in emergency computed tomography with automatic exposure control techniques. Emergency Radiology 11 (May 2005): 267-274.

[18] Kara, K. M., et al. Chest CT performance with Z-Axis modulation: Screening protocol and radiation dose. J Radiology 237 (2005): 303-308

[19] ECRI Institute. 64 slice Computed Tomography systems. Health Devices (Dec 2007): 377-402.

Appendices

Appendix A: Case record form

Radiation Dose

Series No	Scanning Parameter	Filer	CTDIvol (mGy)	DLP (mGy.cm)	Note
1	0.625/NI10/(1)				
2	0.625/NI10/(2)				
3	0.625/NI10/(3)				
4	0.625/NI12.5/(1)				
5	0.625/NI12.5/(2)				
6	0.625/NI12.5/(3)				
7	0.625/NI15/(1)				
8	0.625/NI15/(2)				
9	0.625/NI15/(3)				
10	0.625/NI17.5/(1)				
11	0.625/NI17.5/(2)				
12	0.625/NI17.5/(3)				
13	0.625/NI20/(1)				
14	0.625/NI20/(2)				
15	0.625/NI20/(3)				
16	1.25/NI10/(1)				
17	1.25/NI10/(2)				
18	1.25/NI10/(3)				
19	1.25/NI12.5/(1)				
20	1.25/NI12.5/(2)				
21	1.25/NI12.5/(3)				
22	1.25/NI15/(1)				
23	1.25/NI15/(2)				
24	1.25/NI15/(3)				
25	1.25/NI17.5/(1)				
26	1.25/NI17.5/(2)				
27	1.25/NI17.5/(3)				
28	1.25/NI20/(1)				
29	1.25/NI20/(2)				
30	1.25/NI20/(3)				
31	2.5/NI10/(1)				
32	2.5/NI10/(2)				
33	2.5/NI10/(3)				
34	2.5/NI12.5/(1)				
35	2.5/NI12.5/(2)				
36	2.5/NI12.5/(3)				
37	2.5/NI15/(1)				

Radiation dose (Cont.)

Series No	Scanning Parameter	Filter	CTDIvol (mGy)	DLP (mGy.cm)	Note
38	2.5/NI15/(2)				
39	2.5/NI15/(3)				
40	2.5/NI17.5/(1)				
41	2.5/NI17.5/(2)				
42	2.5/NI17.5/(3)				
43	2.5/NI20/(1)				
44	2.5/NI20/(2)				
45	2.5/NI20/(3)				
46	5.0/NI10/(1)				
47	5.0/NI10/(2)				
48	5.0/NI10/(3)				
49	5.0/NI12.5/(1)				
50	5.0/NI12.5/(2)				
51	5.0/NI12.5/(3)				
52	5.0/NI15/(1)				
53	5.0/NI15/(2)				
54	5.0/NI15/(3)				
55	5.0/NI17.5/(1)				
56	5.0/NI17.5/(2)				
57	5.0/NI17.5/(3)				
58	5.0/NI20/(1)				
59	5.0/NI20/(2)				
60	5.0/NI20/(3)				

CT number Measurement

Series No	Scanning Parameter	Filters	Nodule Size (mm)		
			CT number (nodule)	CT number (background)	S.D. (background)
1	0.625/NI10/(1)				
2	0.625/NI10/(2)				
3	0.625/NI10/(3)				
4	0.625/NI12.5/(1)				
5	0.625/NI12.5/(2)				
6	0.625/NI12.5/(3)				
7	0.625/NI15/(1)				
8	0.625/NI15/(2)				
9	0.625/NI15/(3)				
10	0.625/NI17.5/(1)				
11	0.625/NI17.5/(2)				
12	0.625/NI17.5/(3)				
13	0.625/NI20/(1)				
14	0.625/NI20/(2)				
15	0.625/NI20/(3)				
16	1.25/NI10/(1)				
17	1.25/NI10/(2)				
18	1.25/NI10/(3)				
19	1.25/NI12.5/(1)				
20	1.25/NI12.5/(2)				
21	1.25/NI12.5/(3)				
22	1.25/NI15/(1)				
23	1.25/NI15/(2)				
24	1.25/NI15/(3)				
25	1.25/NI17.5/(1)				
26	1.25/NI17.5/(2)				
27	1.25/NI17.5/(3)				
28	1.25/NI20/(1)				
29	1.25/NI20/(2)				
30	1.25/NI20/(3)				
31	2.5/NI10/(1)				
32	2.5/NI10/(2)				
33	2.5/NI10/(3)				
34	2.5/NI12.5/(1)				
35	2.5/NI12.5/(2)				
36	2.5/NI12.5/(3)				
37	2.5/NI15/(1)				
38	2.5/NI15/(2)				
39	2.5/NI15/(3)				
40	2.5/NI17.5/(1)				

CT Number Measurement (Cont.)

Series No	Scanning Parameter	Filters	Nodule Size (mm)		
			CT number (nodule)	CT number (background)	S.D. (background)
41	2.5/NI17.5/(2)				
42	2.5/NI17.5/(3)				
43	2.5/NI20/(1)				
44	2.5/NI20/(2)				
45	2.5/NI20/(3)				
46	5.0/NI10/(1)				
47	5.0/NI10/(2)				
48	5.0/NI10/(3)				
49	5.0/NI12.5/(1)				
50	5.0/NI12.5/(2)				
51	5.0/NI12.5/(3)				
52	5.0/NI15/(1)				
53	5.0/NI15/(2)				
54	5.0/NI15/(3)				
55	5.0/NI17.5/(1)				
56	5.0/NI17.5/(2)				
57	5.0/NI17.5/(3)				
58	5.0/NI20/(1)				
59	5.0/NI20/(2)				
60	5.0/NI20/(3)				

Image Scoring

Series No	Score				
	5	4	3	2	1
1					
2					
3					
4					
5					
7					
8					
9					
10					
11					
12					
13					
14					
15					
16					
17					
18					
19					
20					
21					
22					
23					
24					
25					
26					
27					
28					
29					
30					
31					
32					
33					
34					
35					
36					
37					
38					
39					
40					

Image Scoring (Cont.)

Series No	Score				
	5	**4**	**3**	**2**	**1**
41					
42					
43					
44					
45					
46					
47					
48					
49					
50					
51					
5					
53					
54					
55					
56					
57					
58					
59					
60					

Score 1 = Visualized partly of 10 mm, completely 12 mm in diameter

Score 2 = Visualized partly of 8 mm, completely 10 mm in diameter

Score 3 = Visualized partly of 5 mm, completely 8 mm in diameter

Score 4 = Visualized partly of 3 mm, completely 5 mm in diameter

Score 5 = Visualized completely 3 mm in diameter

Appendix B: Quality Control of CT system

1. Scan Localization Light Accuracy

Purpose: To test congruency of scan localization light and scan plane.

Method: Tape Localization film to the backing plate making sure that the edges of the film are parallel to the plate edge. Place the film vertically along the midline of the couch aligned with its longitudinal axis. Raise the table to the head position. Turn the alignment light. Mark both internal and external light with unique pin pricks along the midline of the light. Expose the internal light localization using the narrowest slice setting at 120-140 kVp, 50-100 mAs. For external light increment table to light position under software control and expose the film.

Tolerance: The center of the irradiation field from the pin pricks should be less than 2 mm.

Results:

Measured Deviation	External	1.0	mm
	Internal	0	mm

Comments: Pass

2. Alignment of Table to Gantry

Purpose: To ensure that long axis of the table is horizontally aligned with a vertical line passing through the rotational axis of the scanner.

Method: Locate the table midline using a ruler and mark it on a tape affixed to the table. With the gantry untilted, extend the table top into gantry to tape position. Measure the horizontal deviation between the gantry aperture centre and the table midline.

Tolerance: The deviation should be within 5 mm.

Results:

	Table	Bore
Distance from Right to Center (mm)	223	352
Distance from Centre to Left (mm)	220	348
Measured Deviation (mm)*	**1.5**	**2**

**Measured deviation = (Distance from right to center – Distance from center to left)/2*

Comments: Pass

3. Table Increment Accuracy

Purpose: To determine accuracy and reproducibility of table longitudinal motion.

Method: Tape a measuring tape at the foot end of the table. Place a paper clip at the center of the tape to function as an indicator. Load the table uniformly with 150 lbs. From the initial position move the table 300, 400 and 500 mm into the gantry under software control. Record the relative displacement of the pointer on the ruler. Reverse the direction of motion and repeat. Repeat the measurements four times.

Tolerance: Positional errors should be less than 3 mm at 300 mm position.

Indicated (mm)	Measured (mm)	Deviation (mm)
300	229	1
400	398	2
500	498	2
- 300	- 302	2
- 400	- 401	1
- 500	- 501	1

**Deviation = | Indicated – Measured|*

Comments: Pass

4. Slice Increment Accuracy

Purpose: To Determine the accuracy of the slice increment.

Method: Set up as you would for beam profile measurement. Select 120 kVp, 100 mAs, and smallest slit width. Perform several scans with different programmed slice separations under auto control. Scan the film with Epson Expression 10000 XL and measure the distance between the peaks by using Image J software.

Tolerance: Position errors should be less than 3 mm at 300 mm position.

Results:

Slice Separation in mm	Measured Separation (mm)	Deviation (mm)
20	21.80	1.80
30	30.04	0.04
50	49.91	0.09

**Deviation = |Slice separation – Measured separation|*

Comments: Pass

5. Gantry Angle Tilt

Purpose: To determine the limit of gantry tilt and the accuracy of tilt angle indicator.

Method: Tape a localization film to the backing plate making sure that the edges of the film are parallel to the edges of the backing plate. Place the film vertically along the midline of the couch aligned with its longitudinal axis. Raise the table to the head position. Move the table into the gantry. Center plate to alignment light. Expose the film at inner light location using narrowest slit, 120-140 kVp, 50-100 mAs. Tilt the gantry to one extreme from the console. Record the indicated gantry angle. Expose the film using the above technique. Measure the clearance from the closest point of gantry to midline of the table. Tilt the gantry to its extreme in the opposite direction. Record clearance and repeat the exposure. Measure the tilt angles from the images on the film.

Tolerance: Deviation between indicated and measured tilt angles ≤30. Gantry clearance should be ≥30 cm.

Results:

	Away	Toward
Indicated Angle	15º	15º
Measured Angle	15.57º	14.46º
Deviation*	0.57º	0.53
Clearance (mm)	351	354

**Deviation = |Indicated angle – Measured angle|*

Comments: Pass

6. Position Dependence of CT Numbers

Method: Position the water phantom centered in the gantry. Using 5 mm slice thickness, obtain one scan using typical head technique. Select a circular region of interest of approximately 400 sq. mm. and then record the mean C.T. number and standard deviation for each of the positions 1 through 5.

Technique: 120 kVp, 300 mA, 1 sec, slice collimation 5 mm. small head DFOV 250 mm.

Tolerance: The coefficient of variation of mean CT number of the four scans should be less than 0.2

Results:

Position	Mean C.T. #	S.D.	C.V.
1	114.37	3.51	0.031
2	114.62	3.59	0.031
3	115.09	3.84	0.033
4	114.62	3.64	0.032
5	114.47	10.98	0.096

**CV = Standard deviation/mean CT number*

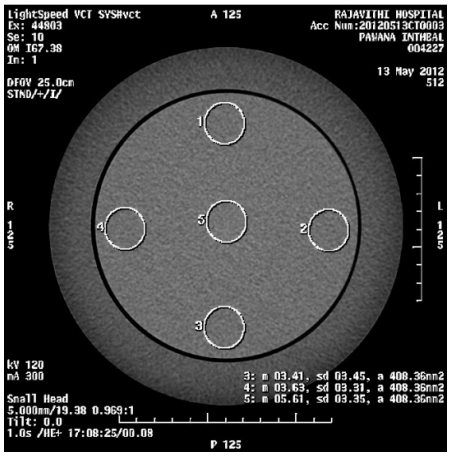

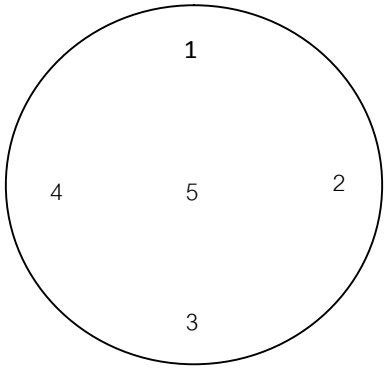

Figure I Position of ROI for CT number measurement.

Comments: **Pass**

7. Reproducibility of CT Numbers

Method: Using the same set up and technique as position dependence, obtain three scans. Using the same ROI as position dependence in location 5, this is the center of the phantom obtain mean C.T. numbers for each of the four scans.

Tolerance: The coefficient of variation of mean CT numbers of the four scans should be less than 0.002.

Results:

Run Number	**1**	**2**	**3**	**4**
Mean CT Number (HU)	5.62	5.63	5.62	5.62

Mean Global C.T. Number	5.62
Standard Deviation	0.008
Coefficient Of variation	0.001

Comments: **Pass**

8. mAs Linearity

Method: Set up the same as position dependence and insert 10 cm long pencil chamber in the center slot of the C.T. dose head phantom. Select the same kVp and time as used for head scan. Obtain four scans in each of the mA stations normally used in the clinic. For each mA station record the exposure in mGy for each scan. Scan should be performed in the increasing order of mA. Compute mGy/mAs for each mA setting.

mA	Exposure in mGy				mGy/mAs	C.V.
	Run 1	Run 2	Run 3	Run 4		
50	2.784	2.809	2.804	2.810	0.06	1.000
100	5.554	5.576	5.551	5.551	0.06	0.004
150	8.303	8.371	8.372	8.312	0.06	0.000
200	11.09	11.06	11.07	11.09	0.06	0.002
250	13.39	13.81	13.86	13.95	0.06	0.003
300	16.57	16.62	16.71	16.74	0.06	0.005
350	19.68	19.78	19.84	19.61	0.06	0.007

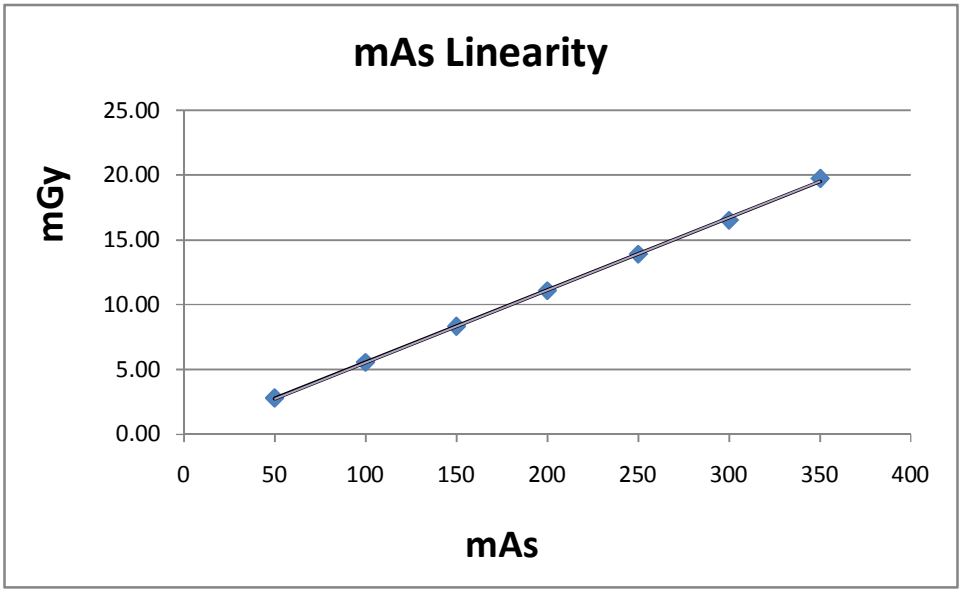

Figure II The relationship of mGy and mAs

Comments: **Pass**

9. Linearity of CT Numbers

Method: Set up the Catphan phantom as described in beam alignment. Select the section containing the test objects of different CT numbers. Select the head technique and perform a single transverse scan. Select a region of interest (ROI) of sufficient size to cover the test objects. Place the ROI in the middle of each test object and record the mean CT number.

Technique: 120 kVp, 300 mA, 1 sec, small head DFOV 250 mm. Slice thickness 5 mm.

Tolerance: R-square between measured CT number and linear attenuation coefficient (μ) more than 0.9

Results:

Material	Expected CT no.(HU)	Measured CT no. (HU)	μ(cm^{-1})
Air	-1000	-941.07	0
Teflon	990	918.13	0.184
Delrin	340	340.14	0.162
Acrylic	120	133.70	0.151
Polysteryline	-35	-34.2	0.136
LDPE	-100	-90.74	0.217
PMP	-200	-173.72	0.305

Note: Expected CT numbers are either the predicted ones or the ones obtained during the previous annual measurement.

Comments: Pass

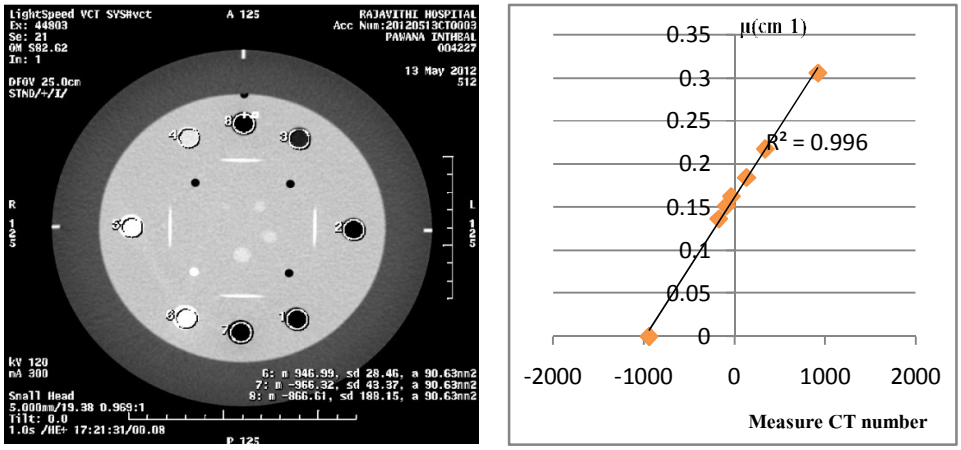

Figure III Linearity of CT number

10. Image uniformity

Method: Set up the Catphan phantom as described in beam alignment. Select the section containing the image uniformity module. Select the head technique. Perform a single transverse scan. Measure the mean value and the corresponding standard deviations in CT numbers within a region of interest (ROI). These measurements are taken from different locations within the scan field.

Technique: 120 kVp, 300 mA, 1 sec, slice collimation 5 mm. small head DFOV 250 mm.

Tolerance: The different of CT number at center and periphery should less than 5 HU

Results:

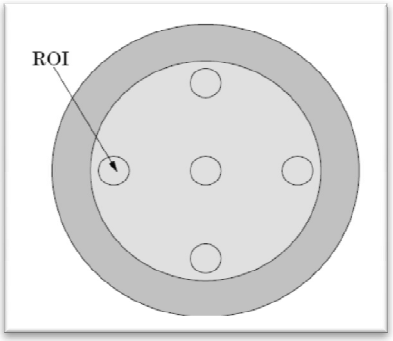

Figure IV Image Uniformity

Position	CT number (HU)	SD	Different (HU)
Center	5.62	3.46	0
3 o'clock	3.38	3.74	2.24
6 o'clock	3.42	3.47	2.20
9 o'clock	3.61	3.29	2.01
12 o'clock	3.45	3.42	2.17

**Different = |CT number center – CT number peripheral|*

Comment: Pass

11. High Contrast Resolution

Method: Set up the Catphan phantom as described in beam alignment. Select the section containing the high resolution test objects. Select the head technique. Perform a single transverse scan. Select the area containing the high resolution test objects and zoom as necessary. Select appropriate window and level for the best visualization of the test objects. Record the smallest test object visualized on the film.

Technique: 120 kVp, 300 mA, 1 sec, slice collimation 5 mm. small head DFOV 250 mm.

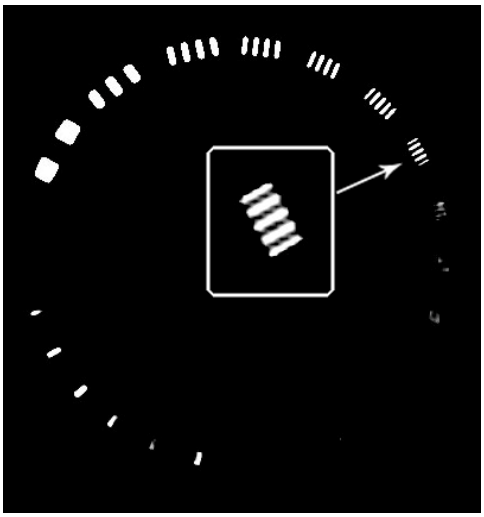

Figure V High contrast resolution

Results:

Slice Thickness in mm	Resolution
5	7 lp/cm (0.071 mm)

12. Low Contrast Detectability

Method: Select the section containing the low resolution test objects in the Catphan phantom. Perform a single transverse scan utilizing the same technique as high resolution**.**

Technique: 120 kVp, 300 mA, 1 sec, slice collimation 5 mm. small head DFOV 250 mm.

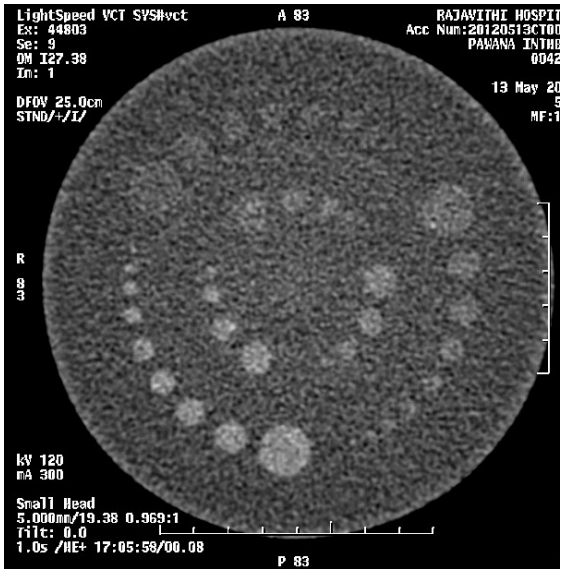

Figure VI Low contrast detectability

Results:

Supra-slice	**Nominal target contrast levels**	**Hole**	**%Contrast**
	0.30%	6	1.5
	0.50%	9	1
	1%	9	2
Sub-slice	**Nominal target contrast levels**	**Hole**	**%Contrast**
	3 mm Length	4	3
	5 mm Length	4	5
	7 mm Length	4	7

13. CTDI Measurement

Purpose: To verify CTDI of the scanner to the published values of ImPACT

Method: The $CTDI_{100}$ measured free in air and in 16 and 32 cm PMMA phantom for head and body were compared the CTDI data spreadsheet of the ImPACT CTDosimetry © 2011. The percent differences were calculated between measured and available ImPACTSCAN values.

Technique: 120 kVp, 100 mA, 1sec, 10 mm collimation

Results:

The measured $CTDI_{100}$ free in air and in 16 and 32 cm PMMA phantom for head and body scans were measured and compared to the CTDI data spreadsheet of the ImPACT CTDosimetry © 2011. [http://www.impactscan.org/ctdosimetry.htm]

The measured $CTDI_{100}$ in air for head and body protocol compared with ImPACTSCAN values for each kVp.

kVp	$CTDI_{100}$ in air (mGy/100mAs)					
	Head		%diff	Body		%diff
	Measured	ImPACT SCAN		Measured	ImPACT SCAN	
80	12.27	14.8	17.09	12.27	14.8	17.09
100	20.01	24.2	17.41	20.01	24.2	17.41
120	28.78	35.0	17.70	28.78	35.0	17.70
140	38.39	46.9	18.22	38.39	46.9	18.22

The measured $CTDI_{100}$ in the head phantom compared with ImPACTSCAN values for 120 kVp

kVp	$CTDI_{100}$ in head phantom (mGy)									
	At center		%diff	At periphery						%diff
	Measured	ImPACT SCAN		North	East	South	West	Average	ImPACT SCAN	
120	18.45	22.40	17.63	18.60	18.56	18.76	18.62	18.63	22.50	17.20

The measured $CTDI_{100}$ in the body phantom compared with ImPACTSCAN values for 120 kVp

kVp	$CTDI_{100}$ in body phantom (mGy)									
	At center		%diff	At periphery						%diff
	Measured	ImPACT SCAN		North	East	South	West	Average	ImPACT SCAN	
120	5.52	6.50	15.07	10.77	11.05	9.79	11.04	10.66	13.10	18.62

$CTDI_{vol}$ of monitor and calculated $CTDI_w$

The $CTDI_w$ was determine by using 16 and 32 cm diameter PMMA cylindrical phantom for head and body phantoms. The scan technique were 120 kVp, 100 mA, 1sec, STD filter for head and body protocol. The displayed $CTDI_{vol}$ on CT monitor were recorded to compared the difference with the calculated values and the ImPACTSCAN values

$CTDI_{vol}$ of monitor and $CTDI_w$ using head technique mA 100, 1 sec, STD filter

kVp	$CTDI_{vol}$ (mGy) in head phantom				
	Calculated	Monitor	% difference monitor and calculated)	ImPACT SCAN	%difference (monitor and ImPACTSCAN)
120	**18.57**	**18.33**	**-1.31**	**19.81**	**-7.47**

$CTDI_{vol}$ of monitor and $CTDI_w$ using body technique mA 100, 1 sec, STD filter

kVp	$CTDI_{vol}$ (mGy) in body phantom				
	Calculated	Monitor	% difference (monitor and calculated)	ImPACT SCAN	%difference (monitor and ImPACTSCAN)
120	**8.95**	**8.39**	**-6.67**	**9.15**	**-8.31**

14. Radiation Profile width

Purpose: To Determine the accuracy of the slice thickness.

Method: Set up as you would for beam profile measurement. Select 120 kVp, 100 mAs, and smallest slit width. Perform several scan with different programmed slice thickness under auto control. Scan the film with VXR-16 scanner and measure the distance between the peaks by using Image J software.

Tolerance: The different of the radiation profile width center and collimation setting should less than ±1 mm

Results:

Collimation (mm)	Measured (mm)	Deviation
2.5 mm(1.25x2)	3	0.5
5 mm (2.5x2)	4.4	0.6
10 mm(5x2)	9.2	0.8

VITAE

Name	Pawana Inthibal
Date of birth	April 13, 1975
Place of birth	Kanchanaburi, Thailand
Education	Bachelor of Science in Radiology Technology program Faculty of Medical Technology Mahidol University 1996
Award	Best oral presentation in Medical Imaging in the title is "Optimization in 64-MDCT of the chest using tube current modulation based on Noise Index: phantom study" from 12th AOCMP and 10th SEACOMP scientific meeting on December 11-14, 2012, Chiang Mai, Thailand
Work Experience	1996- Present Radiological Technologist Department of Radiology, Rajavithi Hospital BKK, Thailand
International Congress	The 68th Japan Radiological Congress (JRC) on April 12-15, 2012, Yokohama City, Japan The 12th Asia-Oceania Congress of Medical Physics (AOCMP) and 10th South-East Asian Congress of Medical Physics (SEACOMP) on December 11-14, 2012, Chiang Mai, Thailand
Address	333 Moo 12 Puttamonthon 3 Rd. Salathamasob Taweewattana BKK, 10170
E- mail	minimiss_mam@yahoo.com